Detail and Contrast Enhancement in Images Using Dithering and Fusion

Sunpreet Sharma

(18547232)

School of Computing, Engineering, and Mathematics

Western Sydney University

A thesis submitted for the fulfillment of the degree of

Master of Philosophy (Engineering)

2018

Dedication

To my mother Sunita, my late father Sham Karan and my brother Yogesh.

Acknowledgements

Because she competes with no one,
No one can compete with her.
~Lau Tzu

I would like to express my gratitude to my supervisor Dr. Ju Jia Zou (Jeffrey) for the useful comments he made and his engagement through the learning process of this master's thesis. Without his encouragement and guidance, this research would not have materialised. Furthermore, I would like to thank my co-supervisor, Dr. Gu Fang, for his assistance and support.

Finally, and most importantly, I would like to thank my partner Katie who has supported me throughout the entire process. Without her, I would never have had the strength to succeed. I am and will always be grateful for her love.

Statement of Originality

I hereby declare that the work presented in this thesis contains no material that has been accepted for the award of any other degree or diploma and that, to the best of my knowledge and belief, the thesis contains no material previously published or written by another person, except when due reference is made in the text of the thesis.

Name: Sunpreet Sharma

Signatur  Date: 31/05/2018

Table of Contents

List of Figures

List of Tables

Acronyms and Definitions

WT	*Wavelet Transform*
DWT	*Discrete Wavelet Transform*
IDWT	*Inverse Discrete Wavelet Transform*
DT-CWT	*Dual Tree Complex Wavelet Transform*
PSNR	*Peak Signal to Noise Ratio*
AM	*Amplitude Modulation*
FM	*Frequency Modulation*
MATLAB	*Matrix Laboratory*
RMSE	*Root Mean Square Error*
MSE	*Mean Square Error*
DB	*Density of Black Pixels*
DW	*Density of White Pixels*
FT	*Fourier Transform*
ED	*Error Diffusion*
IR	*Infrared Image*
B&W	*Black and White*
PAN	*Panchromatic*
MS	*Multi Spectral*
dB	*Decibels*

Publications

1. S. Sharma, J. J. Zou, and G. Fang. "Detail and contrast enhancement for images using dithering based on complex wavelets," *In Proceedings of IEEE Region 10 Conference (TENCON), Singapore, November 22-25, 2016*, vol. 1, pp. 1388-91.
2. S. Sharma, J. J. Zou, and G. Fang. "Contrast enhancement using pixel based image fusion in wavelet domain," *In Proceedings of IEEE 2nd International Conference on Contemporary Computing and Informatics (IC3I), Noida, India, December 14-17, 2016*, vol. 1, pp. 285-90.
3. S. Sharma, J. J. Zou, G. Fang, "Detail and Contrast Enhancement for Images using Region-Based Fusion in Wavelet Domain," *In Proceedings of International Symposium on Robotics and Mechatronics (ISRM 2017), Springer, Sydney, Australia, November 29-December 01,2017.* (Paper in press).
4. S. Sharma, J. J. Zou, G. Fang, "Contrast Enhancement of Dithered Images Using Complex Wavelets and Novel Amplification Factors," *In Proceedings of IEEE 12th International Conference on Signal Processing and Communication Systems (ICSPCS), Cairns, Australia, December 17-December 19, 2018.* (Paper in press).

Abstract

Silence is the language of the GOD,
All else is poor translation.
~Rumi

This thesis focuses on two applications of wavelet transforms to achieve image enhancement. One of the applications is image fusion and the other one is image dithering.

Firstly, to improve the quality of a fused image, an image fusion technique based on transform domain has been proposed as a part of this research. The proposed fusion technique has also been extended to reduce temporal redundancy associated with the processing. Experimental results show better performance of the proposed methods over other methods. In addition, achievements have been made in terms of enhancing image contrast, capturing more image details and efficiency in processing time when compared to existing methods.

Secondly, of all the present image dithering methods, error diffusion-based dithering is the most widely used and explored. Error diffusion, despite its great success, has been lacking in image enhancement aspects because of the softening effects caused by this method. To compensate for the softening effects, wavelet-based dithering was introduced. Although wavelet-based dithering worked well in removing the softening effects, as the method is based on discrete wavelet transform, it lacked in aspects like poor directionality and shift invariance, which are responsible for making the resultant images look sharp and crisp. Hence, a new method named complex wavelet-based dithering has been introduced as part of this research to compensate for the softening effects. Image processed by the proposed method emphasises more on details and exhibits better contrast characteristics in comparison to the existing methods.

Chapter 1- Introduction

Kindness in words creates confidence,
Kindness in actions creates profoundness,
Kindness in giving creates LOVE.
~Lau Tzu

Image enhancement is probably one of the most extensively studied areas in image processing. There are many factors that affect the quality of the acquired, transmitted or reconstructed image. Some factors are directly related to the image acquisition process, such as the illumination, whereas others are related to the physical properties of the sensor and the observed scene. The perceptual image quality is also affected by the common limitations of coding and transmission technologies. The main objective of contrast and detail enhancement is to improve the perceptual quality of a given image so that the features of the transformed image become more visible than the features of the original image. Contrast enhancement (CE) can be expressed as an optimisation problem where the objective is to maximise the average local contrast of an image. Contrast enhancement methods can be classified by means of various criteria. One way to classify CE techniques is to divide them into two classes, depending on the domain where the image is analysed and processed (spatial domain) and the way of transforming the contrast (transform domain).

This thesis investigates image enhancement problems using two image processing techniques, namely, image fusion and image dithering. Wavelet transforms have been used to achieve contrast and detail enhancement in these two applications. Hence, this thesis is an illustration of the use of wavelet transforms to solve these problems.

1.1. Existing methods and applications

1.1.1. Image fusion

Image fusion is defined as a process by which two or more images are combined into a single image, which retains the important features from each of the original images [1].

There are some requirements for achieving image fusion, which are mentioned below.

1. It should not discard any important information contained in any of the input images.
2. It should not introduce any information from outside into the fused output.
3. It must be reliable and tolerant to imperfection such as misregistration or noise.

Today there are large **applications** of image fusion and one can predict that with the advancement of this technology there will be more and more fields where image fusion will be beneficial. Advantages of image fusion have been postulated for navigation, surveillance, fire control and missile guidance to improve accuracy and for the accomplishment of these

tasks. As image fusion solves the problem by overlapping the two or more images into one therefore it is extensively used in biomedical, robotics, military and many other fields. In medical imaging, image fusion is extensively used for the simultaneous evaluation of a combination of computer tomography (CT), nuclear magnetic resonance (NMR), and positron emission tomography (PET) images. The images of the same scene are acquired at different time instances either to find and evaluate changes in the scene or to obtain a less degraded image of the scene. With image fusion it is also important to achieve high spatial and spectral resolutions by combining images from two sensors, one of which has high spatial resolution and the other high spectral resolution.

Some of the existing methods which have been studied during this research are mentioned below in Figure 1.1. An extended discussion on methods mentioned in Figure 1.1 can be found in Chapter 2 of this thesis. At this moment an idea of making a suitable selection of fusion level can be seen as dependent on the information type available. For example, when the sensors are alike, fusion at pixel level can be opted since it takes all the data into account. However, they produce spatial distortions in the fused image. Feature level fusion can be considered when the features as found by the processing of the different sensors can be appropriately associated. When sensors are very different, fusion at decision level will be more suitable and is also computationally more efficient. In this thesis two methods have been proposed, one of which uses pixel level fusion and the other uses region or feature level fusion.

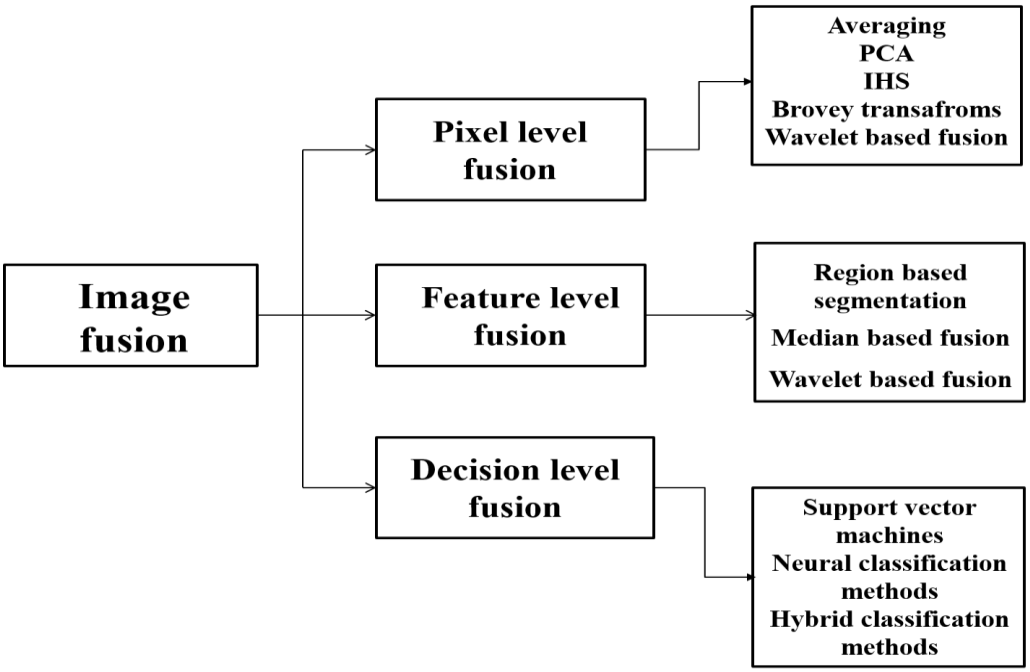

Figure 1.1 Existing fusion methods

1.1.2. Image dithering

Devices such as printers have a limited set of colours with which the colour rich or grey scale image must be represented. This often degrades the image quality or the image may not be pleasing to the human eyes. **Dithering** is a process in which an image with a limited colour depth can be transformed to provide an augmented perception of a pleasing image [2].

Here are some **applications** and some hardware that employ different image dithering techniques. Dithering plays an important part in achieving image compression [3,4], improving image quality in LCDs [5] and feature extraction [6,7]. Rendering devices including computer display units, cameras with LCD displays, mobile phones that are not capable of operating with a large number of colours. Web browsers use different dithering algorithms to display different kind of images. Let us assume a web browser needs to display a 256 colours image while a computer has 64 colours in its display. In this case, an adjustment to the original image is vital for browsers to display the image to the user. Another useful application of dithering is in situations in which the graphic file format is the limiting factor. The commonly used GIF format is restricted to 256 or fewer colours in many graphics editing programs. The graphics editing software is responsible for dithering images prior to saving them in such restrictive formats.

Existing dithering methods discussed in this thesis and their classification is provided in Figure 1.2. An insight on these methods can be gained from Chapter 2 of this thesis. The disadvantages associated with some of these methods have been mentioned in Section 1.2.

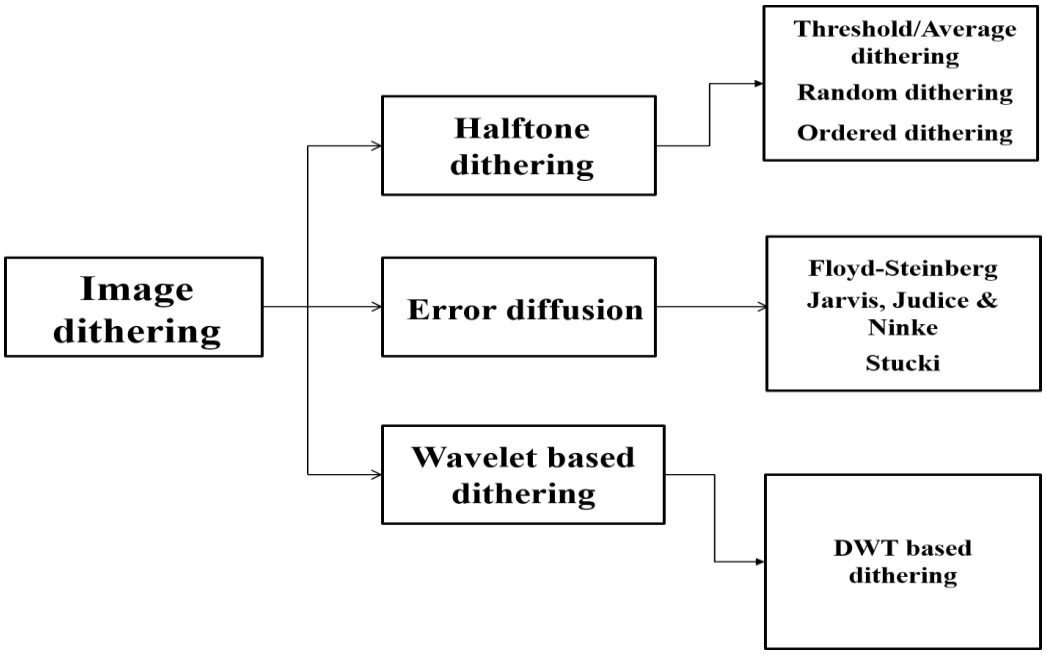

Figure 1.2 Existing dithering methods

1.2. Problem statement and aim

- ***Limitations of existing fusion methods***

1. ***Loss of contrast:*** A small change or shift in the input signal causes a large change or variation in the energy distribution of the wavelet coefficients at different scales or levels that can result in contrast loss [8].

2. ***Loss of processing time or Temporal redundancy:*** Image fusion which is based on a pixel-based process must process each and every pixel present in the source images before the right selection is made for the processed image. Hence this process is very lengthy and time-consuming and often leads to temporal redundancy [42]. In this thesis temporal redundancy of a method means by a process which is lengthy in terms of processing time.

- ***Shortcomings of existing dithering methods***

1. ***Softening of images:*** Softness in an image can make an image look coarser than the original image and make an image look greyish. This has an adverse effect on the contrast associated with the original image as crisp black and white regions appear to get lost in a uniform grey tone.

2. ***Loss of image information or details:*** Wavelet-based dithering can reduce the softening effects caused by error diffusion and can preserve the contrast [9]. However, the other thing which is also true is that wavelet-based dithering is also responsible for the loss of information or details present in the original image [2].

The **aim** of this research is to enhance the contrast and details present in a processed image. The author has considered image dithering and image fusion as two individual pathways to achieve the aim. Hence by contrast enhancement in the processed image, the author means that the final image after using image dithering and fusion should be able to exhibit better characteristics associated with contrast and image details respectively. As image dithering and image fusion will serve as pathways to achieve the aim, the study of existing methods have also been defined as **objectives** of this research.

When it comes to image fusion the proposed work should be able to enhance the original image or set of images itself, whereas in the case of image dithering the proposed work should be able to produce better output than the existing methods.

1.3. Original contributions

Digital images find numerous applications in civilian and military image processing systems that require sufficient contrast to analyse the image. Due to the poor quality of the imaging device, lack of expertise of the operator and possibly external adverse conditions, the quality of the image or video may be seriously affected leading to poor contrast. Regarding these issues, the proposed work has the following advantages, thus is making the following contributions to the field of image processing.

1. The proposed work can be applied to improve the details and contrast in an image. It can significantly improve the contrast and simultaneously preserves the details and the brightness of low contrast images without introducing any artefacts.
2. Two image fusion methods have been proposed in the present thesis. First is a pixel-based fusion method and the second one is region based fusion method. These methods have demonstrated their versatility by being able to fuse images of various types for example aerial images, multifocal images, IR images and so on. The proposed fusion methods in the present thesis have illustrated a success of 94% over existing methods, when it comes to achieving fusion and improving performance metrics such as peak signal to noise ratio and entropy.
3. The proposed work on image fusion produces a superior fused image with a reduction in processing time when compared with existing methods. The final fused image also exhibits enhanced contrast characteristics.
4. A new method for dithering is proposed which produces a superior dithered image, compared to existing methods, with emphasis on detail enhancement and contrast enhancement. The proposed work on dithering has successfully processed a data set of images and the dithered images produced by it are pleasing to the Human Visual System (HVS).
5. The proposed dithering method shows an improvement in metrics such as black and white difference or peak signal to noise ratio. This objective assessment is true in 89% of the total dataset images when compared to existing methods.

1.4. Thesis outline

The thesis consists of five chapters, organised as follows:

1. **Chapter 1** presents the introduction with a comprehensive description of the central theme of the research and an outline of the thesis.
2. **Chapter 2** accounts for the literature review and this has been organised into three parts. The chapter opens with a background of image fusion methods and ongoing trends. This discussion is then extended with an overview of the key existing image fusion methods.

As wavelet transform is the backbone of this thesis, an account of this method is included in the chapter. Finally, the last part of this chapter covers image dithering. Limitations of the existing image fusion and image dithering methods have also been addressed. The chapter concludes with a summary.

3. **Chapter 3** focuses on image fusion, one of the objectives of this research. This chapter starts with an explanation of the proposed method for image fusion, which is based on Wavelet Transforms (WTs). This is illustrated with an implementation of the proposed method, achieved using MATLAB. The last part of the chapter presents a discussion of both the visual and mathematical analysis of the proposed method for image fusion and summarises the chapter respectively.
4. **Chapter 4** explores image dithering, the other objective of this research. It begins by explaining the proposed method based on Complex Wavelet Transforms (CWTs). This is followed by an explanation of the implementation of the proposed method using MATLAB. Chapter 4 ends with a discussion on the subjective and objective analysis of the proposed image dithering method and a chapter summary.
5. **Chapter 5** presents a summary of the thesis, the conclusions drawn from the research and recommendations for further study.

Chapter 2- Literature Review

Be a LAMP, a LIFEBOAT, a LADDER.
Help someone's SOUL heal.
Walk out of your house like a SHEPARD.
~Rumi

2.1.Image fusion background

As mentioned in Section 1.1.1, image fusion happens at three levels [1]. Those three levels are illustrated in Figure 2.1 and discussed below.

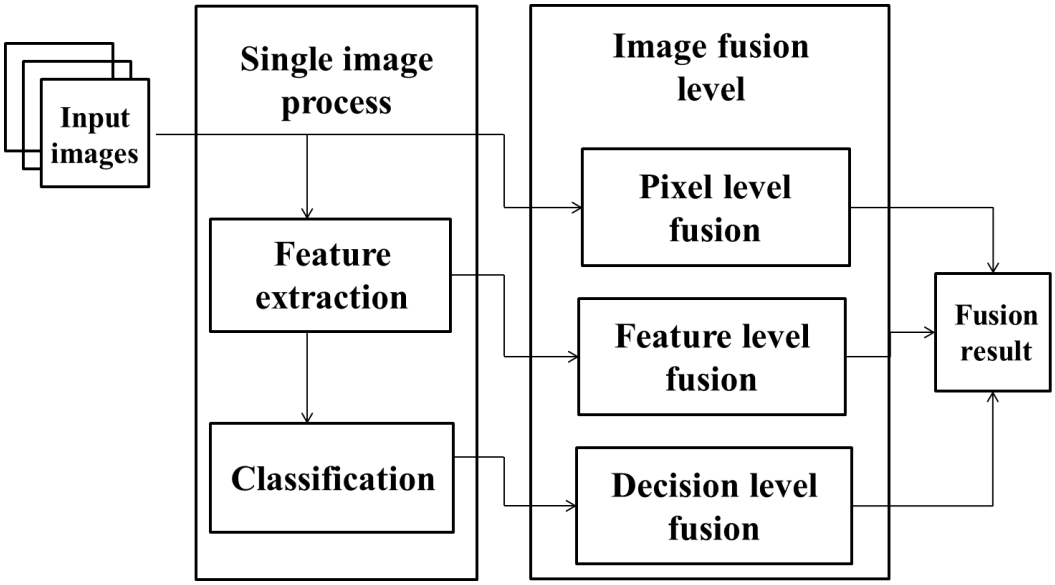

Figure 2.1 Image fusion block scheme of different abstraction levels: pixel-level fusion, feature level fusion, and decision level fusion.

Pixel level fusion: Pixel-based fusion is performed on a pixel by pixel basis. It generates a fused image in which the information associated with each pixel is determined from a set of pixels in source images.

Feature level fusion: Feature-based fusion at feature level requires an extraction of objects recognized in various data sources. It requires extraction of salient features which are dependent on their environments such as pixel intensities, edges or textures. After the extraction is finished the selected features can be combined to generate the fused image.

Decision-level fusion: Decision-based fusion consists of merging information at a higher level of abstraction, combines the results from multiple algorithms to yield a final fused decision. Input images are processed individually for information extraction. The obtained information is then combined by applying decision rules to reinforce common interpretation.

As fusion using wavelets is possible at both pixel level and feature level. So the present thesis focuses primarily at these two levels. Fusion techniques exist in two domains. One is in the spatial domain and the other is in the transform domain. Both of these are discussed right below.

- ***Fusion in spatial domain***

This approach of fusion happens primarily at the pixel level. A classical approach to image fusion is to take each pixel in the fused image as the weighted average of the corresponding pixels in the input images [1, 10-12]. Generally, the weights are determined according to the activity-level of different pixels in the input images. However, this kind of approaches may generate block artifacts on object boundaries [13-16]. Instead of performing the blockwise fusion, region-based image fusion methods perform fusion to the regions with irregular shapes which are obtained by image segmentation [1, 16]. A common limitation of segmentation-based methods is that they are mainly dependent on an accurate segmentation of the input images, which is another topic of research in image processing. Various colour space and dimension reduction-based image fusion methods have been proposed. These methods are usually designed for fusion of colour and greyscale images, and thus, are limited to some specific applications, such as the pan sharpening problems.

Pixel-level fusion is performed on a pixel-by-pixel basis and is widely used in remote sensing [1, 17], medical imaging [1, 17-19], and computer vision [19, 20]. It generates a fused image in which information associated with each pixel is determined from a set of pixels in source images to improve the performance of image processing, e.g. fusing thermal and visible images for a night vision surveillance system or for segmentation. The most common pixel level fusion algorithms include pixel average technique, principal components analysis (PCA), Brovey transforms (BT), IHS and others. These techniques are not complex when it comes to implementation. However, although the fused images obtained by these methods have high spatial quality, they usually suffer from spectral degradation [21]. Because in the real-world objects have different shapes and scales, multi-resolution techniques have attracted more and more interest in image fusion. The interest in these techniques originated in pyramid and wavelet transforms.

- ***Fusion in transform domain***

The idea of an image pyramid was first discussed in the early 1980s [22]. Using this method, the input images are first transformed into their multi-resolution pyramid representations [23]. Then, with the help of a certain fusion rule, the fusion process creates a new fused pyramid from the input image pyramids. Finally, the fused image is reconstructed by performing an

inverse multi-resolution transform. Some of the illustrations of this work include the Laplacian pyramid [24], the gradient pyramid [25], the contrast pyramid [26], the ratio-of-low-pass pyramid [27], and the morphological pyramid [28]. However, because the pyramid method fails to introduce any spatial orientation selectivity in the decomposition process, the above methods often cause artefacts in the fusion [29]. Liu et al. propose a general image fusion framework based on multiscale transform in [14]. In their work, the source images at first are decomposed using multiscale decomposition. Then, the low-frequency components are fused using the sparse representation method, while the high-frequency details are fused with traditional fusion rules. Finally, an inverse multiscale transform is performed to obtain the fused image. This general framework is followed by the majority of the methods in transform domain. Upcoming next paragraphs in the present section address more on the methods of this nature i.e. methods based on multiscale transform.

A tutorial of the wavelet-based image fusion methods is provided by Zhang and Blum [30], in which they present a comprehensive comparison of different pyramid merging methods, different resolution levels and different wavelet families. Besides the pyramid and wavelet transform, in recent years some new multiscale transforms such as dual-tree complex wavelet [31], curvelet [32, 33], contourlet [34, 35, 36] and shearlet [37, 38] have been introduced for image fusion. However, the most commonly used multiscale decomposition or transform domain fusion methods for image fusion are the pyramid and wavelet transforms [1, 36, 38].

In the past Zhang et al.[39] reviewed some classical fusion schemes, e.g. coefficient based fusion, window and region-based fusion, median-based fusion and so on. Recently, some new fusion schemes have been designed, for example, fusing the base components using the principal component analysis-based method in which the detail coefficients at each transform level are selected by choosing the maximum value and followed by a neighbourhood processing step [40, 41]. This can increase the consistency of coefficient selection thereby reducing the distortion in the fused image. A novel weighted average method to fuse the multiscale decompositions has been proposed [1, 42] in which the weight parameters in different scales of the transform are determined by combing global and local weights; this method is able to preserve the image details and is insensitive to the noise. Recently a novel cross-scale fusion rule for multiscale decomposition has been proposed based on the fusion of medical images, taking into account both intrascale and interscale consistencies [17, 18]. Moreover, the weights of different scales are optimised by using a generalised random walkers method which can effectively exploit the spatial correlation among adjacent pixels instead of using a global optimisation method.

In [43], Matsopoulos and Marshall first applied the morphological pyramid method to fuse the MR and CT images, but this method can occasionally create many spurious edges. Another family of multi-resolution fusion techniques is the wavelet-based method, which usually uses the discrete wavelet transform (DWT) in the fusion. Since the DWT of image signals produces a non-redundant image representation, it can provide a better spatial and spectral localisation of the image information compared with other multiresolution representations. The DWT schemes have some advantages over pyramid schemes such as increased directional information, no blocking artefacts that often occur in pyramid fused images and better signal-to-noise ratios [44]. Therefore, the wavelet-based methods have been widely used for image fusion [30, 44], and two detailed surveys on this method can be seen in [45] and [46]. In the contourlet transform, the Laplacian pyramid has been used to capture the point discontinuities, and then a directional filter bank links the point discontinuities into linear structures. Due to its effectiveness in representing spatial structures, contourlet transform has been successfully applied in medical imaging [47].

Since 1998, many scientific papers on image fusion have been published, which emphasised on improving the fusion quality and reducing the distortion. There is a wide range of techniques for the image fusion out of which the most popular and efficient methods are mentioned right below. Visual illustrations of each of the methods discussed in Section 2.1.1 can be found in Appendix B of this thesis.

2.1.1. Overview of existing fusion techniques.

- ***Principal Components Analysis (PCA)***

PCA is another general tool for coordinate transformation and data reduction in remote sensing and in many other image processing devices. The PCA is useful for image encoding, image compression, image enhancement and image fusion. The principal component analysis converts intercorrelated Multi-Spectral (MS) bands into a new set of uncorrelated components. The first Principal Component (PC) also resembles a panchromatic image. It is, therefore, replaced by a high-resolution panchromatic for fusion. The panchromatic image is fused into the low-resolution multispectral bands by performing a reverse PCA transformation. One of the transform's targets might be to analyse the image patches into uncorrelated components.

PCA is a linear transformation technique which aims at reducing redundant information in the source images. PCA is mainly applicable in remote sensing where multispectral images are to be merged with high-resolution data. As the name implies, PCA technique generates a

projection of non-correlated images called principal components on orthogonal axis from the inter-related source data. The source data is compressed by linear transformation into a reduced set of sub-images known as principal components, which contain all the useful data for analysis. The variance of principal components is calculated and those with higher variance will have more information.

Comments

1. PCA method has the advantages of reducing the number of variables by creating combined independent principal components for representing important information. Thus it reduces the dimensional structure of the source data.

2. PCA is an assumption based technique[1]. Some of the assumptions that PCA follow are linearity, orthogonality etc. When these assumptions go incorrect especially in higher dimensions then PCA tends to give false results.

- ***Intensity, Hue and Saturation (IHS)***

IHS is one of the essential techniques of image fusion methods widely used in remote sensing applications and has been used as a standard procedure in many commercial software solutions. Here 'Intensity' corresponds to the brightness of the color, 'Hue' corresponds to the average wavelength of color and 'Saturation' to the color purity. The images obtained from multiple sensors of the same scene may contain information which is complementary to each other. An example can be described for fusing remote sensing multispectral (MS) and panchromatic (PAN) images. After representing the low-resolution, multispectral image in IHS notation based on an RGB color model, its intensity (I) component is replaced with the high-resolution PAN component, thus changing the highest resolution component in MS image to PAN image. It is assumed that the recovered intensity component and the panchromatic image contain similar information [1]. Most literature recognizes IHS as a third order method because it employs a 3 x 3 matrix as its transform kernel in the RGB-IHS conversion model. A matrix with 3 rows and 3 columns is a third order matrix. This is the case for IHS kernel. The linear RGB-IHS conversion system is given by Equation 2.1.

$$\begin{bmatrix} I \\ v1 \\ v2 \end{bmatrix} = \begin{bmatrix} 1/3 & 1/3 & 1/3 \\ -\sqrt{2/6} & -\sqrt{2/6} & \sqrt{2/6} \\ 1/\sqrt{2} & -1/\sqrt{2} & 0 \end{bmatrix} \bullet \begin{bmatrix} R \\ G \\ B \end{bmatrix}, \tag{2.1}$$

here variables $v1$ and $v2$ can be considered as x and y axes in the Cartesian coordinate system, while intensity I corresponds to the z axis. In this way, the hue (H) and the saturation (S) can be represented by $H = \tan^{-1}\left(\frac{v2}{v1}\right), S = \sqrt{v1^2 + v2^2}$.

Comments

1. The main advantage of IHS is its capability of maintaining colour through the fusion process. This is possible as this process does not alter the HUE component, which is a direct measure of the colour intensity. As almost all applications require colour intactness throughout the fusion process this is the reason that this technique is one of the most widely used ones.
2. This technique is only limited to three bands at a time.
3. It can severely distort the spectral values of the original colour of the MS image.

- ***Brovey Transform (BT)***

BT is a simpler and widely-used RGB colour fusion method. This method of image fusion is similar to IHS method where the intensity component is substituted by high-resolution PAN image. The transformation decomposes the phase space of the MS image into colour and intensity, which essentially substitute the *I* component of the MS image with high-resolution image. It further simplifies the image transformation coefficient to reserve the multi-band image information, and all the intensity information is transformed into high-resolution PAN image. In this method, the replacement takes place by applying Equation 2.2.

$$\begin{bmatrix} Rf_i \\ Gf_i \\ Bf_i \end{bmatrix} = \frac{PAN}{I} \begin{bmatrix} R_i \\ G_i \\ B_i \end{bmatrix}, \tag{2.2}$$

where,
Rf_i, Gf_i, Bf_i, represents the R,G,B components of the fused image at pixel value i.
I represents the average intensity of the R,G,B components at pixel value i.
R_i, G_i, B_i, represents the R,G,B components of the input band at pixel value i.

Comments

1. This operation is lighter than IHS in terms of processing time. Hence this technique can be preferred where temporal redundancy is a limitation.

2. The Brovey transform provides excellent contrast characteristics but affects the spectral characteristics greatly. The Brovey sharpened image is not suitable for pixel-based classification as the pixel values change drastically in this sort of process.

- ***Wavelet transforms and fusion***

Wavelet transforms (WTs) are an integral part of the present thesis. So, the author at this point wants to highlight some of the important and useful aspects of wavelet transforms. Once an insight has been gathered on wavelet transform the discussion on wavelet-based fusion will be continued both in the present Chapter 2 and in Chapter 3 respectively.

A **wavelet** is a smooth oscillating function or waveform of finite duration such that its energy is concentrated in time, its average is zero, and it allows simultaneous time/frequency analysis [48].

To be more flexible in extracting time and frequency information, a family of wavelets can be constructed from a function $\psi(t)$, also known as the 'Mother Wavelet', which is confined in a finite interval. 'Daughter Wavelets' $\psi_{u,s}(t)$ are then formed by translation (shifts) with a factor u and dilation (scaling) with a scale parameter s in time (frequency) domain; this relation has been given by Equation 2.3.

$$\psi_{u,s}(t) = \frac{1}{\sqrt{s}} \bullet \psi\left(\frac{t-u}{s}\right) \tag{2.3}$$

By using Wavelet Transform (WT) the time resolution is increased when one analyses a high-frequency portion of the signal, and the frequency localisation is increased when analysing a low-frequency part of the same signal. This type of analysis is suitable for signals that have both low-frequency components with long time duration and high-frequency components with short time duration, which is the case for most signals. The thesis uses Discrete Wavelet Transform (DWT) to achieve image fusion, so this is going to be the focus of the further discussion. An excellent insight on WT from the context of its history, evolution and more can be gained from [48].

DWT uses the frames to yield coefficients. The coefficients correspond to points on a two-dimensional grid or lattice of discrete points in the scale-translation domain. This lattice will be indexed by two integers: the first integer, j, will correspond to discrete scale steps while the second integer, n, corresponds to discrete translation steps (the grid is indexed by j and n). The dilation parameter s is now $s = s_0^j$ and the translation, u, is now $u = nu_0 s_0^j$, where

s_0 and u_0 are the discrete scale and translation steps, respectively. Therefore Equation 2.3 can be rewritten as Equation 2.4.

$$\psi_{j,n}(t) = \frac{1}{\sqrt{s_0^j}} \psi\left(\frac{t - nu_0 s_0^j}{s_0^j} \right) \tag{2.4}$$

It is important to note that wavelet function fulfills the admissibility condition given in [49] as Theorem 2.3.1. It is necessary because by the wavelet function should exhibit the characteristics of a band pass filter and should ultimately converge. If it will not do so the chosen frame will not converge and hence will become not defined.

Assuming $C_f(j,k)$ and $D_f(j,k)$ are the scaling coefficients (approximations) and wavelet coefficients (details) of the projection of a signal *f*. The successive lower resolution coefficients are then recursively derived with Multi Resolution Analysis (MRA) are described in Equation 2.5, where h_0 stands for lowpass filter and h_1 is a highpass filter respectively.

$$\begin{aligned} C_f(j+1,k) &= \sum_n h_0[n-2k] C_f(j,n) \\ D_f(j+1,k) &= \sum_n h_1[n-2k] C_f(j,n) \end{aligned} \tag{2.5}$$

These equations can be implemented as a tree-structured filter bank as shown in Figure 2.2 [50]. Because of the orthonormal wavelet basis, this 3-level analysis filter bank also satisfies the synthesis of high-resolution scaling coefficients from the next immediate level lower resolution scaling and wavelet coefficients as in Equation 2.6.

$$C_f(j,k) = \sum_n h_0[k-2n] C_f(j+1,n) + \sum_n h_1[k-2n] D_f(j+1,n) \tag{2.6}$$

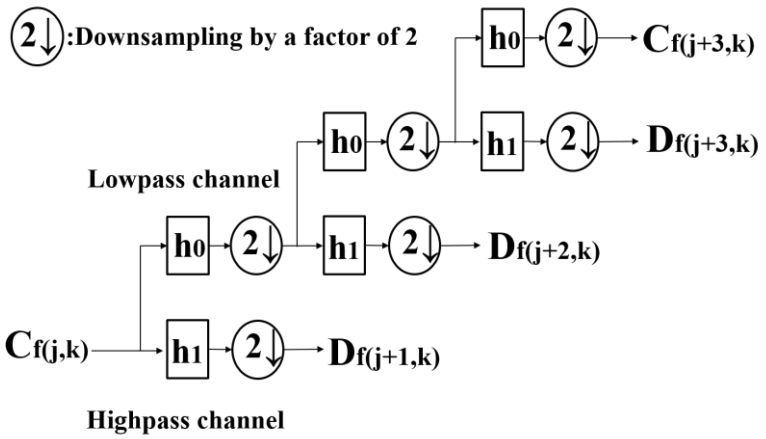

Figure 2.2 Two-channel, three-level analysis filter bank with 1-D DWT.

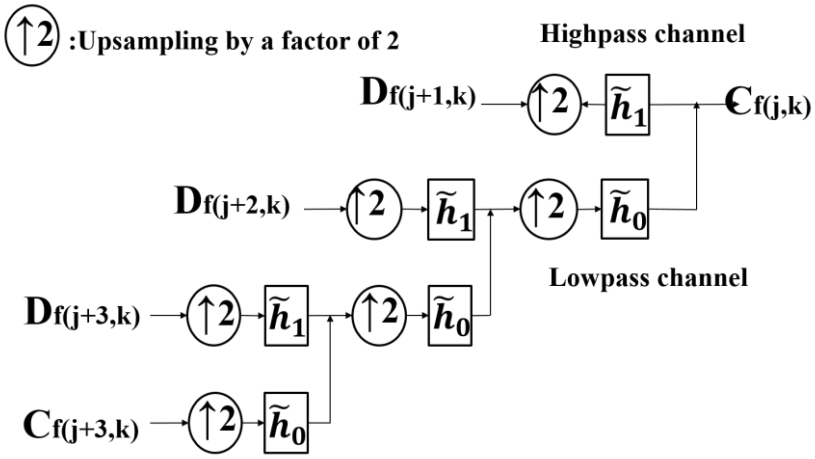

Figure 2.3 Two-channel, three-level synthesis filter bank with 1-D DWT.

For a sampled signal, the filter bank tree is also viewed as an implementation of 1-D DWT with initial maximum resolution component $C_f\left(j=0,k\right)$ and its decomposition into a number of details $D_f\left(j,k\right)$ at successive lower resolution scales.

For the standard DWT, the size of approximate (scaling) coefficients and detail (wavelet) coefficients decreases by a factor of 2 at each successive decomposition level. Thus, the standard DWT is perfectly non-redundant in multi-scale environment. The sparse representation with energy compaction makes the standard DWT widely accepted for signal compression. The reconstruction filter bank structure shown in Figure 2.3 follows the recursive synthesis similar to Equation 2.6 with reconstruction filters $\tilde{h}_0$ and $\tilde{h}_1$, which are identical to their corresponding decomposition filters h_0 and h_1 but with time reversal. The most important criterion with filter bank implementation (sub-band decomposition) of DWT is the proper retrieval of signals, which is commonly known as perfect reconstruction. The perfect reconstruction imposes certain constraints on analysis and synthesis filters. More

about these constraints can be found in the literature [51-53]. The implementation of an analysis filter bank for a single level 2-D DWT is shown in Figure 2.4. This structure produces three detailed sub-images (LH, HL, HH), corresponding to three different directional orientations (Horizontal, Vertical and Diagonal), and a lower resolution sub-image LL. The filter bank structure can be iterated in a similar manner on the LL channel to provide multilevel decomposition. A multilevel decomposition hierarchy of an image is illustrated in Figure 2.5.

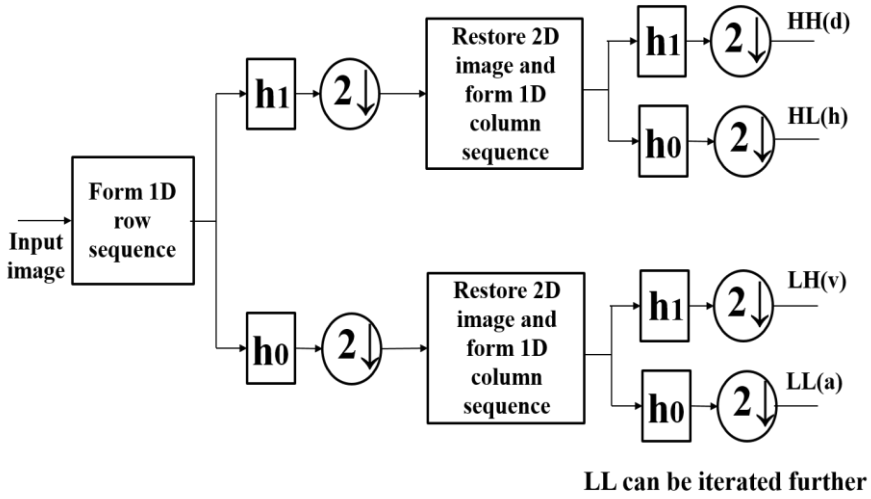

Figure 2.4 Single-level analysis filter bank for 2-D DWT.

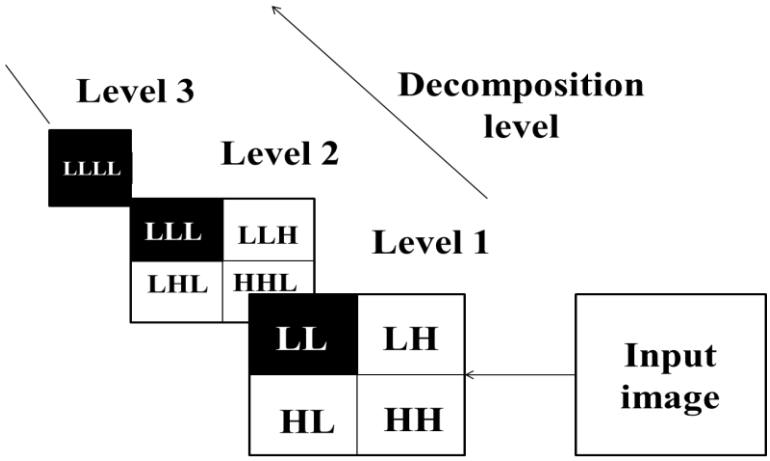

Figure 2.5 Multi-level decomposition hierarchy of an image with 2-D DWT.

Each decomposition breaks the parent image into four child images. Each of such sub-images is one fourth the size of a parent image. The sub-images are placed according to the position of each sub-band in the two-dimensional partition of the frequency plane as shown in Figure 2.6. If $\psi(x)$ is the one-dimensional wavelet associated with the one-dimensional scaling function $\phi(x)$, then three 2-D wavelets associated with three sub-images are given as

$$\psi^V(x,y) = \phi(x) \otimes \psi(y) \rightarrow LH$$

$$\psi^H(x,y) = \psi(x) \otimes \phi(y) \rightarrow HL$$

$$\psi^D(x,y) = \psi(x) \otimes \psi(y) \rightarrow HH\,.$$

$\otimes$: stands for tensor product.

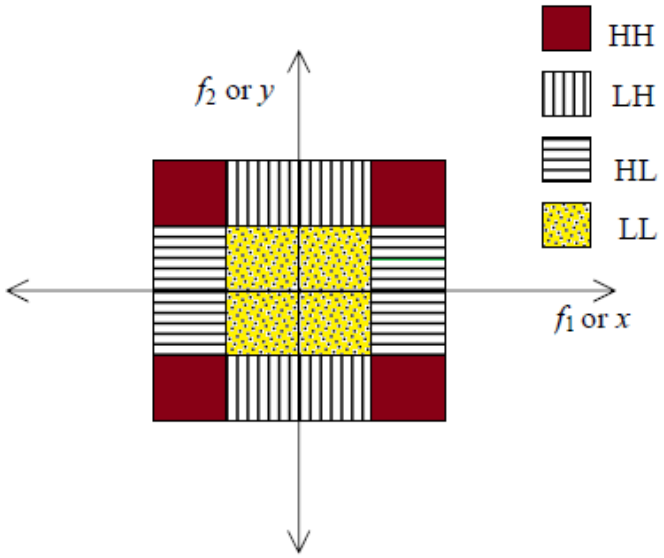

Figure 2.6 Frequency plane partitioning with 2-D DWT.

A test image 'pattern' and its 2-D DWT decomposition is shown in Figure 2.7. This decomposition is done with the help of the 'wavelet toolbox' of MATLAB. There are also various extensions available for 2-D wavelet transforms in a non-separable form. There are also non-separable multidimensional filter banks and wavelets bases with their applications to image coding [54-56]. Non-separable methods offer true multidimensional processing, freedom in filter design and non-rectangular sub-sampling. Although the non-separable methods have several advantages, separable filtering is a common choice because of the simplicity of its implementation.

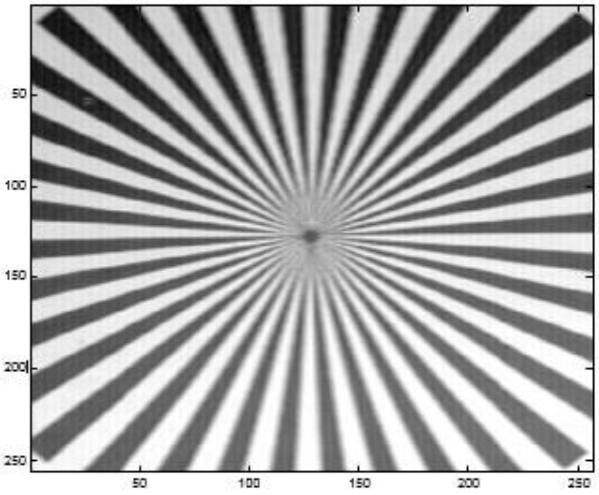

(a) Test image

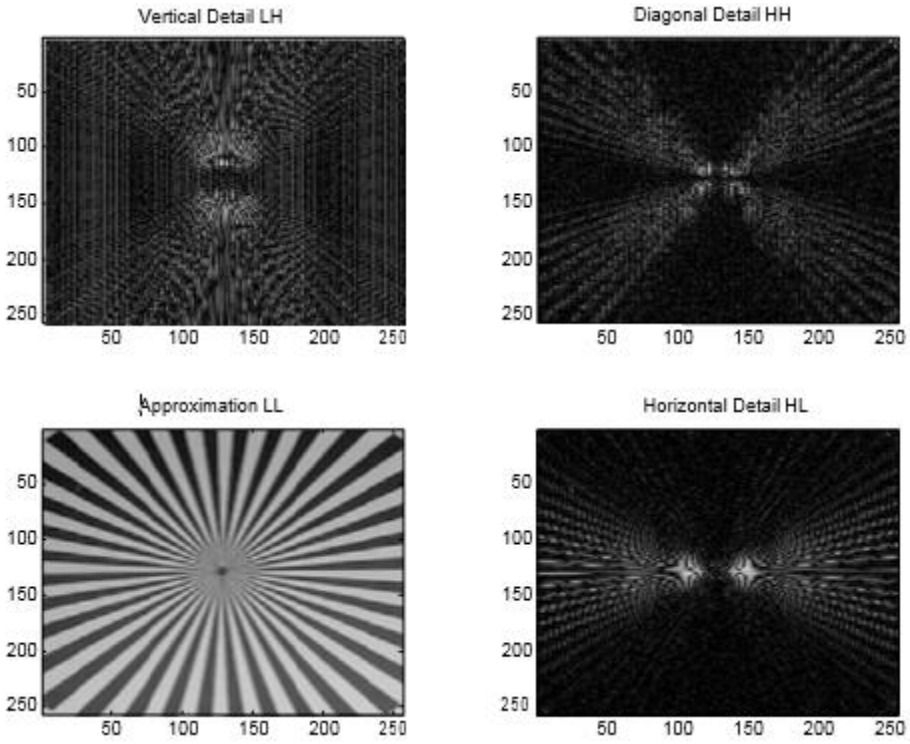

Figure 2.7 Extraction of coefficients with 2-D DWT.

In wavelet transformation, fusion is more formally defined by considering the wavelet transform ω of the two already registered images A and B along with the fusion rule ϕ. Once the fusion has been completed, the inverse wavelet transform ω^{-1} can be performed to get back the final fused image C. This process can be expressed below in Equation 2.7. The basic framework of DWT based fusion is illustrated in Figure 2.8.

$$C = \omega^{-1}\left(\phi\left(\omega(A), \omega(B)\right)\right) \tag{2.7}$$

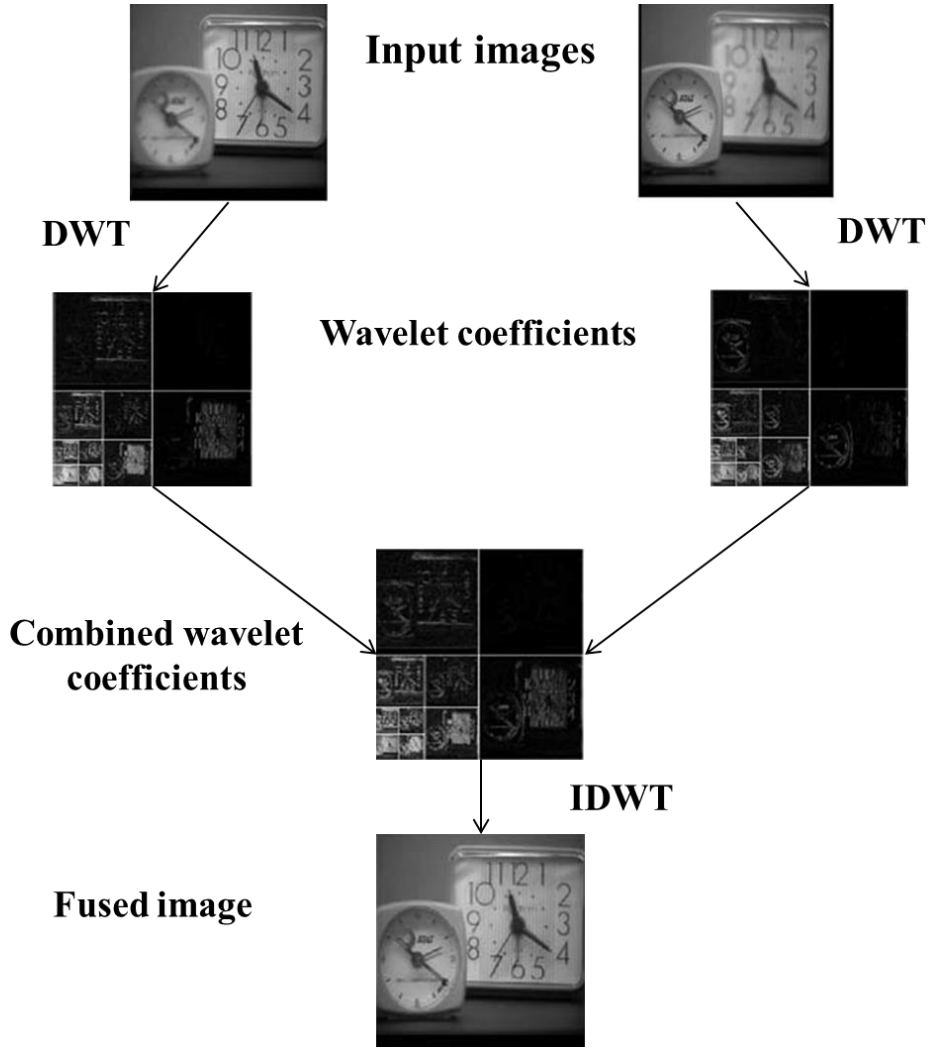

Figure 2.8 Framework of DWT based fusion.

2.1.2. Drawbacks of existing image fusion methods

1. ***Loss of processing time or temporal redundancy:*** Pixel-based image fusion processes have to process each and every pixel present in the source images. This is required before the right selection is made for the processed image. Hence, the process is lengthy, time-consuming and often leads to temporal redundancy.
2. ***Loss of contrast:*** Shift sensitivity may arise from down samplers in the DWT implementation [52,57-58]. This is an undesirable property because it implies that DWT coefficients fail to distinguish between input signal shifts. The shift variant nature of DWT is demonstrated with three shifted step-inputs in Figure 2.9. The input shifted signals in Figure 2.9 have been decomposed up to j = 4 levels using Daubechies 5 (db5) wavelet. This figure shows the unpredictable variations in the reconstructed detail signal at various levels and in final approximation. A small change or shift in the input signal causes a large change or variation in the energy distribution of the DWT coefficients at different scales or levels and this can result in contrast loss [23] as shown in Figure 2.10.

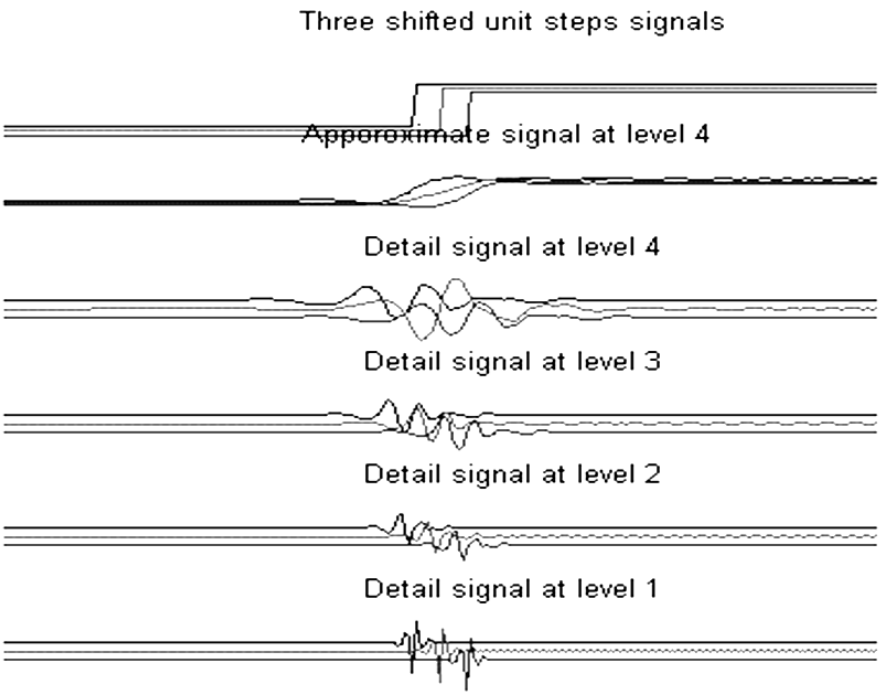

Figure 2.9 Shift-sensitivity of standard 1-D DWT [49].

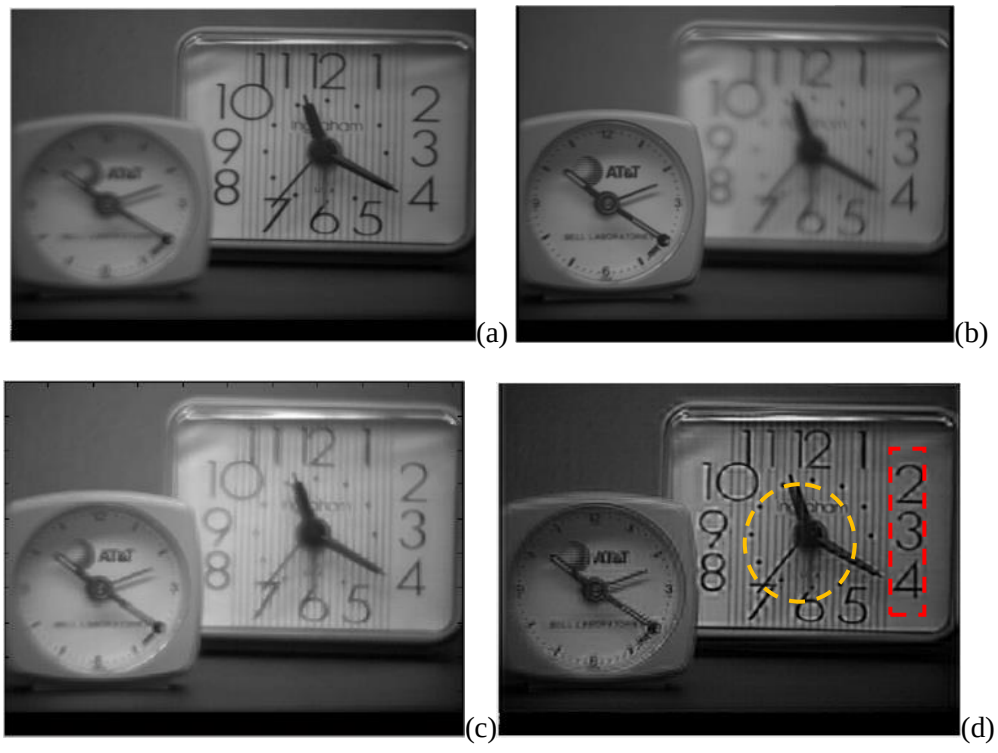

Figure 2.10 Parent images (a) and (b) are fused together to give image (c) and image (d). Although image (c) has less noise in comparison to both the parent images, it has lost sharpness and contrast. Image (d) has been achieved by using a contrast enhancement technique while achieving image fusion. In comparison to image (c) it has further supressed the noise and has also maintained better contrast characteristics (yellow oval) along with better detail preservation (red rectangle).

2.2. Image dithering methods

Image dithering reduces the colours of an image to provide rendering capabilities to different hardware devices. It helps hardware to find the closest match to the colours from its current colour palette and create a dithered image, not exactly the same as the original image but an approximation. Consequently, it makes it possible to display or print a true colour image using a device which has fewer colours available to display or print. There are different types of colour palettes such as fixed colour palette and optimised colour palette. The disadvantage of a fixed colour palette is that one may not have the colours necessary for the image being processed and one may not need the colours that are available in the palette. The optimised colour palette is the one in which available colours are chosen depending on how often those colours are used in the original image. The process of selecting a suitable palette and mapping each pixel in the original image to an entry in the palette is called **quantisation** [59].

(a) Original image (b) Dithered image

Figure 2.11 Effect of image dithering.

Figure 2.11 reveals the difference between the greyscale image and the dithered image. Therefore, if the printing device or the display device cannot handle a particular colour, the only solution is to apply dithering algorithms to convert that colour to the most suitable one that can be handled. Although a dithered image uses a limited number of colours, it looks quite close to the original image because of the limited spatial resolution of the human eye, which is a process of averaging neighbouring pixels. The reason for the spatial resolution is that human eyes act as low-pass filters, so if an image consists of high-frequency components it provides fewer details. Therefore, whenever a dithering technique is being executed, it must preserve the low-frequency components, which in return help human eyes to localise the necessary pictorial information about an image.

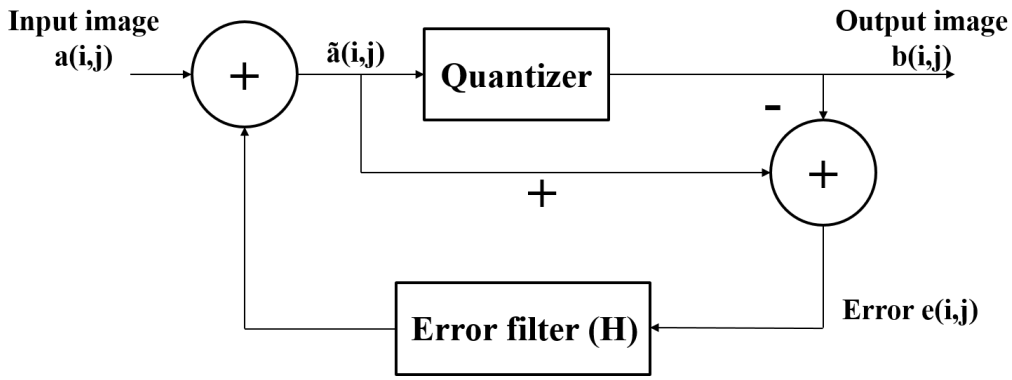

Figure 2.12 Block diagram for image dithering.

The block diagram in Figure 2.12 explains the implementation of image dithering using a block diagram. Generally, the process consists of three main blocks: quantizer, error filter and summation operator which are being represented by the circle. The given figure has been described from the perspective of error diffusion-based dithering; therefore error diffusion filter H has been used. More insight on error diffusion-based dithering can be gained from Section 2.2.2. Here $a(i, j)$ is the input image that is to be dithered. The pixels in the image are modified because of the quantization. The modified input pixels are given by $\tilde{a}(i, j)$.

After quantization an error is produced as the pixel value after quantization and the original pixel value are different. The error $e(i, j)$ is the difference between the modified input and the quantized output pixel value. It can be calculated by using Equation 2.1.

$$e(i, j) = \tilde{a}(i, j) - b(i, j) \tag{2.1}$$

The error calculated above is diffused to neighbouring pixels through the error filter, H. The error diffused to neighbouring pixels is different when different diffusion filters are used. This process continues until the entire input image is mapped and an output dithered image is generated.

2.2.1. Background

Finding the dithered image is an iterative process. The time taken to reach convergence depends on various factors, such as mask or kernel size, etc. Generally, quantisation and dithering operations are performed one after another, i.e., the first quantisation will be performed and later the dithering operation is carried out. Here the quantiser tries to minimise the quantisation error without taking into consideration the fact that the ditherer will change the quantised results. As a result, the error that the quantiser tries to minimise may be increased during the dithering operation. This problem arises because of the independent design of the quantiser. One can overcome this problem by designing a

quantiser which takes dithering into consideration. Such a quantiser is mentioned in [60]. There are different types of quantisers [61-64], for example, in the median-cut quantiser, a colour palette is built such that each colour in the palette is allocated with a nearly equal number of pixels in the image. This palette can be improved using the Linde-Buzo-Grey (LBG) algorithm. Braudway [62] proposed building a primary palette by centering colours at peaks in the colour value histogram. Subsequently, this can also be improved using the LBG algorithm. A faster binary tree splitting (BTS) method is proposed in [64]. In this algorithm, colour clusters are formed in the leaves of a binary tree which was formed by iteratively splitting the colour space along its principal axis.

Common problems occurring in the standard dithering include textual contours, colour impulses and colour shifts [65-67]. The adaptive methods proposed in these papers aim to remove these unnecessary effects. Dithering makes use of the averaging property of the eye to create the illusion of more colours. Error diffusion achieves this effect by spreading the quantisation error to the neighbouring pixels. There are different types of error diffusion filters such as Floyd-Steinberg, Stucki, Jarvis, Judice, and Ninke [68,40,41]. The error diffusion filters use a fixed kernel, i.e. the coefficients of the error diffusion filters are fixed. Contrary to these filters, the new algorithms are designed to find the optimum coefficients for the given image or to change the coefficients adaptively. When quantisation is performed on an image, the colour present in a region is approximated to the closest colour present in the colour palette. When approximation is done, there is a shift in the colour which is noticeable to the eye. Also, in the quantised image, there are appearances of false edges. These two problems are solved mostly by error diffusion. Sometimes all the quantisation errors accumulate, resulting in a colour impulse which is very disturbing. Also, there are unacceptable distortions around the edges. To overcome these effects, a new adaptive vector error diffusion technique is proposed in [34]. The error diffusion filter coefficients in [34] are obtained by minimising the mean square error between the average colour of the original image and the dithered image. The use of the Least Mean Square-type (LMS type) adaptive algorithm to solve the minimisation problem has been done in [34]. Using this adaptive technique, one can produce images in which the average colour shade is similar to the colour shades in the original image. Also, the occurrence of colour impulses and false textual contours is significantly reduced.

In [9], a wavelet-based image enhancement technique was proposed, which has served as a motivation for this research. In [9] an adaptive histogram equalisation technique that uses wavelet-based gradient histograms has been suggested. Applying wavelet transform to an image concentrates energy in a small subset of the wavelet coefficients, mostly along the edges. This feature is useful in image processing applications. Some contrast enhancement

algorithms use wavelets to improve the image contrast. Yang et al. [69] proposed a technique to enhance the contrast of medical images by using the Haar wavelet and histogram stretching. Of all the image dithering methods mentioned below, error diffusion-based image dithering has been most widely investigated and used. Existing image dithering methods which have been studied as a part of this research are mentioned below. The visual illustrations of each of the methods discussed in Section 2.2.2. can be found in Appendix B of this thesis.

2.2.2. Analysis of existing dithering methods

- ***Halftone dithering*** [59]

This technique is referred to as traditional printing technique. This method involves the printing of dots of different sizes in an order and pattern to stimulate various intensities. **Halftone** is the reprographic technique that simulates continuous tone imagery through the use of dots, varying either in size, in shape or in spacing [59]. The engineers realized that when humans view a very small area at normal viewing distances, our eyes automatically perform blending or smoothing function on fine details of that area. Because of this function of the human eye, humans perceive the overall intensity of the area that they are viewing.
There are two halftoning methods; amplitude modulation (AM) based halftoning and frequency modulation (FM) based halftoning [63]. There are different types of dots that can be used like elliptical dots and square dots but most commonly used are round shaped dots. The elliptical dots are useful for images with a multiple number of objects while square dots are best for images with more detail. Halftoning is also used to print colour images. The density of four primary colours cyan, magenta, yellow and black (CMYK) are varied to produce shades. The components that affect the result of output image include screen ruling (number of dots per linear inch), screen angle, screen dot shape and range, highlight and shadow dot size and mid-tone dot size. The resolution of a halftoned screen is measured as a number of lines of dots per inch in parallel with screen angle. The higher screen resolution means greater detail that can be reproduced.

- ***Thresholding/Average dithering*** [76]

Threshold or average dithering works on a basic principle of choosing a threshold value and all pixels darker than the chosen value become black and other pixels (lighter than the threshold value) become white. Images processed through this method are monochromatic (black and white). The threshold is decided by selecting an average value of image pixels and all pixels with intensity level more than the average threshold are quantized to 1 and the remaining pixels (with values less than the average threshold) get a value of 0.

Comments

1. This is a simple dithering method to implement that produces adequate results on most images.
2. Method tends to lose details as well as introduces visible contour artefacts i.e. an unwanted distortion in images.

- ***Random dithering*** [77]

Random dithering was the first attempt to correct the contouring produced by threshold/average dithering. The main aspect of random dithering is the generation of the threshold values. The threshold values can be generated using a random number generator. A random generator can generate values from 0-255. These values are used as the threshold values. These values are then compared with the corresponding image pixel value. If the value of the image pixel is greater than the corresponding threshold value generated by the random generator, then the pixel is set to '1' (or 'white') and if the value of the image pixel is less than the corresponding threshold value generated by the random generator, then the pixel is set to '0' (or 'black'). Thus using random dithering, one can convert a greyscale image to a monochrome image (or binary image).

Comments

1. The advantage of using the random dithering technique is that the image produced has fewer artefacts.
2. Random dithering introduces white noise, so the output image looks like badly tuned TV picture with 'snow' effect.
3. Random dithering technique is more suitable for low-frequency images where the priority of absence of artefacts is higher than noise.

- ***Ordered dithering*** [60]

This method is an improvement on random dithering as there is a consideration of how neighbouring pixels should be treated. The image is distributed in different regions and those regions are treated one by one. In this method, the comparison is made with a threshold matrix. One of the standard 2 x 2 matrix is defined right below as D.

$$D = \begin{bmatrix} 0 & 128 \\ 192 & 64 \end{bmatrix}.$$

The matrix D is cascaded until the size of the dithering matrix is equal to the size of the image. The pixels in the original image are compared with the corresponding pixels in the dithering matrix *D*. If the pixel in the image is greater than the corresponding value in the dithering matrix (which is generated by cascading the standard dithering matrix D), then the pixel in the image is set to '1' (or 'white') and if the pixel in the image is less than the corresponding value in the dithering matrix, then the pixel in the image is set to '0' (or 'black'). Thus, using ordered dithering, one can convert a greyscale image to a monochrome image (or binary image) and this type of dithering technique gives proportionally a good quality image. It is possible to use a smaller subset of the above mask. The Bayer's method is commonly used and can be identified by cross-hatch artefacts on dithered image [60].

Comments

1. This method is simple, fast and deterministic (it can be used in animations) and it is mostly used in computer displays with limited palettes.
2. A major flaw in the process is that it exhibits crosshatch pattern. As a result, human eyes can easily view the blocking effect in the processed image.

- ***Error diffusion***

Error diffusion (ED), unlike other classical methods, is a lengthy method. Because it processes a particular position in the image matrix one at a time, the results of the process will affect the rest of the image matrix and hence ED requires more time and greater computational power. Furthermore, error diffusion creates dithering patterns dynamically, which will enhance the edges of the images. This characteristic can be applied to images consisting of texts.

ED can be divided into two main parts: one-dimensional ED and two-dimensional ED. The one-dimensional error diffusion process is such that it scans the image from left to right. The process goes to each image matrix and compares the image matrix value with its half-grey value. The comparison is made in a manner such that if the image value is less than the half-grey value, a black colour is placed otherwise the white colour is placed. This method gives only full black or full white output. When employing the one-dimensional method an error is created which is added to the next image value, with the same method repeated. Unlike one-dimensional error diffusion, two-dimensional ED is more complicated because the two-dimensional ED scans the image matrix from left to right, top to bottom and processes each value and diffuses the error to more than one matrix. How the diffused error is distributed to

neighbouring cells varies with different ED methods. The error diffusion technique generates a more pleasing image output than the other dithering methods discussed above. The low-frequency noise is not visible in the image which leads to a good spatial resolution, and the output does not contain artefacts such as cross-hatch patterns. There are many error diffusion techniques available. The main idea of every error diffusion technique is to diffuse the error but each method has its own way of spreading the error to neighbouring pixels, which will determine the quality of each error diffusion algorithm. Some of the famous error diffusion methods that have been considered to achieve the objectives of this research are discussed below.

1. Floyd-Steinberg ED [68]

The Floyd-Steinberg algorithm is considered to give the best dithered output of the classical dithering methods. It was first introduced by Floyd and Steinberg in [68] and the method itself has been named after them. Figure 2.13 below is the kernel (α) used in their method.

$$\alpha = \frac{1}{16}\begin{bmatrix} & * & 7(\alpha 1) \\ 3(\alpha 4) & 5(\alpha 3) & 1(\alpha 2) \end{bmatrix}$$

Figure 2.13 Kernel of error diffusion for Floyd-Steinberg.

The quantisation error is diffused in such a way that the 7/16th of the error is diffused to pixel α1, the 3/16th of the error is diffused to pixel α4, the 5/16th of the error is diffused to pixel α3 and the 1/16th of the error is diffused to pixel α2. The main reason for its popularity is due to the pleasingly isotropic output.

When processing the current pixel, one compares the pixel with the value 128 (for an 8 bit per pixel image). If the pixel value is less than 128, then it is replaced with '0' and if the pixel value is greater than 128, then it is replaced with '1'. When the quantisation is done, the original pixel value is replaced with some other value. The difference between the original pixel value and the new pixel value is the error produced. The image is scanned from left to right and from top to bottom. The pixels are quantised and the error is diffused to the neighbouring pixels as explained above, without disturbing the pixels that have already been processed or quantised. In this dithering technique, the quantisation error is nearer to zero.

2. Jarvis, Judice & Ninke ED [76]

This method was proposed by Jarvis, Judcie and Ninke respectively and was called as the 'Minimum Average Error'. This method consists of 12 weights to diffuse the error to the neighbouring pixels. The kernel of the dither matrix is given in [76] and here it has been

shown as alpha (α). In Figure 2.14 asterisk shown in the kernel represents the current position of the operation.

$$\alpha = \frac{1}{48}\begin{bmatrix} 1 & 3 & 5 & 3 & 1 \\ 3 & 5 & 7 & 5 & 3 \\ 15 & 7 & * & 0 & 0 \end{bmatrix}$$

Figure 2.14 Kernal of error diffusion for Jarvis, Judcie and Ninke.

This method diffuses the errors to 12 neighbouring pixels. The values chosen for the matrix do not affect the output image greatly although some microscopic patterns can be observed. These microscopic patterns become smaller and randomly appearing as more number of matrix elements has non-zero values. This method is coarser but has fewer visual artefacts.
It is slower than Floyd Steinberg that has been discussed below and computation is higher due to division by 48 which is not a power of 2 to make use of the shift operators.

Comments

1. On comparison with Floyd-Steinberg error diffusion algorithm, here error diffusion is done to eight extra pixels. Therefore, more time and large memory is required.
2. In Floyd-Steinberg dithering method, the error is diffused to 4 pixels and in this method the error is diffused to 12 pixels. Hence, it requires more computational power.

3. Stucki ED [77]

The Stucki error diffusion method is an improvement to Jarvis et al. method and the difference in this algorithm comes from the way the error diffusion is performed on the neighbouring pixels. This is relatively faster than Jarvis et al. in computation and provides a clean and a sharp output image.

$$\alpha = \frac{1}{42}\begin{bmatrix} 0 & 0 & 0 & 0 & 0 \\ 0 & 0 & * & 8 & 4 \\ 2 & 4 & 8 & 4 & 2 \\ 1 & 2 & 4 & 2 & 1 \end{bmatrix}$$

Figure 2.15 Kernel of error diffusion for Stucki.

Comments

1. It can be seen in Figure 2.15 that division by 42 is quite slow to calculate but after the initial 8/42 is calculated, the same can be used to compute the other coefficients using shifts.
2. The slow processing time is offset by the clean and sharp output.

- ***Wavelet-based dithering***

This method was developed by Ovidu Cosma [9] to compensate for the softening effect produced by error diffusion and to enhance the edges of the images. In this technique, the original image is decomposed using DWT, which produces a series of coefficients that are placed in several sub-bands. When an image is decomposed it will have an approximation coefficient and detail coefficients (horizontal, vertical and diagonal). Once the coefficients are extracted, they can be amplified by multiplying coefficients with sub-band weights (Table 4.1) to enhance the details and contrast of an image. The same image can be passed through an error diffusion algorithm to produce the dithered image. This type of dithering is called wavelet-based dithering with error diffusion (DWT-ED). This method was specially developed to overcome the softening effects arising due to error diffusion algorithms.

2.2.3. Limitations of existing dithering methods

1. ***Softening of images:*** The main drawback of the existing error diffusion techniques is that the resulting images are softer than the original because each pixel colour is represented as the average of a group of pixels. Softness in an image can make an image look coarser than the original image and make an image look greyish. This has an adverse effect on the contrast associated with the original image as crisp black and white regions appear to get lost in a uniform grey tone; this effect can be observed in Figure 2.16.

(a) Original image (b) Processed Image

Figure 2.16 Effect of Floyd-Steinberg error diffusion.

2. ***Loss of image information or details:*** Figure 2.17(b) shows the result of the wavelet-based dithering that has been achieved from the original image in Figure 2.17(a). One thing which is evident is that wavelet-based dithering can reduce the softening effects caused by error diffusion and can preserve the contrast. But the other thing which is also

true is that wavelet-based dithering is also responsible for the loss of information or detail present in the original image.

(a) Original Image (b) Processed image

Figure 2.17 Effect of wavelet-based dithering.

2.3. Summary

This chapter consists of a two-part literature review. It starts with a background of image fusion methods both in spatial and transform domain. This discussion is then extended with an overview of the key existing image fusion methods. As wavelet transform is the backbone of this thesis, an account of this method is included in the chapter followed by a brief discussion on wavelet-based fusion. Drawbacks of existing image fusion methods include (a) Loss of processing time or temporal redundancy, (b) Loss of contrast. The second part of this chapter covers existing image dithering methods such as random dithering, ordered dithering, error diffusion etc. This part also points two out the limitations of existing image dithering methods. One of the limitations is the softening of images and the other is the loss of image information or details. Next, Chapter 3 on image fusion addresses solutions for the mentioned problems. Whereas Chapter 4 focuses on solving or minimising the mentioned shortcomings related to image dithering.

Chapter 3- Image Fusion

If you grow in LOVE, you grow in AWARENESS,
If you grow in AWARENESS, you grow in LOVE.
~OSHO

3.1. The proposed pixel-based fusion and implementation

Image fusion has been achieved by using pixel level methods based on multiresolution Biorthogonal Wavelet Transforms (BWT) [69,70]. BWT has been preferred because of two important properties, namely, wavelet symmetry and linear phase, which can preserve edge information and hence reducing the distortions in the fused image. The fusion rule selected in these papers is known as an absolute maximum rule and the same rule has been used in the proposed method to achieve the desired results.

Nirmala et al. [14] has proposed a fusion method which has been based on standard deviation. In their method, they have used DWT for multi-level image fusion. They have proposed that standard deviation can be performed on the approximate coefficients before the final fused image is reconstructed. The method suggested by them was novel, and this thesis has focused on making further improvements regarding enhancing the contrast and keeping the details intact in the fused image. The proposed method can capture more information from input images and as a result, makes the fused image appear sharp and clear. Consequently, the fused image is pleasing from a visual perspective. An improvement in contrast also makes observations of the features present in an image easier and as a result, the observer can effectively locate details like boundaries, edges etc. present in an image.

3.1.1. Fusion rule used

Certain pixels in a picture correspond to image features such as edges, lines and boundaries. These features of the picture are necessary to describe image content and visual performance. The proposed method is based on the application of DWT [71] to the fusion of source images. Therefore, in the proposed method of image fusion, an absolute maximum selection rule in the transform domain has been used. Let *A(x,y)* and *B(x,y)* be the two images to be fused and their wavelet coefficients corresponding to low frequency sub-bands *CAA(i.j)* and *CAB(i,j)* respectively, then the maximum selection rule to combine wavelet coefficients is defined as in Equation 3.1.

$$CAF(i,j) = \begin{cases} CAA(i,j) \text{ if } |CAA| \geq |CAB| \\ CAB(i,j) \text{ if } |CAB| \geq |CAA| \end{cases} \tag{3.1}$$

where *CAF(i,j)* is the value that will be present in the final fused image [72].

For a simpler understanding of how the selected fusion rule works two matrices have been fused in this section. Suppose there are two matrices *A* and *B* each of dimensions two by three and an element by element comparison can be made among them that will give an element with maximum (larger) value. Matrix *C* can then be created which will contain the elements of maximum value. Figure 3.1(b) shows the resultant matrices of the two parent matrices shown in Figure 3.1(a). The author has performed the discussed pixel-based fusion on a set of images shown in Figure 3.2(a) and illustrated the effect of the achieved fusion in Figure 3.2(b). Another important point that one should keep in mind is that the dimensions of the images or matrices have to be the same to achieve fusion. Otherwise this process will not be feasible.

(a)

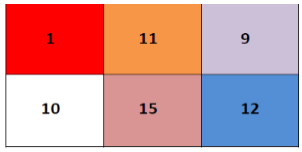

(b)

Figure 3.1 Fusion of two matrices using maximum selection rule: (a) Two individual matrices to start with; (b) Processed matrix with maximum values.

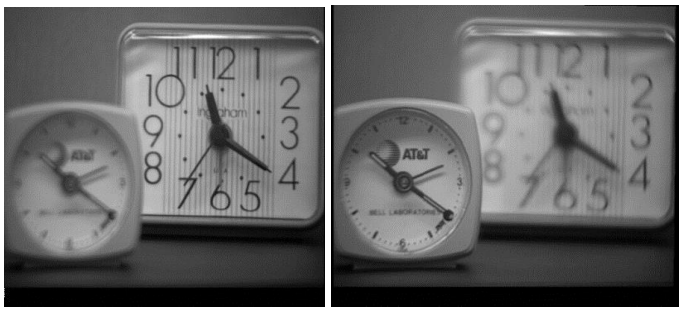

Clock A (a) Clock B

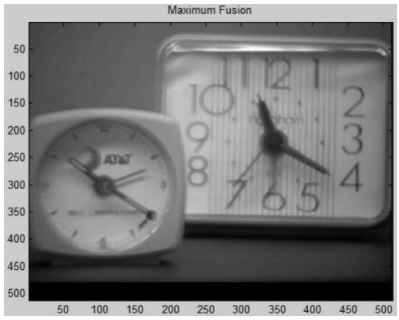

(b)

Figure 3.2 Fusion of two multi-focus images using maximum selection rule: (a) Two original images; (b) Processed image with maximum values.

3.1.2. Pixel-based fusion in the transform domain

As the working of the fusion rule has been made clear, now it can be applied using the wavelet transforms. In order to undestand image fustion using DWT, the pixel-based algorithm in the transform domain will first be implemented at a wavelet decomposition of level 1. Later, the decomposition level will reach to level 3.

- ***Transform domain fusion at level 1.***

DWT provides a flexible multi-resolution of an image and in this section decomposition at level 1 has been made on the test images named as clock A and clock B in Figures 3.3 and 3.4 respectively. These figures also show the extracted coefficients from level 1 decompositions. These coefficients include one approximate coefficient CA and three detail coefficients CH, CV and CD as shown in Figure 3.3 and CA1, CH1, CV1 and CD1 for image clock B in Figure 3.4 respectively.

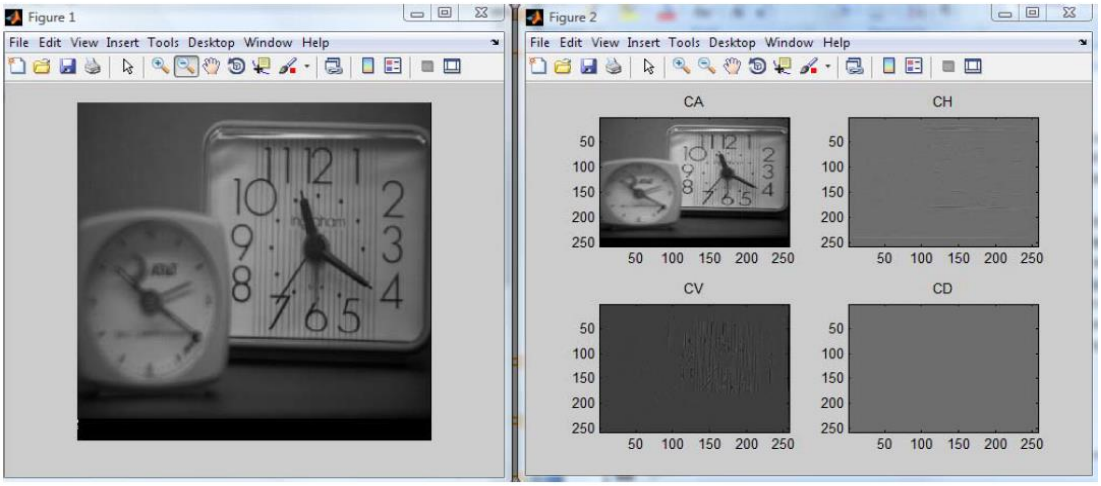

Figure 3.3 DWT of image clock A.

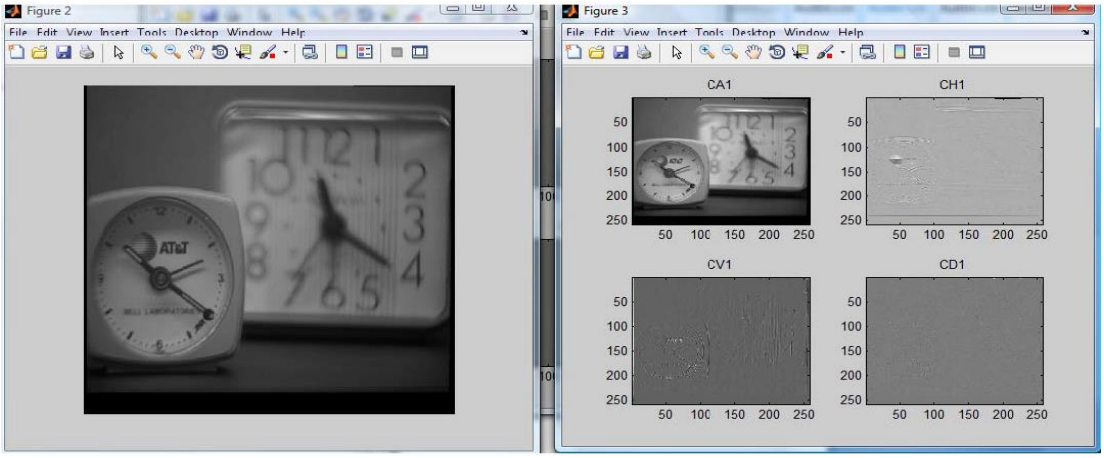

Figure 3.4 DWT of image clock B.

Once DWT has been performed, both images can be fused by comparing the coefficients of one image with those of the other image, using the maximum fusion rule defined above. Figure 3.5 shows a schematic implementing wavelet-based fusion on images.

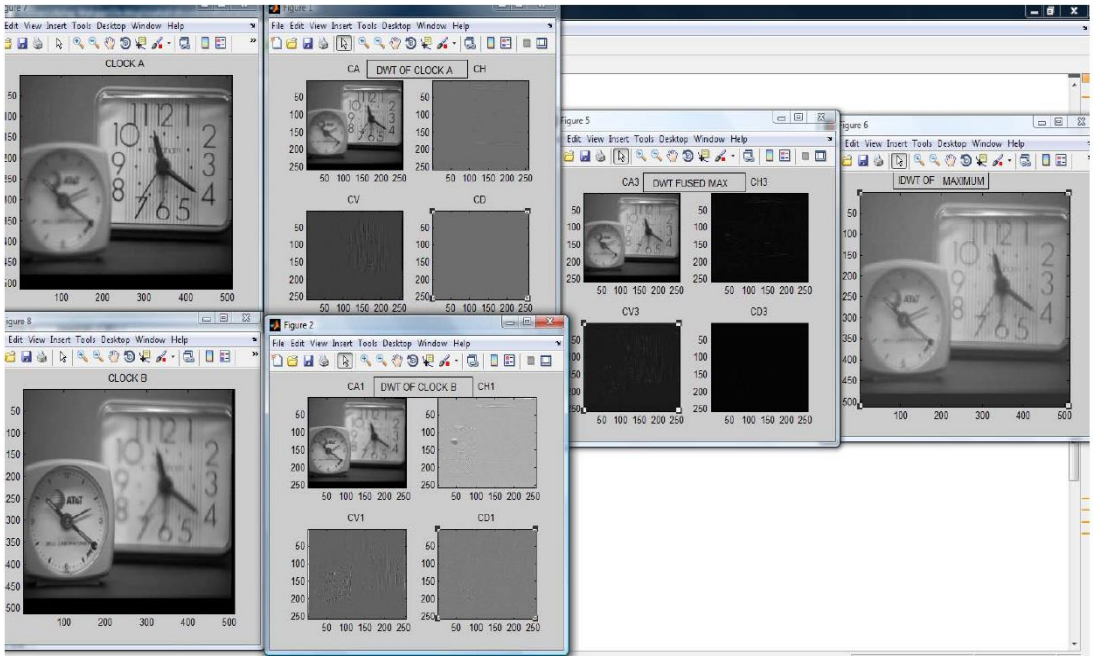

Figure 3.5 Level 1 DWT fusion using maximum rule.

Figure 3.5 shows two images, clock A and clock B, with their DWT at level one, i.e. generating four coefficients which include one approximate coefficient and three detail coefficients. Once we have taken the DWT for both the images, fusion has been achieved by comparing each wavelet coefficient of clock A with its corresponding wavelet coefficient of clock B with the help of a pixel based-algorithm using the maximum rule. Once the comparisons have been made of the coefficients, the next step is to reconstruct the image. This is done by performing the inverse discrete wavelet transform (IDWT) of the fused wavelet coefficients in order to get the final output corresponding to the selected fusion rule which will be more meaningful than the input images.

So far, the process of appling the pixel-based algorithm in the transform domain has been established, as has the process of decomposing the image into its wavelet coefficients at level one. Continuation of this concept includes an increase in the level of decomposition and to investigate its effect on the clarity of the final fused image.

- ***Transform domain fusion at level 2 and level 3***

As shown in Figure 3.6(a) image fusion at level one using DWT decomposes the input image into one approximate coefficient and three detail coefficients (horizontal, vertical and diagonal). In Figure 3.6 these components have been illustrated using subscripts i.e. A1

stands for approximate coefficient at level one and H1, V1, D1 stands for horizontal, vertical and diagonal components at the same level.

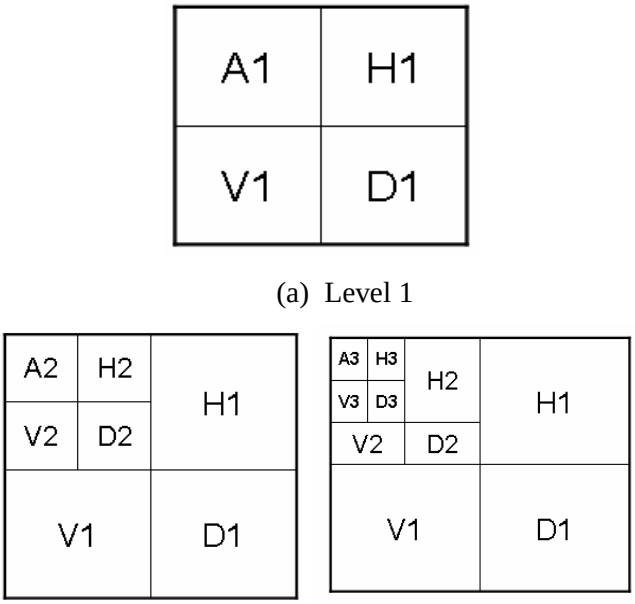

(a) Level 1

(b) Level 2 (c) Level 3

Figure 3.6 DWT decomposition illustration.

In order to apply the pixel-based algorithm at the wavelet decomposition of level 2, A1 component in Figure 3.6(a) can further be decomposed. This process yields four more coefficients namely A2, H2, V2, D2 at level two. As the level increases, the further decomposition is only performed on the low-low(LL) or approximate frequency band. Decomposition at level two gives one approximate coefficient and six detail coefficients for each input image. Once the decomposition is done the coefficients of the first input image with those of the other image can be compared using the fusion rule.

In the proposed method decomposition has been carried to three levels and most of the steps for the wavelet decomposition at level three are similar to the ones at the level 2 of decomposition. The only thing that changes is the number of detail coefficients. As in the second level decomposition there is one approximate coefficient and six detail coefficients, and at level three this number changes to one approximate coefficient and nine detail coefficients. As approximate coefficients are the result of low pass filtering, they have most of the energy associated with them and hence they are the deciding factor for the contrast within an image. Whereas the detail coefficients are the result of high-pass filtering, they are responsible for features or details such as edges, boundaries, etc. After comparing and generating the relevant coefficients, reconstruction can be completed in order to get the output fused image.

Once image fusion has been achieved using the maximum fusion rule, it can be observed that the resultant fused image is better than the two original images, but still possess quite a degree of blurriness associated with it. To overcome this drawback approximate coefficient has been scaled by multiplying it by a factor of 0.75 which has been selected empirically. By doing this, the overall energy within the fused image reduces. In other words, the image became less bright, but the features present within became more prominent and definite. A brief example can be seen in Figure 3.7, but a better perspective can be seen in Section 3.1.2. Upto this point the proposed method has been to capture the features. The next focus is on improving the contrast so that the end fused image will look sharper and crisper. To achieve it, one of the image enhancement techniques famously known as ***Gamma Correction*** has been used, which is given below in Equation 3.2. The main reason behind this selection is that it is a straight forward process and as a result it is fast in processing time [73].

$$S = P * R^{\gamma} \tag{3.2}$$

where S is the output pixel value, R is the input pixel value and P & γ are real numbers. Empirically $\gamma = 1.1$ has been chosen for the proposed method.

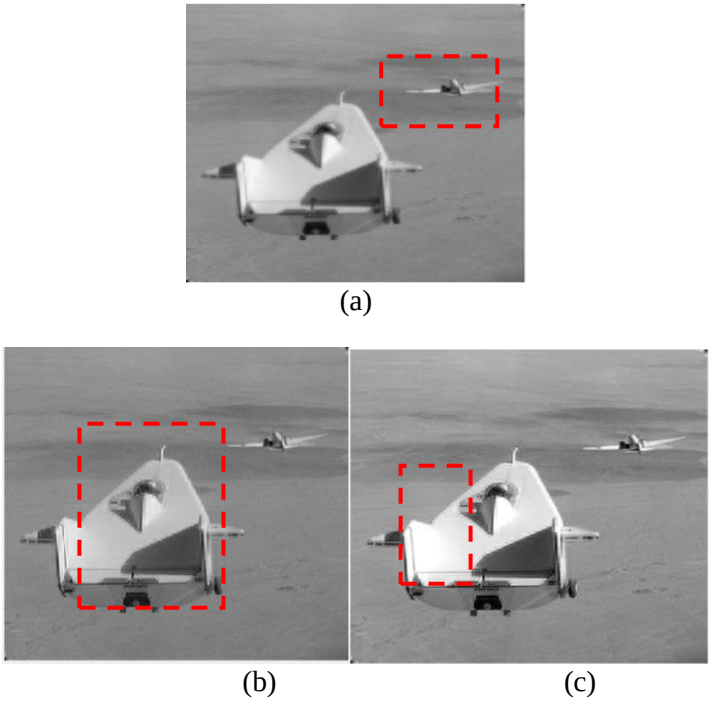

(a) (b) (c)

Figure 3.7 Effect of contrast enhancement technique in fused image (c) from two images (a) and (b). Rectangles show regions where the change in contrast can be observed.

- ***Flowchart for the proposed pixel-based method***

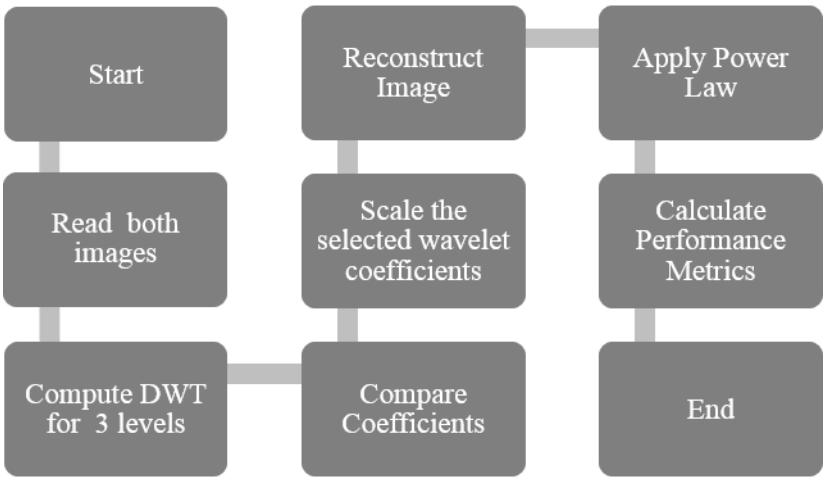

Figure 3.8 Flowchart for the proposed pixel-based method.

In the proposed method, we have used DWT for multilevel signal decomposition. In Figure 3.8, the method starts by reading two input images, followed by performing DWT on three levels that generates approximate and detail coefficients respectively. In the next step, comparison of CAA (an approximate coefficient of image A) with the corresponding CAB (an approximate coefficient of image B) is made and this generates the approximate CAF using the maximum fusion rule as shown in Figure 3.9. In a similar fashion, the rest of the six detail coefficients of images A and B can be compared and this generates six detail coefficients. After analysing and generating the appropriate coefficients, reconstruction to get the fused image can be done. Once the method gets to this point, the power law to enhance the contrast of the fused image can be used to get the final image.

$$For\ i = 1 : number\ of\ rows\ in\ CAA$$
$$For\ j = 1 : number\ of\ columns\ in\ CAA$$
$$Compare\ CAA(i, j)\ with\ CAB(i, j)$$
Using Maximum Rule
$$if\ \ CAA(i, j) \geq CAB(i, j)$$
$$CAF(i, j) = CAA(i, j)$$
$$Else\ CAF(i, j) = CAB(i, j)$$

Figure 3.9 Pseudo-code for fusion rule.

3.1.3. Results and discussion of the proposed pixel-based method

Figure 3.10 Test images from left to right: plane and Lena.

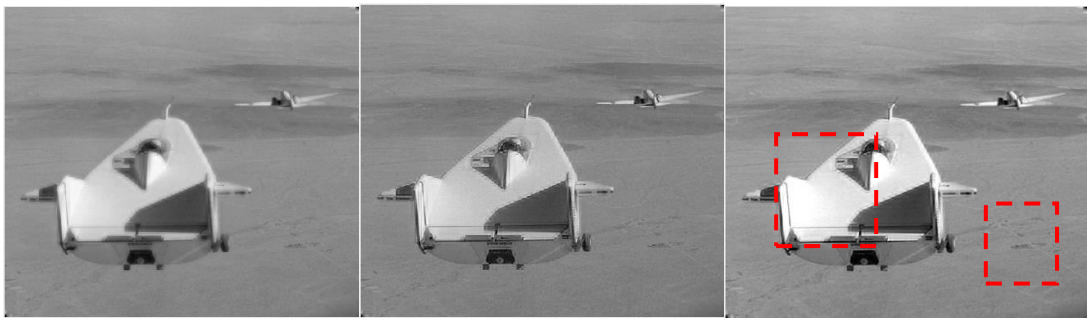

(a)

(b)

Figure 3.11 Comparison of reconstructed images from left to right: Method used in [70], pixel-based method using absolute maximum rule with contrast enhancement [14], **the proposed pixel-based method**.

Figure 3.10 shows two of the test images which have been used to test the proposed method. Test images in these figures are part of data set for image fusion, which have been included in Appendix A of the present thesis. Mentioned data set can be located using [78, 79] and consists of multifocal images, infrared (IR) images, aerial images and miscellaneous images. Yellow circles in Figure 3.10 show blurry or out of focus regions which have been removed by fusing the images together. Figure 3.11 compares the proposed method with two existing methods. The results in the left column are obtained from the pixel-based fusion using the maximum rule without contrast enhancement [70]. It can be observed that the reconstructed images seem to have a grey texture throughout. The reconstructed images also lack in quality of edges and features, due to greyish images appearing blurry and soft. The results in the

middle column were obtained from the method proposed in [14]. It can be observed that both reconstructed greyscale images in the middle column appear subtly less greyish in comparison to the images in the left column in Figure 3.11. Images in the middle column are better in contrast, which makes edges and features more evident. The blur associated with the reconstructed images has been reduced as well. The results in the right column in Figure 3.11 were obtained from the proposed method. It can be clearly seen that the overall contrast has been improved compared to the other two methods. An improvement in contrast leads to better feature and edge quality which are considered the details of an image. Improved features and edges have been marked using red rectangles in the proposed method column. In Figure 3.11(b), the red rectangle shows the eyes are more prominent in contrast, and the yellow oval shows the clarity in hair follicles. In Figure 3.11(a), the red rectangles also show visible improvements in contrast making them look sharp and crisp.

- ***Performance parameters***

The quality parameters taken into consideration are Root Mean Square Error (RMSE) [73], Peak, Signal to Noise Ratio (PSNR) and entropy [31]. If *I(i, j)* represents the grey level in the reference image (error-free image) at the *ith* row and *jth* column and *D(i, j)* represent the value in the output image, then an error *e(i, j)* is defined in Equation 3.3.

$$e(i,j) = I(i,j) - D(i,j) \tag{3.3}$$

The mean-square error and root-mean-square (RMSE) error are defined below in Equation 3.4.

$$MSE = \frac{1}{MN} \sum_{\substack{0 \le i < M \\ 0 \le j < N}} \left[I(i,j) - D(i,j) \right]^2$$
$$RMSE = \sqrt{MSE} \tag{3.4}$$

where *M* and *N* are the numbers of rows and columns of the image.

Once RMSE is calculated, PSNR can be calculated using the following expression given in Equation 3.5

$$PSNR = 10 \log_{10} \left(\frac{Max_i^{\,2}}{MSE} \right) \tag{3.5}$$

where $Max_i = 255$. PSNR should be as high as possible in the fused image. In Table 3.1 test images represents the input images which have been gained after corrupting the reference image with an error on purpose. The reason behind such a corruption is that it gives a clear indication of PSNR comparison between the reference image and input images. Also, the same comparison is valid when a fused image is compared to the reference image

and in this manner the difference in the PSNR between the input images and fused image can also be gathered. So if the PSNR value of the input images can be improved by a fusion method, then this can indicate the effectiveness of such a method. The entropy of an image is the measure of the information contained in the fused image. Higher values of entropy indicate that the fused image contains more information. The entropy is given by the Equation 3.6.

$$E = -\sum_{L=0}^{L-1} P_l \log_2 P_l \tag{3.6}$$

where L represents the number of grey levels, P_l is the ratio between the number of pixels with grey level l and the total number of pixels. From Table 3.1 it can be clearly seen that the proposed method is better in terms of both PSNR and RMSE than the other two methods and input images themselves. In addition, the fused image gained as a result of the proposed method contains more information when compared to the other fusion methods. It is indicated by the higher entropy value in Table 3.1. Reference image for test images in Table 3.1 can be found in Appendix A in Figure A1.

Table 3.1 Comparison between existing methods with the proposed pixel-based method.

Test images (Individual PSNR values)	**Method**	**RMSE**	**PSNR(dB)**	**Entropy**
Plane A PSNR (24.564) Plane B PSNR (26.9845)	Method in [70]	3.3279	37.0561	7.4152
	Method in [14]	2.7421	40.6107	7.5623
	Proposed Method	**2.5161**	**41.7999**	**7.7028**
Lena A PSNR (23.564) Lena B PSNR (24.9845)	Method in [70]	3.1989	37.8980	7.3906
	Method in [14]	3.0863	38.6053	7.4456
	Proposed Method	**2.7410**	**40.6179**	**7.6423**

Figure 3.12 shows more test images taken from the data set of 100 images given in Appendix A. These test images have been fused using the proposed pixel-based method and the other existing methods mentioned in Table 3.1. Visual and objective comparison among these methods has been illustrated through Figure 3.13 and Table 3.2 respectively.

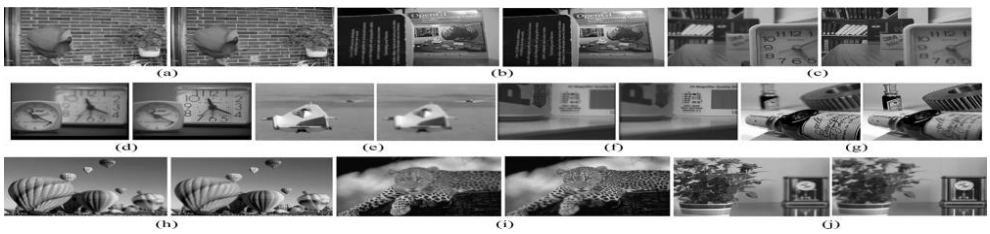

Figure 3.12 Test images from dataset in Appendix A: (a) flower, (b) book, (c) bookshelf, (d) clock, (e) plane, (f) Pepsi, (g) bottle, (h) parachute, (i) leopard, (j) flower wage.

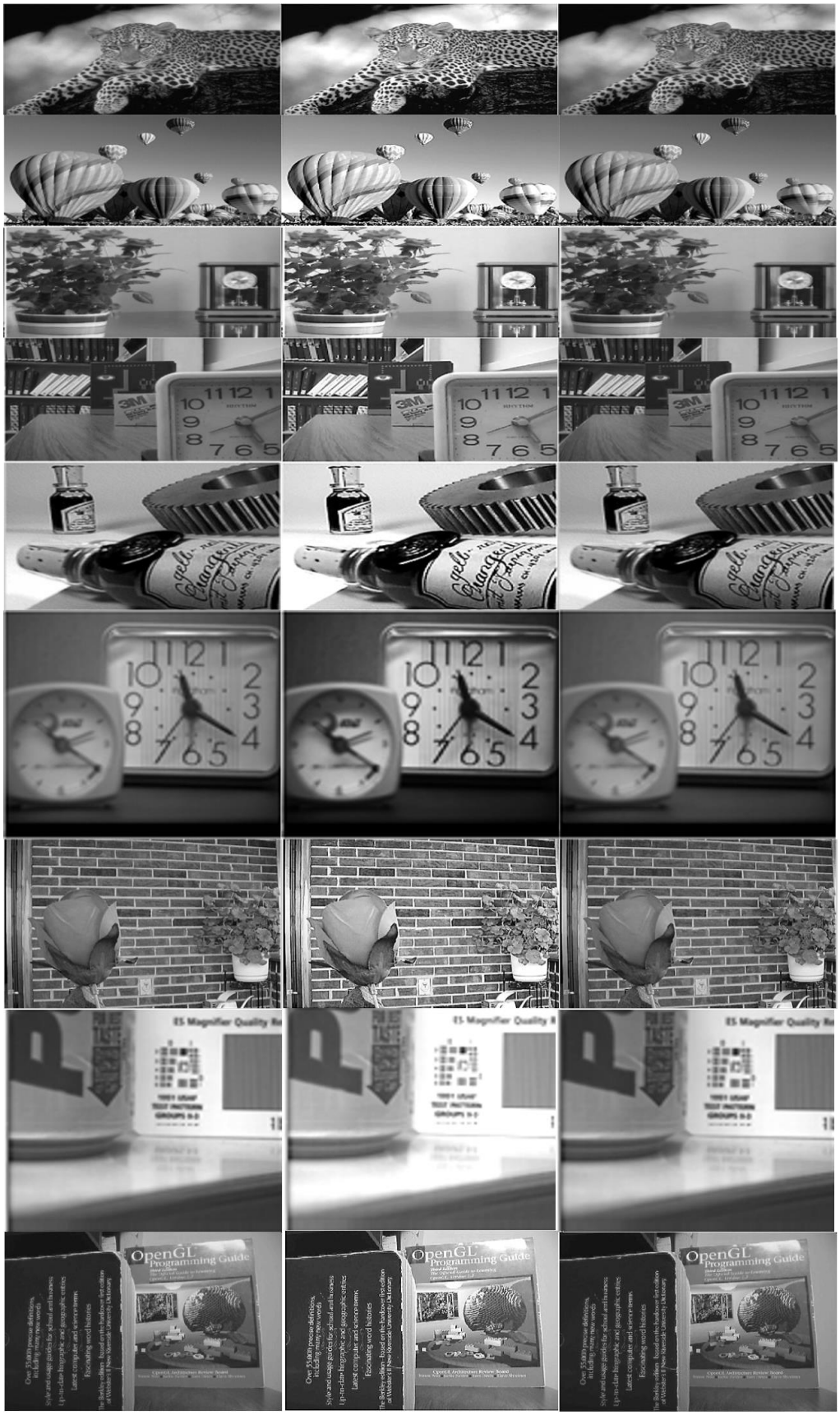

Figure 3.13 Comparison of data set from left column to right column: Method used in [70], **the proposed pixel-based method**, pixel-based method using absolute maximum rule with contrast enhancement [14].

Table 3.2 Dataset comparison for the proposed pixel-based method.

Test images (Individual PSNR values)	PSNR(dB)		
	Method in [70]	Method in [14]	**Proposed method**
Flower (24.2364, 24.2364)	36.5836	36.929	**41.1423**
Book (22.8624, 22.8624)	36.8507	37.0724	**39.9267**
Book shelf (27.135, 27.135)	38.509	37.642	**41.641**
Clock (18.8642, 18.8642)	36.5496	**37.1675**	33.6497
Plane (23.9524, 23.9524)	37.0561	40.6107	**41.7999**
Pepsi (28.5988, 28.5988)	37.5043	38.2989	**41.4455**
Bottle (29.5264, 29.5264)	31.9329	38.7198	**41.9115**
Parachute (28.2332, 28.2332)	37.7547	39.5679	**41.1646**
Leopard (26.5527, 26.5527)	37.5468	38.5485	**40.9335**
Flower wage (23.7824, 23.7824)	41.175	39.6219	**41.0499**
Average	37.37957	38.33962	**39.95813**
	Entropy		
Test images	Method in [70]	Method in [14]	**Proposed method**
Flower	6.3519	6.7124	**7.6795**
Book	6.4877	6.6681	**8.0645**
Book shelf	6.3676	6.3524	**7.2066**
Clock	6.3889	7.2506	**7.3248**
Plane	7.4152	7.5623	**7.7028**
Pepsi	6.487	7.1471	**7.3046**
Bottle	6.6033	6.8676	**7.6795**
Parachute	6.7292	6.9889	**8.0645**
Leopard	6.5875	6.7255	**7.2066**
Flower wage	6.8968	7.1066	**7.3248**
Average	6.63151	6.93815	**7.55582**

Figure 3.13 and Table 3.2 makes it evident that the proposed method works better when compared to existing pixel based fusion methods. Another table is available in Appendix A as Table A1, that shows the results of the proposed method and existing methods performed over 100 images. Table A1 illustrates that on average the proposed pixel-based method has improved entropy value by 0.9355 and 0.5717 when compared to methods in [70] and [14] respectively. Images fused using the proposed method exhibits better contrast characteristics as it can be seen in Figure 3.13 in the middle column. Better contrast makes an image to look sharp and clear, hence the fused image is pleasing from a visual perspective. An improvement in entropy also make the features present in an image easier to observe, as entropy is a direct measure of the information present in an image. From Table 3.2 it can be noticed that entropy is higher in the proposed method and as a result, the observer can effectively locate image details like boundaries and edges present in the fused image.

Out of the 100 processed images the proposed pixel-based method has better quality in 94 cases. Whereas in others one of the existing methods has outperformed the proposed method. The cases where the proposed method has been outperformed by other methods have been

highlighted and can be observed in Table A1 in Appendix A. The versatility of the proposed method can be noticed from the various types of images it is capable of fusing. Illustrations can be seen from the experiments shown below in figures ranging from Figure 3.14 to Figure 3.16.

Test Image 1a

Test Image 1b

Method in [70]

Method in [14]

The proposed pixel-based method

Figure 3.14 Illustrates multifocal image fusion results using, method in [70], pixel-based method used in [14] and the proposed method.

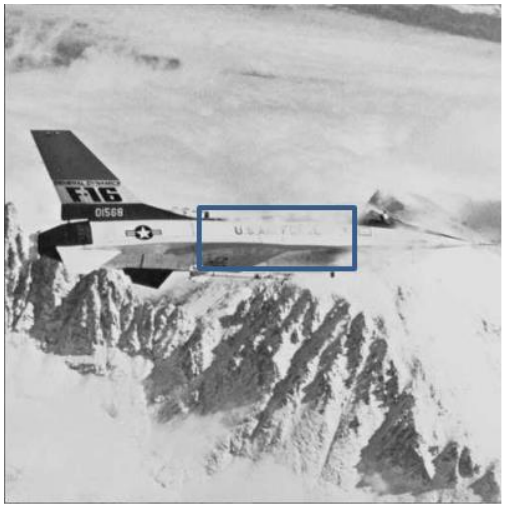

Test Image 2a

Test Image 2b

Method in [70]

Method in [14]

The proposed pixel-based method

Figure 3.15 Illustrates aerial image fusion results using, method in [70], pixel-based method used in [14] and the proposed method. Blue box in test images shows missing information.

Test Image 3a

Test Image 3b

Method in [70]

Method in [14]

The proposed pixel-based method

Figure 3.16 Illustrates IR image fusion results using, method in [70], pixel-based method used in [14] and the proposed method.

3.2. The proposed region-based fusion and implementation

The proposed pixel-based image fusion is simple and gives good contrast images. However, in some situations where the salient features of an image are more than one pixel or where edge details are important, the pixel-based fusion technique may not be an appropriate measure. In such situations instead of concentrating on the individual pixels one needs to concentrate on the particular region or feature of an image. The fusion technique that fuses the particular region of the two images is known as region-based image fusion and it falls under the category of feature level fusion.

In this section image fusion using the region-based algorithm is performed. In the majority of the applications for image fusion schemes, the main focus is in the regions within an image, and not in the actual pixels. Therefore, it seems reasonable to incorporate feature information into the fusion process [74]. There are several perceived advantages of this method and some are mentioned below.

1. **Efficiency in processing time:** The proposed work in Section 3.1.2 is based on pixel-based processing, so each and every pixel present in the source images need to be processed before the right selection is made. Hence this process is very lengthy and time-consuming. In region-based fusion a group of pixels or a mask is dealt with one at a time, which makes this method time efficient.
2. **Reduced sensitivity to noise:** Processing semantic regions rather than individual pixels or arbitrary regions can help in overcoming some of the problems with pixel-based fusion methods such as blurring effects and sensitivity to noise [74].

Zhang et al. [39] and Yingjie and Liling [72] have concentrated on region-based fusion rather than the conventional pixel-based algorithms. Zhang et al. proposed a region-based image fusion method for medical images that involves the calculation of energies of each window of a particular size in the image. The results obtained from experiments conducted with this fusion rule are compared with the pixel-based technique and conclusions are drawn by [39]. By interpreting the results and the error tables it is clear that this method performs better than the pixel-based method.

Some researchers have given considerable importance to the fused images giving a good visual perception rather than good performance values. Burt and Kolezynski [83] have proposed a fusion rule involving calculation of local energies of a neighbourhood around the salient features. A comparison of the different pixel-based and region-based approaches in fusion is given by Sasikala and Kumaravel [74]. Other popular image fusion techniques using region-based rules are edge fusion [61] and local gradients [74].

The word region stands for a group of pixels combined together. There are many available region-based image fusion algorithms, but the present thesis has concentrated mostly on the region-based image fusion using energy estimation. The method reads two registered images of the same object, for example one of which is out of focus on the right-hand side and the other is out of focus on the left-hand side. Next a mask can be created which is generally smaller than the actual size of the image. For example, if the input image is of the size 512 x 512 pixels, then a mask of 3 x 3 or 4 x 4 pixels can be created respectively. Once the desired mask is created, it is convolved with both input images simultaneously step by step. At every step it should compute the energy of the region that comes under the mask (i.e. squaring and adding all the pixel values that come under the mask). Once the energy is computed for a particular region both the images (for example image *A* and *B* in Figure 3.17), a comparison is made of the energies between both regions of image *A* and image *B* using the maximum rule. While comparing the energies it is assumed that the energy of image *A* is found to be higher than the energy of the same region of image *B*. In this case, the region that comes under the mask of image *A* for that particular energy is taken and is put into the region that needs to be generated within image *C*. This process continues until the mask has traversed the whole of the image size and image *C* is filled up completely.

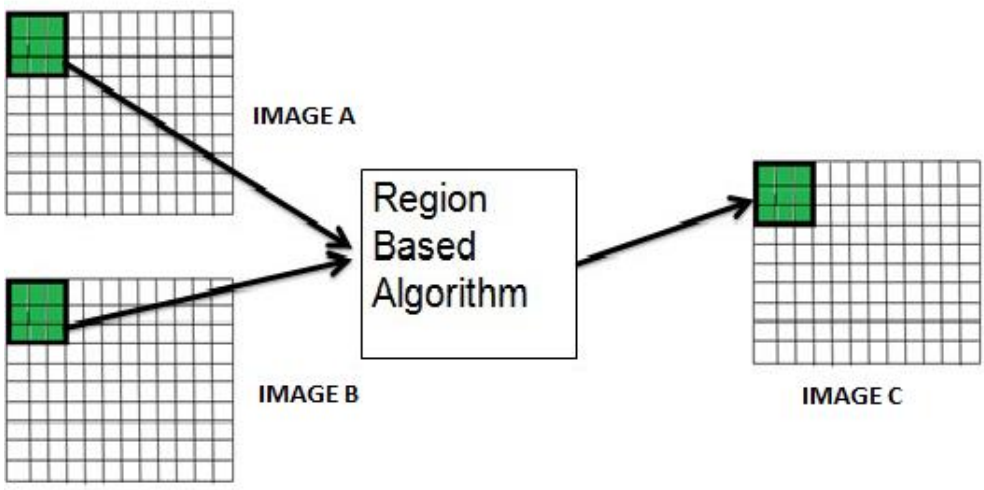

Figure 3.17 Schematic of region-based fusion.

In the proposed method, an absolute maximum selection rule given in Equation 3.7 has been used in the transform domain. Let $A(i, j)$ and $B(i, j)$ be the two images to be fused and their approximate wavelet coefficients corresponding to low-frequency sub-bands are $CAA(i, j)$ and $CAB(i, j)$ respectively. Therefore, a 3 x 3 mask for these coefficients is defined and the energy associated with this mask can be calculated using the pseudo-code given in Figure 3.18. M and N in Figure 3.18 stand for the total number of rows and columns of the image,

the size of an image is $M \times N$, i and j are the row and column location of the pixel, with *n* representing the centre point of the mask. Here α stands for the value of wavelet coefficients corresponding to separate input images.

The pseudo-code that can represent the region-based image fusion is given below in Figure 3.18.

$$For\ i = 1\ :\ M$$
$$For\ j = 1\ :\ N$$
$$ECAA(i, j) = \sum_{n=-1}^{1} \alpha_{AA}(i+n, j+n)^2$$
$$ECAB(i, j) = \sum_{n=-1}^{1} \alpha_{AB}(i+n, j+n)^2$$
$$Compare\ ECAA(i, j)\ with\ ECAB(i, j)$$
Using Maximum Rule
$$if\ \ ECAA(i, j) \geq ECAB(i, j)$$
$$ECAF(i, j) = ECAA(i, j)$$
$$Else\ ECAF(i, j) = ECAB(i, j)$$

Figure 3.18 Pseudo-code for region-based fusion.

3.2.1. Fusion rule used

Once the energy is calculated both regions can be compared by the absolute maximum rule in the following manner:

$$ECAF(i, j) = \begin{cases} ECAA(i, j) \text{ if } |ECAA| \geq |ECAB| \\ ECAB(i, j) \text{ if } |ECAB| \geq |ECAA| \end{cases} \quad (3.7)$$

In Equation 3.7, $ECAF(i, j)$ is the energy value of the region that will be present in the final fused image. The same steps need to be repeated until the mask has fully mapped both input images and the final image C is filled up completely. Similarly, the coefficients corresponding to the high-frequency sub-bands or detail coefficients are processed by the defined fusion rule and are made present in the final image.

To understand how region-based energy estimation works the algorithm has been applied to the two 6x6 matrices. Firstly, two 6x6 matrices have been built by filling them up with some random numbers. After creating the matrices, the energy of the particular region of both the matrices has been calculated with the help of a three by three mask. Once the energy is calculated for a particular region for both images a comparison among energies can be made. Using the maximum rule, the mask with higher energy can be selected and the particular

values of the pixels inside the higher energy mask can be taken and placed in the generated matrix. Some of the hand done calculations for the region-based energy estimation algorithm have been included below in Figure 3.19.

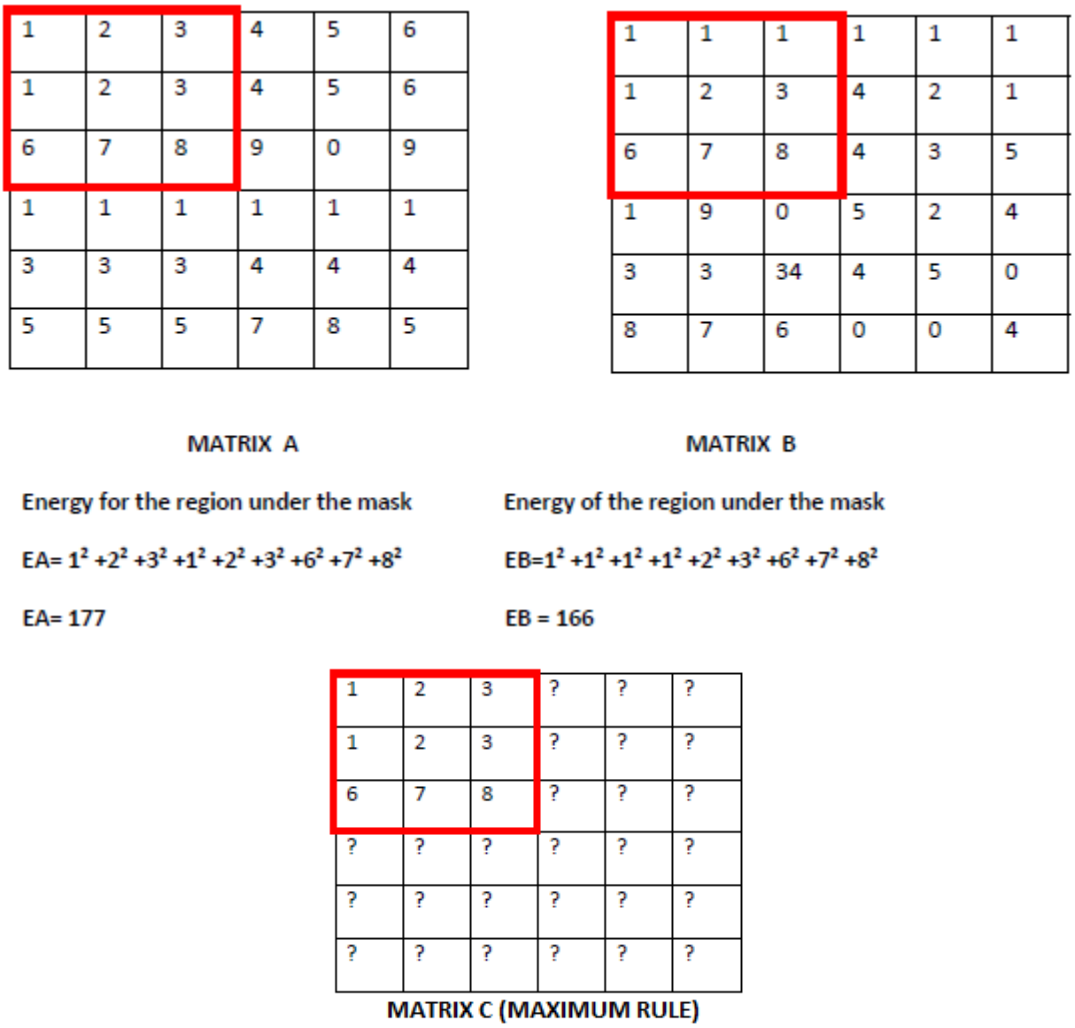

Figure 3.19 Calculations of energy estimation.

As the proposed method is using the maximum rule, it can be noticed from the above calculations that the EA is greater than the EB and therefore the region under the mask of matrix A can be considered and put into the matrix C. An illustration of how the region-based (energy estimation-based) algorithm works can be gained from Section 3.2.2, where it has been extended to and performed on actual images.

Implementation of the region-based image fusion using DWT in the MATLAB, starts by reading the two registered images. The next step is the decomposition of both input images into its wavelet coefficients, which depends upon the chosen level of decomposition. After decomposing the images into the approximate coefficients and the detail coefficients the pseudo-code given in Figure 3.18 can be used to fuse the images and to get an output image C.

- ***Flowchart for the proposed region-based method***

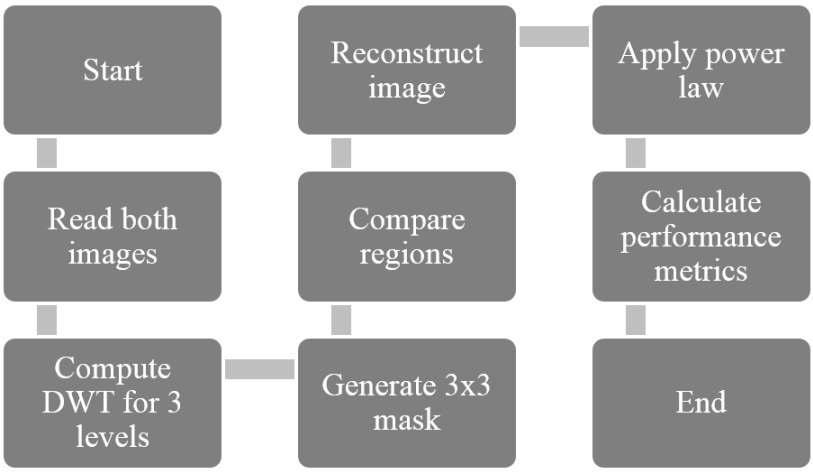

Figure 3.20 Flowchart for the proposed region-based method

As indicated in Figure 3.20, the proposed method starts by reading two test images. This is followed by performing DWT on three levels that yield approximate and detail coefficients respectively. The next step is to generate masks and calculate energies of the defined regions. The following step is the comparisons between the regions comprising approximate coefficients, i.e. $ECAA$ and $ECAB$. This results in the generation of the region corresponding to $ECAF$ using the maximum fusion rule in the final image. In a similar manner comparisons between the regions comprising detail coefficients of the images *A* and *B* can be made. After analysing and generating the appropriate regions, reconstruction can begin to get the output fused image using IDWT. Finally, the power law can be incorporated to achieve contrast enhancement.

3.2.2. Results and discussion of the proposed region-based method

Test images which have been used to demonstrate the research work are shown in Figure 3.21. Yellow circles in Figure 3.21 represent out of focus or blurry regions. Figure 3.22 compares the proposed method with the existing method. The left column represents the results from related work in [45] and in Section 3.2.1. It can be observed that both of the reconstructed greyscale images in the left column appear less greyish in comparison to the images in the far right column and the blur associated with the reconstructed images has been reduced as well. In Figure 3.22 the far-right column shows the results obtained from the method proposed in [14]. It can be observed that the reconstructed images seem to have a grey texture throughout. Also, reconstructed images lack in edges and features as greyish images look blurry and soft. The middle column in Figure 3.22 shows the results obtained from the proposed method. It can be clearly seen that the overall contrast has been improved compared to the other two methods. An improvement in contrast leads to better feature and

edge quality which are considered as details of an image. Improved features and edges have been marked using red rectangles in the proposed method column. In Figure 3.22 the red rectangle shows that linings are more prominent in contrast, and the yellow oval shows the clarity in hair follicles. In Figure 3.22(a) the red rectangles also project the visible improvements in contrast, making markings on the surface look crisper and clearer.

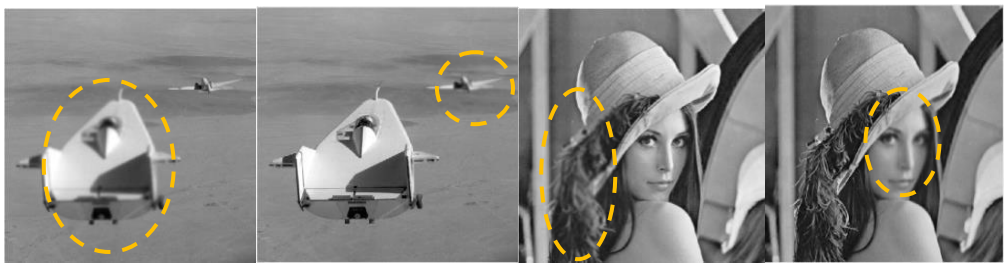

Figure 3.21 Test images from left to right: plane and Lena.

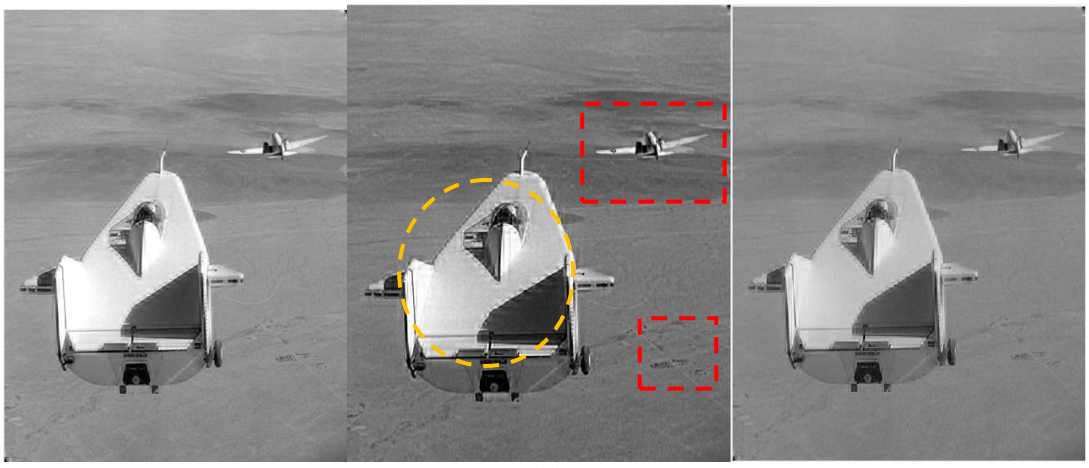

(a)

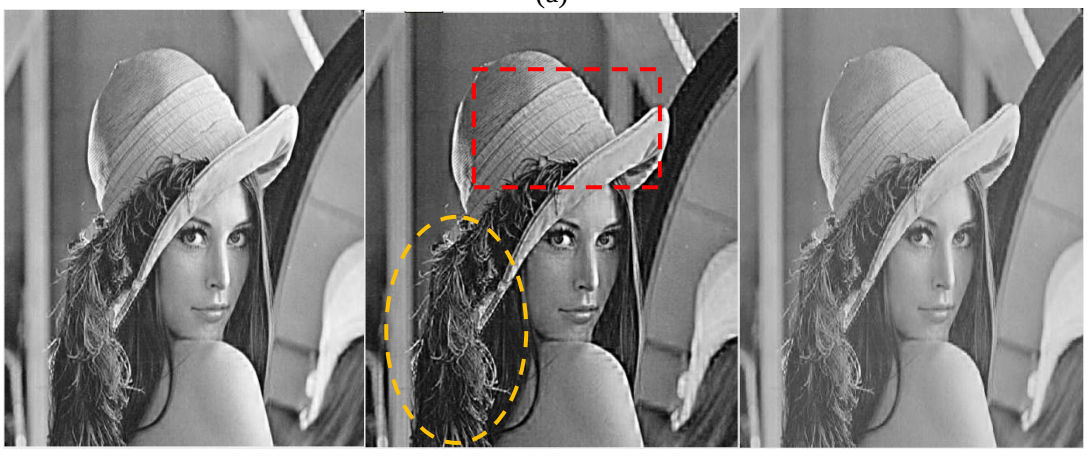

(b)

Figure 3.22 Comparison of reconstructed images from the left to the right: method used in [45], **the proposed region-based method**, method used in [14].

Table 3.3 Comparison of existing methods and the proposed region-based method.

Test images	Method	Time (Seconds)	PSNR(dB)	Entropy
Plane A PSNR (24.564)	Method in [45]	7.72	41.7999	7.7028
	Proposed Method	**5.39**	**43.2156**	**7.7235**
Plane B PSNR (26.9845)	Method in [14]	6.43	40.6107	7.5623
Lena A PSNR (23.564)	Method in [45]	7.54	40.6179	7.6423
	Proposed Method	**5.32**	**41.8953**	**7.6649**
Lena B PSNR (24.9845)	Method in [14]	6.24	38.6053	7.4456

Table 3.4 Dataset comparison for the proposed region-based fusion.

	Time(seconds)		
Test images	Method in [45]	Method in [14]	**Proposed method**
Flower	6.424	5.757	**5.564**
Book	8.553	6.616	**5.956**
Bookshelf	5.153	5.641	**4.569**
Clock	5.569	5.687	**5.167**
Plane	7.72	6.43	**5.39**
Pepsi	5.458	5.002	**5.132**
Bottle	7.201	5.808	**4.920**
Parachute	4.925	4.849	**3.821**
Leopard	6.965	5.515	**3.354**
Flower wage	5.11	5.265	**4.368**
Average	6.22	5.657	**4.857**
	Entropy		
Test images	Method in [45]	Method in [14]	**Proposed method**
Flower	7.6795	6.7124	**7.8440**
Book	8.0645	6.6681	**7.4407**
Book shelf	7.2066	6.3524	**7.7649**
Clock	7.3248	7.2506	**7.7351**
Plane	7.7028	7.5623	**7.7168**
Pepsi	7.3046	7.1471	**8.0460**
Bottle	7.6795	6.8676	**7.8277**
Parachute	8.0645	6.9889	**7.8829**
Leopard	7.2066	6.7255	**7.0673**
Flower wage	7.3248	7.1066	**7.6446**
Average	7.55582	6.93815	**7.6970**

In Tables 3.3 and 3.4, it can be observed that the entropy is higher in the proposed method in comparison to the other two existing methods. As the entropy is higher in the proposed method, it means that more information is contained in the fused image. On observing the computational time taken, it can be noticed that the proposed method is also more time efficient.

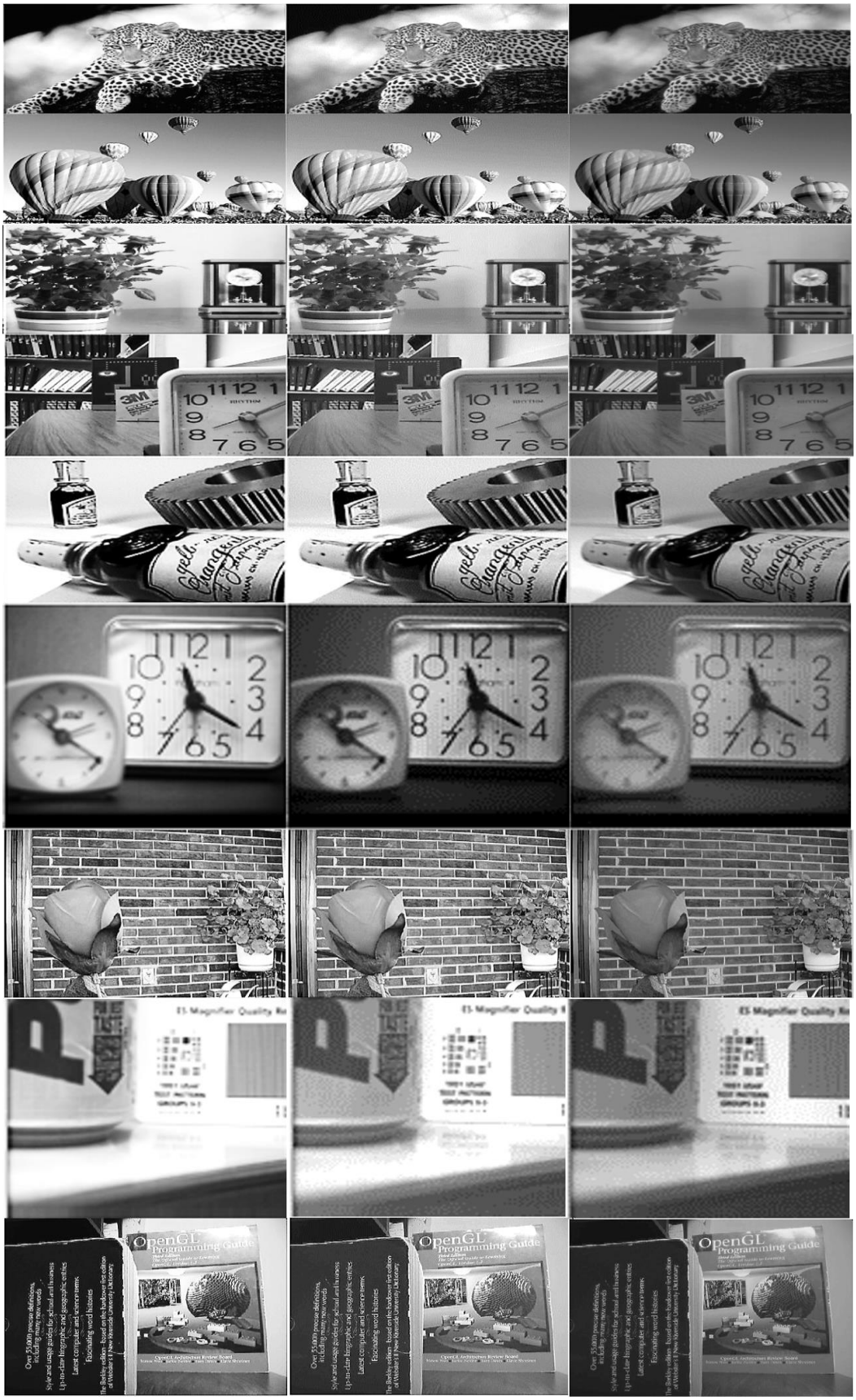

Figure 3.23 Comparison of data set from left column to right column**: the proposed region-based method**, method used in [45], the method used in [14].

Alike in Section 3.1.3 the proposed region-based method is performed on same data set of 100 images given in Figure A1 and results have been recorded in Table A1. Results in Table A1 projects that the proposed region-based method has improved the entropy of test images by a factor of 0.5324 compared to the proposed pixel-based method, 1.4678 compared to [70] and by 1.104 when compared to one in [14] respectively. It can also be observed that the proposed region-based method consumes 1.53 seconds less time when compared to the method in [45] and 3.01 seconds less in comparison to the method in [14]. The proposed region-based method has successfully worked better in 97 out of the 100 processed images from the image fusion data set. Cases in which the existing methods have done better from the perspective of entropy value or processing time than the proposed method have been highlighted in Table A1.

Comparisons between the proposed pixel-based method from Section 3.1 and the proposed region-based method has been shown in Figures 3.23 and Figure 3.24. It can be observed from the comparison that the proposed region-based method further improves the quality of the contrast in the fused image. This has been demonstrated with the help of the red boxes in Figure 3.24. The proposed pixel-based method is better in preserving the details or information present in an image. Orange colour boxes in Figure 3.24 have been used to focus on the areas where this phenomenon can be easily observed.

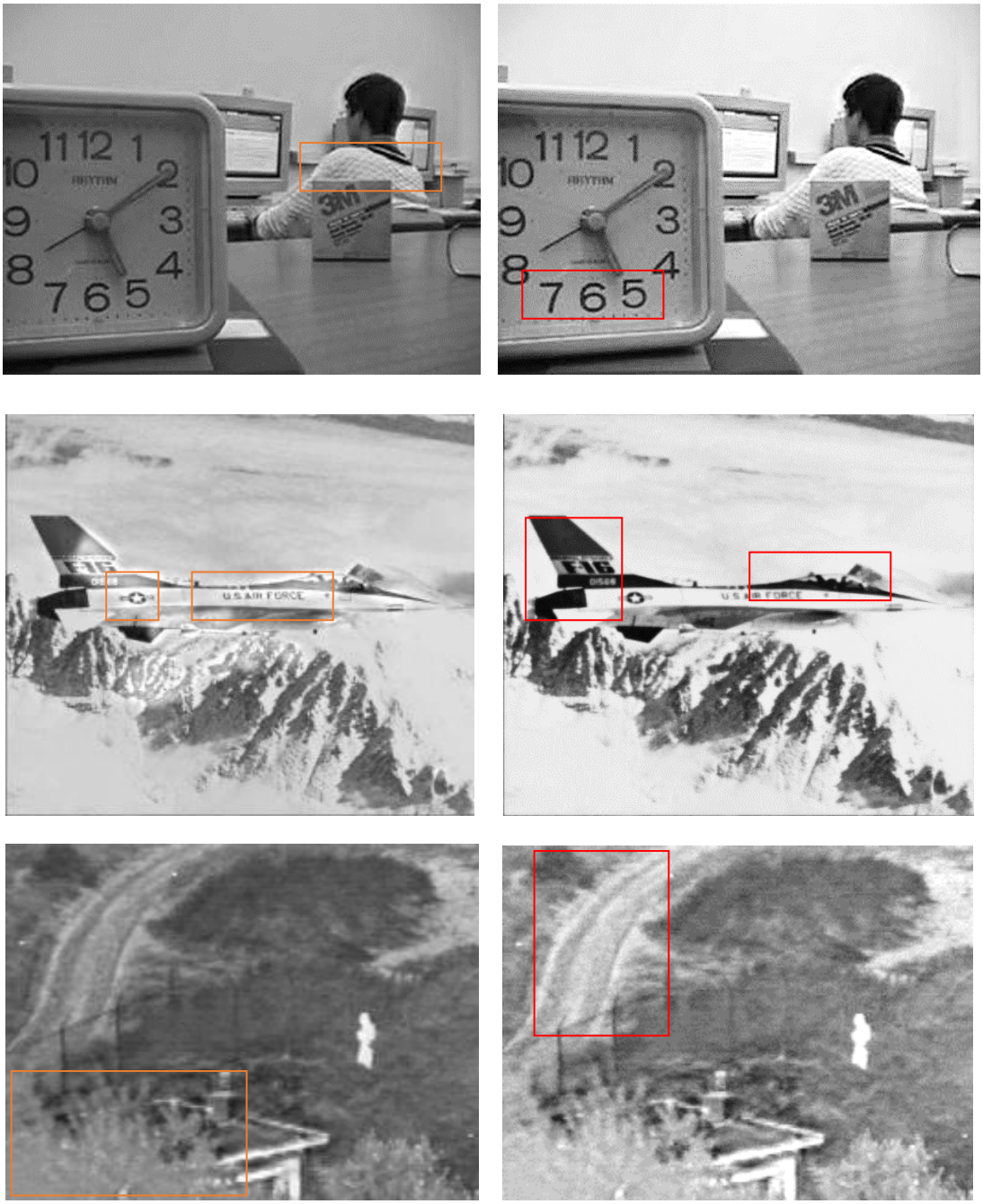

Figure 3.24 Comparison of the two proposed methods. Results of the proposed pixel-based method are represented by left column and results of the **proposed region-based method** can be seen in right column.

3.3. Summary

This chapter has focused on the proposed research of image fusion, which is one of the objectives of the thesis. The chapter starts with one of the proposed methods that use pixel level fusion using DWT. As the chapter progresses it explains the selected fusion rule and implementation of the pixel level proposed method. Moving forward from the implementation chapter progresses to the results and discussion section of the first method. In this section, visual and mathematical assessments were completed and the results show an

improvement in the contrast in the final fused image. Results also have shown an improvement in entropy value by 0.9355 when compared to first existing method and 0.5717 when compared to the second existing method. The second half of the chapter focused on the other proposed method which utilised feature or region level fusion based on DWT. The second half of the chapter flowed from the first half and the results revealed an improvement in the processing time in comparison to the first proposed method and other existing methods. The chapter concluded with an objective and subjective analysis of the proposed region-based method. The proposed region-based method has shown an improvement in entropy of 1.468 and 1.104 compared to existing methods respectively. Consecutively the proposed region-based method has also improved the processing time by a factor of 1.53 seconds when compared to the first existing method and 3.01 seconds compared to the second existing method.

Chapter 4- Image Dithering

The secret of change is to focus all of your energy,
Not on fighting the OLD,
But on Building the NEW.
~Socrates

4.1. The proposed dithering method and implementation

Error diffusion-based dithering is the most widely used and explored of all the present methods. Error diffusion, despite its great success, has been lacking in image enhancement aspects because of the softening effects caused by this method. To compensate for the softening effects, wavelet-based dithering [9] was introduced. Although wavelet-based dithering worked well in removing the softening effects, as the method is based on DWT, it lacked in aspects such as poor directionality and shift invariance which are responsible for making resultant images look sharp and crisp.

To compensate for the drawbacks of error diffusion and wavelet-based dithering, a new method called **complex wavelet-based dithering** has been proposed in this research. In comparison to the existing methods, the proposed method has been able to emphasise the details and improve the contrast in the dithered image.

4.1.1. Complex wavelet-based dithering

The proposed method uses special wavelet transform with shift invariance property and better directionality, called the Dual Tree Complex Wavelet Transform (DTCWT) [38]. Figure 4.1 shows two fully decimated trees, i.e. *Tree-a* and *Tree-b*, have been used in which *Tree-a* gives the real part and *Tree-b* the imaginary part of the complex wavelet coefficients at each level [47]. Complex wavelets are used to analyse and represent both real-valued signals (resulting in symmetries in the coefficients) and complex-valued signals. In either case, the CWT enables new multilevel signal processing algorithms that exploit the complex magnitude and phase. In particular, a large magnitude indicates the presence of a singularity while the phase indicates its position within the support of the wavelet [47]. Imaginary coefficients of DTCWT correspond to the phase information of signals and thus suggest most structural information of the image. An extension of 2D-DTCWT is achieved by separable filtering along columns and then rows of an image.

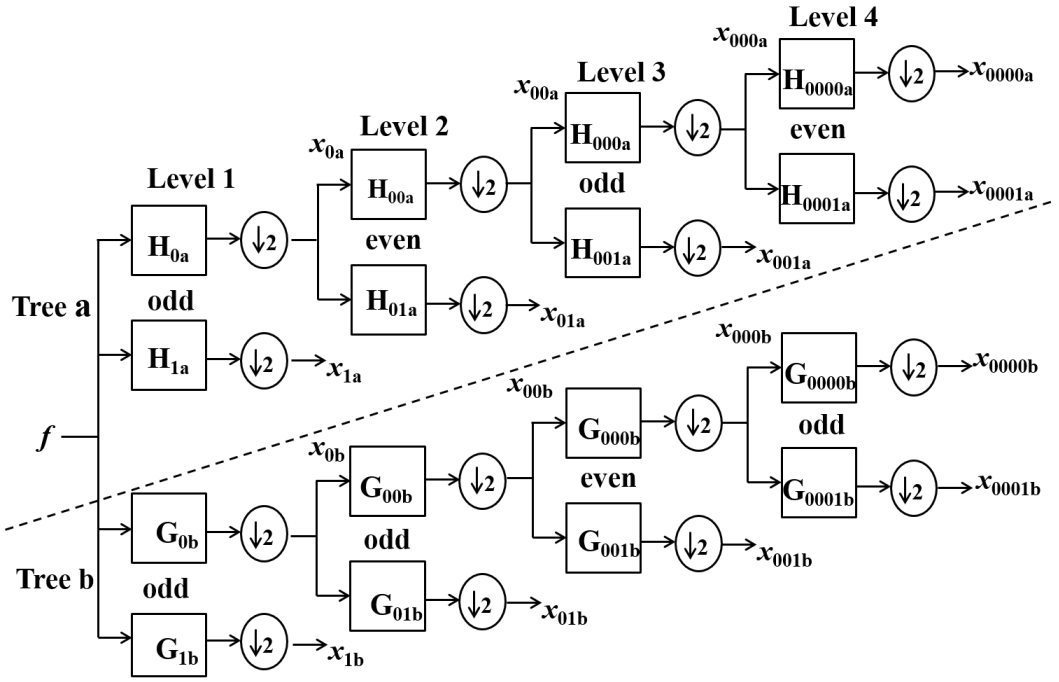

Figure 4.1 Analysis tree using odd-even filters.

In Figure 4.1 the filters are themselves real, and no complex arithmetic is required for the implementation of the DTCWT and the filter bank structure produces real-valued coefficients. However, because the outputs from the two trees are interpreted as the real and imaginary parts of complex coefficients, the transform becomes complex. The CWT decomposes an image using dilation and translations of a complex scaling function and six complex wavelet functions. The real and imaginary parts of DTCWT are computed using a separate filter bank structure shown in Figure 4.1 with wavelet filters H_0 & H_1 for the real part and G_0 & G_1 for the imaginary part. This type of one-dimensional filtering yields six real-oriented wavelets which have been used to find the real and imaginary parts of the complex wavelet.

These six wavelet sub-bands are strongly oriented in six different directions represented as θ and are shown as below

$$\theta = \left\{+15^0, +45^0, +75^0, -15^0, -45^0, -75^0\right\},$$

whereas in DWT there are only three wavelet sub-bands, which are oriented at

$$\theta = \left\{0^0, 30^0, 45^0\right\}$$

and as a result DTCWT captures more features or details present in an image [47]. Similarly, a two-dimensional signal or an image can be decomposed into twelve band pass-oriented sub-bands using 2D-DTCWT for the first level of decomposition. The magnitude of

corresponding real and imaginary coefficients of each corresponding sub-band is then obtained. The 2-D-DTDWT structure has an extension of conjugate filtering in 2-D case. The filterbank structure of 2-D dual-tree is shown in Figure 4.2. The 2-D structure needs four trees for analysis as well as for synthesis. The pairs of conjugate filters are applied to two dimensions (*x* and *y*), which are expressed in Equation 4.1.

$$(H_x + jG_x)(H_y + jG_y) = (H_xH_y - G_xG_y) + j(H_xG_y + G_xH_y) \tag{4.1}$$

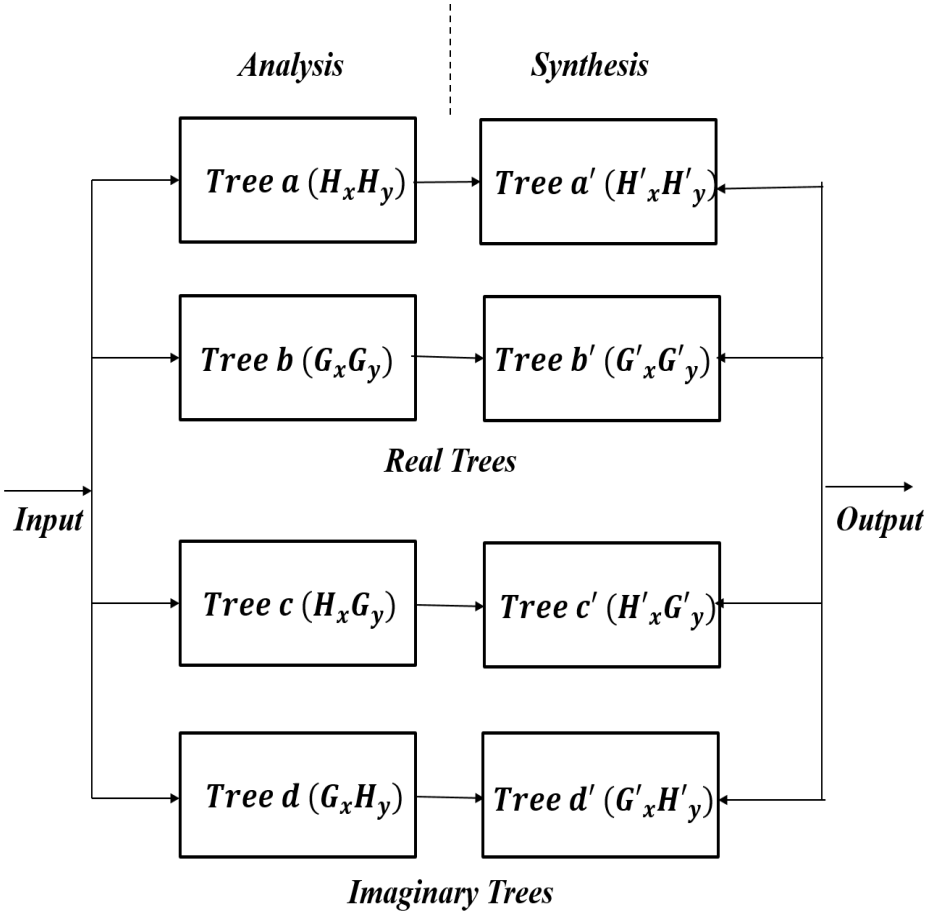

Figure 4.2 Filterbank structure for 2D-DTCWT.

The filterbank structure of *tree-a* is similar to standard 2D-DWT above in Figure 2.4. All other *trees-(b, c, d)* have similar structures with the appropriate combinations of filters for row- and column- filtering. The overall 2-D dual-tree structure is 4-times redundant (expensive) than the standard 2-D DWT. The *tree-a* and *tree-b* form the real pair, while the *tree-c* and *tree-d* form the imaginary pair of the analysis filterbank. *Trees-*(a', b') and *Trees-*(c', d') are the real and imaginary pairs respectively in the synthesis filterbank similar to their corresponding analysis pairs.

As mentioned in the last paragraph, DTCWT uses two separate filterbanks, hence the coefficients generated by these filter banks can be analysed and synthesised separately. In the proposed method the real and imaginary coefficients have been amplified using a set of sub-band weights from Table 4.1. Subsequent steps shown in Figure 4.3 include the reconstruction using the amplified coefficients, performing Floyd-Stenberg ED and finally calculating performance parameters.

Table 4.1 Sub-band weights for coefficients [9]

Sub-band level	1	2	3	4	5	6	7	8	9
Wavelet dithering weights	10	40	19	12	10	8	8	8	8

- ***Flowchart for the proposed dithering method***

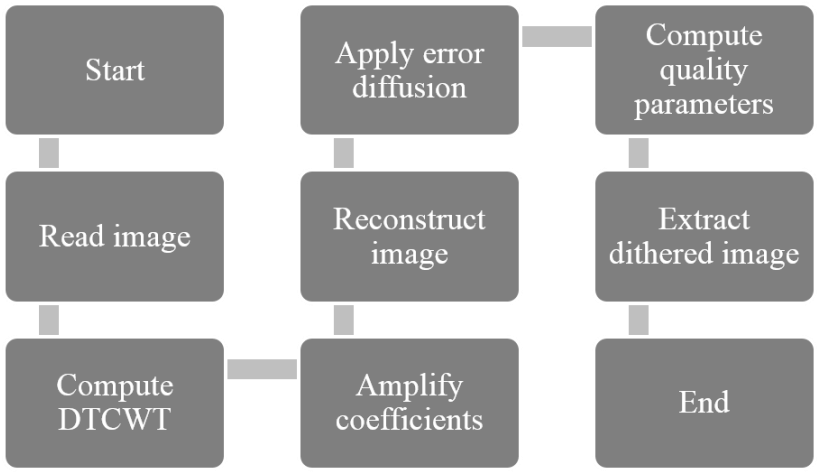

Figure 4.3 Flowchart depicting DT-CWT-based image dithering.

If the coefficients in sub-band 3 need to be amplified, then according to Table 4.1, the corresponding weight or amplification factor for sub-band 3 is going to be 19. Figure 4.4 is a block diagram that has been used to demonstrate the working of the proposed method. The example considers an input 2D matrix of size 4 x 3, performs the second level 2D-DTCWT, computes the dithered and reconstructed matrix. As seen in Figure 4.4, the output is a 4 x 4 matrix.

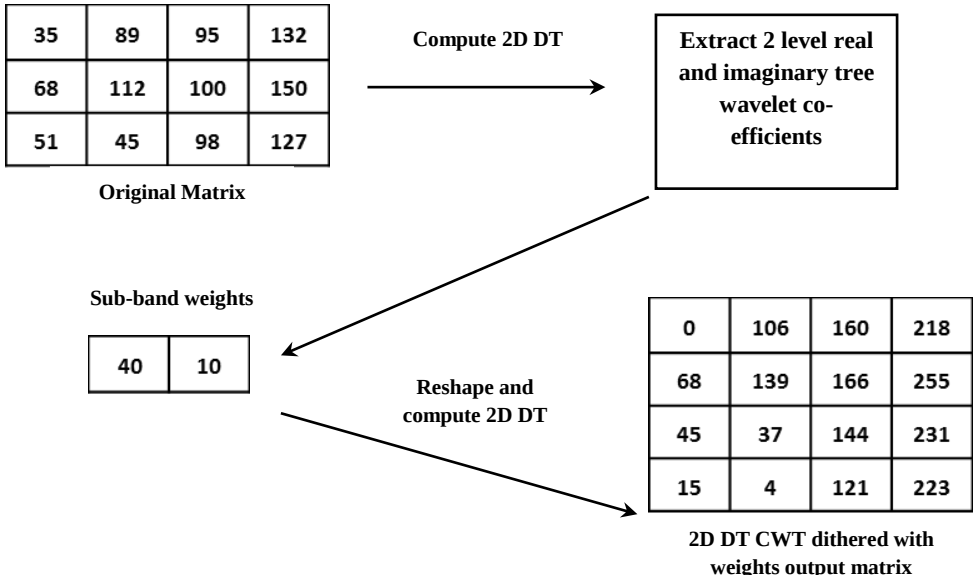

Figure 4.4 Example for computing complex wavelet-based dithering.

MATLAB has been used for the implementation of the proposed method. The source code for the 2D -DTCWT has been reused from Nick Kingsbury's code [51]. The forthcoming bullet points within the present section have illustrated breakdown of the proposed method.

- ***2D DT Real Weight CWT dithering***

In this method, the real-tree wavelet coefficients are amplified with the sub-band weights and so in theory, since these are the low-frequency components, this should provide a considerably better-dithered image. Amplification of the lower frequency has suppressed the higher frequency signals in the image and pixels have been uniformly distributed; an illustration of this can be seen in Figures 4.5 and 4.6 respectively.

(a) (b)

Figure 4.5 (a) WT-based dithered image, (b) 2D DT Real CWT-based dithered with ED.

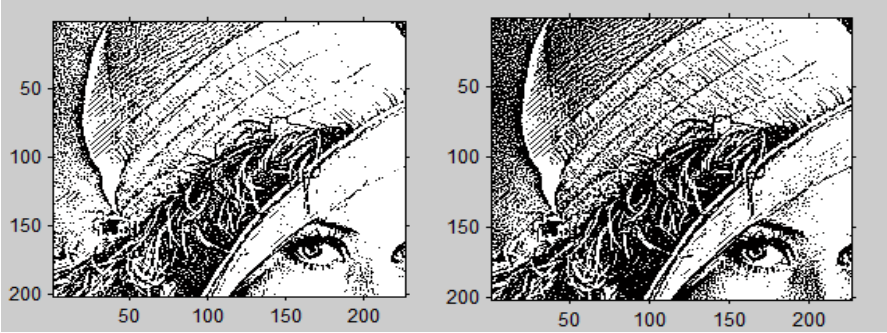

(a) (b)

Figure 4.6 (a) Section of WT-based dithered image, (b) Section of 2D DT Real CWT with Floyd ED.

- ***2D DT Imaginary CWT dithering***

In this method, the imaginary tree wavelet coefficients are amplified with the sub-band weights and so in theory, since these are high-frequency components, the output image may not be good enough as seen in Figures 4.7 and 4.8. It may be noticed that the 2D DT imaginary weights CWT output image is not good enough to see although the details have been preserved. Amplification of the higher frequency has suppressed the lower frequency signals in the image. The section images show that the ED dithering has further enhanced the details present in the processed image.

(a) (b)

Figure 4.7 (a) 2D DT Imaginary CWT-based dithered image, (b) 2D DT Imaginary CWT with Floyd Steinberg.

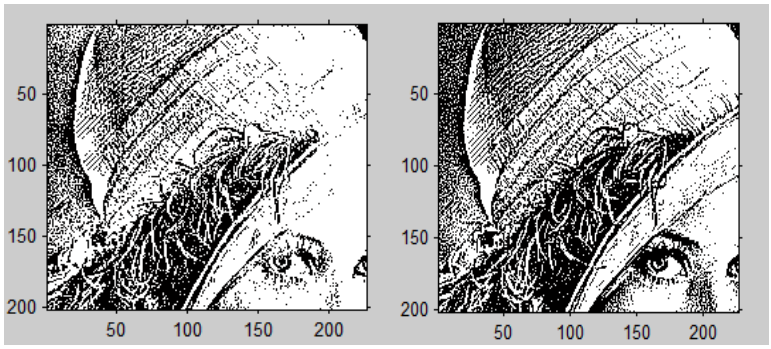

(a) (b)

Figure 4.8 (a) Section of 2D DT Imaginary CWT-based dithered image, (b) Section of 2D DT Imaginary CWT with Floyd-Steinberg.

- ***2D-DTCWT dithering***

The output image is given in Figure 4.9. It may be noticed that the 2D-DTCWT is much better than the DWT-based dithering as it provides finer details in the image. This is due to the fact that this method has improved directional selectivity and is able to pick up the finer details on amplifying with the sub-band weights. Overall, the photographic quality, image details and features are well preserved. With the addition of the Floyd-Steinberg ED the image appears aesthetically pleasing when compared to the direct method, since the grainy appearances are reduced due to the errors diffused to neighbouring pixels. Figure 4.8 shows a section of the image Lena, with the lines in the hat (especially the vertical as well as horizontal lines) being more prominent. Figure 4.9 also shows Lena's clear and enhanced hair strands, which are better than the existing methods shown in Figure 4.9.

Figure 4.9 2D DTCWT-based dithered image.

- ***The proposed set of sub-band weights***

From the above discussion on the proposed dithering method it is evident that the sub-band weights or amplification factor play an integral role. The selection of the amplification weight should be such that it should be able to achieve the desired result, which has better contrast characteristics in this case. Initially, the sub-band weights were taken from Table 4.1, which are the weights proposed by Ovidiu Cosma to achieve DWT dithering. The proposed method has also used the same weights to achieve the DT-CWT based dithering.

As part of this research a new empirical set of sub-band weights were selected, as shown in Table 4.2. These empirical weights have been able to further enhance contrast and details in a dithered image. The visual effects of these amplification weights are evident and can be observed in Figure 4.10.

Table 4.2 The proposed set of sub-band weights for coefficients

Sub-band level	1	2	3	4	5	6	7	8	9
Wavelet dithering weights	15	8	6	6	6	3	3	1	1

(a) (b)

(c) (d)

(e) (f)

(g) (h)

Figure 4.10 Results of the proposed method due to weights from Table 4.1 are represented by (a)(c)(e)(g) and results of the proposed method due to weights from Table 4.2 are presented by (b)(d)(f)(h).

4.2. Results and discussion of the proposed method

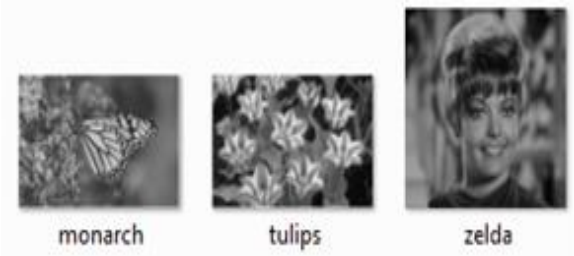

Figure 4.11 Test images from left to right: monarch, tulips and Zelda.

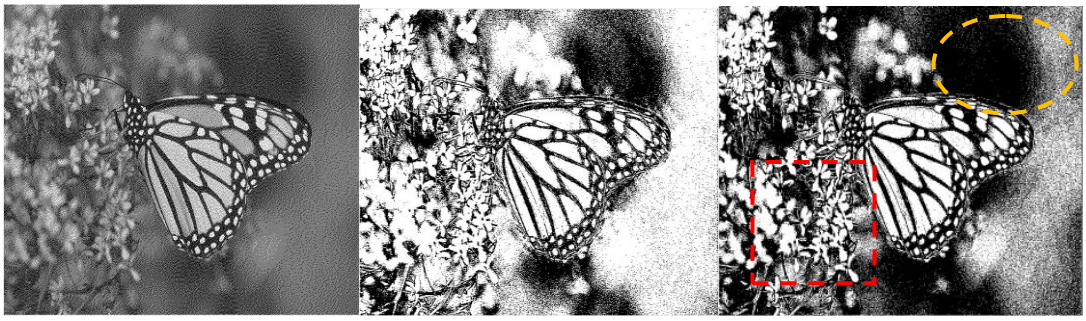

(a)

(b)

(c)

Figure 4.12 Comparison of reconstructed images from left to right: Floyd-Steinberg-ED, wavelet-based dithering, and the **proposed method**.

Figure 4.11 shows three out of the 102 test images that have been chosen for illustration of the proposed method. Dataset consisting of all the test images for dithering can be found in

Appendix A as Figure A2. Figure 4.12 compares the proposed method with two existing methods. In the left column, results are obtained using Floyd-Steinberg ED dithering. It can be observed that the reconstructed images seem to have a grey texture throughout. In addition, reconstructed images lack in edges and features as greyish images appear blurry and soft. The middle column shows the results obtained from wavelet-based dithering. It may be observed that all three reconstructed images in the middle column appear less greyish in comparison to the images in the left column in Figure 4.12. Images in the middle column are better in contrast, which makes edges and features more evident. The blur associated with the reconstructed images has been reduced as well due to wavelet-based dithering.

The right column in Figure 4.12 shows the results obtained from the proposed method. It can be clearly seen that the overall contrast has been improved and is better than that obtained from the other two methods. An improvement in contrast leads to better feature and edge quality which are considered details of an image. Improved features and edges have been marked using red rectangles in the proposed method column. In Figure 4.12(c) the red rectangle shows the lips are more prominent and the yellow oval shows an improvement in preserving two edges. In Figure 4.12(b) and Figure 4.12(c) the red rectangles show visible improvements in contrast that makes images to look sharp and crisp. Also, the yellow oval clearly shows the enhanced features or details of the image.

- ***Performance parameters***

The quality parameters taken into consideration are RMSE, PSNR from Equations 3.4, 3.5 and Black and White (B & W) difference [2] respectively.

The black and white pixel density of an image provides the proportion in which the black and white pixels are distributed in the image. It is calculated by

$$\text{Density of black(DB) or white pixels(DW)} = \frac{\text{Number of black or white pixels}}{\text{Total pixels}}$$

Once the individual densities are calculated, the density variation is calculated by

$$\text{Density variation(DV)} = \left|\text{DB-DW}\right|$$

Once DV is calculated, the $\text{B \& W difference}$ is calculated by

$$\text{B \& W difference} = 20\log\frac{255}{\text{DV}}.$$

A high value of the B&W difference implies that the pixel levels have been distributed uniformly. PSNR should be as high as possible whereas the lower the RMSE, the better is the

reconstructed image. Table 4.3 shows that the proposed method is better in terms of PSNR, RMSE and B&W difference than the Floyd-Steinberg ED and wavelet-based dithering respectively.

Table 4.3 Comparisons between existing methods and the proposed method.

Test Image	Method	RMSE	PSNR (dB)	B & W difference(dB)
Monarch	Floyd Steinberg ED	4.1518	35.7660	59.4731
	Wavelet-based dithering	1.1818	46.6803	57.6429
	Proposed method	**0.9354**	**50.3881**	**55.7323**
Tulips	Floyd Steinberg ED	5.1408	33.9102	56.7981
	Wavelet-based dithering	2.5100	40.1373	54.3468
	Proposed method	**0.9629**	**51.9467**	**50.4368**
Zelda	Floyd Steinberg ED	4.8831	34.3568	56.7032
	Wavelet-based dithering	0.8964	49.0810	54.1241
	Proposed method	**0.9478**	**50.9940**	**50.5433**

In Appendix A, data set for image dithering has been shown by using Figure A2. Dataset for image dithering consists of 102 standard images and they have been processed using Floyd Steinberg ED, Wavelet-based dithering and the proposed method. Once the images were processed the performance parameters have been calculated and arranged in Table A2 to establish a comparison.

On observing Table A2 it can be noticed that on average the proposed image dithering method provides better results. This is when compared to Floyd Steinberg ED and wavelet-based dithering, in terms of both PSNR and B&W difference values respectively. When it comes to PSNR, it can be noticed that on average the proposed method gives a higher value of 5.135dB when compared to Floyd Steinberg ED, whereas this value difference becomes 2.44dB in case of wavelet-based dithering. A similar kind of conclusion can be drawn when the B&W difference values are calculated. In this case, the proposed method works better by a value of 8.342dB compared to Floyd Steinberg ED and by 5.131dB in relation to wavelet-based dithering respectively. The proposed method has worked successfully in 89 out of 102 images by giving better results in comparison to other existing methods. In contrast, with reference to the rest of the other 13 images, only one of the other existing methods has performed better in one way or other when compared with the proposed method. Table A2 in Appendix A can be consulted in this context.

To extend the ongoing discussion on the newly proposed amplification weights, a comparison with existing methods has been made. Figure 4.13 shows a set of test images and Figure 4.14 exhibits the changes made on them by the empirical weights given in Table 4.2.

Figure 4.13 Test images from left to right: cameraman, Zelda.

(a)

(b)

Figure 4.14 Comparison of reconstructed images from left to right: Floyd-Steinberg-ED, wavelet-based dithering and the **proposed method**.

Figure 4.13 shows two images which have been used to test the proposed method. Figure 4.14 compares the proposed method with two existing methods. The results in the left column are obtained using Floyd-Steinberg ED dithering. It can be observed that the reconstructed images seem to have a grey texture throughout. In addition, reconstructed images lack in edges and

features as greyish images appear blurry and soft. The middle column shows the results obtained from wavelet-based dithering. It can be observed that both reconstructed images in the middle column appear less greyish in comparison to the images in the left column in Figure 4.14. Images in the middle column are better in contrast, which makes edges and features more evident. The blur associated with the reconstructed images has been reduced as well due to wavelet-based dithering.

The right column in Figure 4.14 shows the results obtained from the proposed method. It can be clearly seen that the overall contrast has been improved compared to the other two methods. An improvement in contrast leads to better feature and edge quality which are considered details of an image. Improved features and edges have been marked using red rectangles in the proposed method column. In Figure 4.14(b) the red rectangle shows the lips are more prominent in contrast and the yellow oval shows an improvement in detecting two edges. In Figure 4.14(a) and Figure 4.14(b) the red rectangles also show visible improvements in contrast, making them look sharp and crisp. In addition, the yellow oval clearly shows the enhanced features or details of the image. From Table 4.4 it can be clearly seen that the proposed method is better in terms of PSNR, RMSE and B&W difference than Floyd-Steinberg ED and wavelet-based dithering respectively.

Table 4.4 Comparison between existing methods and the proposed method using sub-band weights from table 4.2.

Test Image	Method	RMSE	PSNR (dB)	B&W Difference
Cameraman	Floyd Steinberg ED	5.1408	33.9102	59.6921
	Wavelet-based Dithering	1.6280	43.8980	57.4452
	Proposed method	**0.5597**	**53.1722**	**52.5388**
Zelda	Floyd Steinberg ED	4.8831	34.3568	59.7053
	Wavelet-based Dithering	0.8964	49.0810	56.1244
	Proposed method	**0.2126**	**61.5787**	**52.5533**

Table 4.5 shows the comparison among classical dithering techniques mentioned in Section 2.2.2 and the proposed method. All the methods have been implemented on test image Lena of size 256 x 256 pixels. ID in Table 4.5 stands for Image Dithering.

Table 4.5 Comparison of classical methods and the proposed method.

Image	Dither type	PSNR(dB)	B & W Difference(dB)	Time(seconds)
Lena	Random thresholding	31.39267	66.64911	2.330251
	Fixed threshold	27.09227	73.45082	0.91218
	Ordered dither	31.86811	70.98415	1.460832
	Floyd Steinberg	31.50421	62.86755	1.177894
	Jarvis, Judice & Ninke	31.61605	77.29922	4.260904
	Stucki	31.57646	77.15074	4.145102
	DWTID	39.8365	57.43506	1.559448
	DWTID + ED	39.8566	57.4452	3.253142
	2D DT CWT ID	44.0831	59.69215	1.200825
	Proposed method	**45.0971**	**83.9405**	**1.998821**
	2D DT RWT ID	41.253	56.10699	1.379807
	2D DT RWT ID + ED	41.8566	56.12442	2.024887
	2D DT IWT ID	39.2843	57.57305	1.121416
	2D DT IWT ID + ED	39.3038	57.59885	1.908025

Figure 4.15 shows the graphs that are based on Table 4.5. These Graphs demonstrates the trends of PSNR, B & W difference and time taken for processing in seconds respectively. More implementation results on test images can be found in Appendix A. Based on the experiments the following comments have been made.

Comments

1. The ED-based dithering techniques have the highest running time.
2. For a pleasing output, the ED methods are the best choice out of all the classical methods.
3. In terms of details and contrast enhancements the wavelet-based methods perform better in the existing methods and there are no patterns observed in the wavelet-based dithers as observed in some of the classical methods.
4. The complex coefficients using weights produce a superior dithered image with detail enhancement.
5. In general, the proposed method provides a good output image visually and is better than moderate when it comes to processing time.
6. The imaginary co-efficient with weights does not provide a good output. As the higher frequency components are amplified, which may contain a lot of noise in the output image.

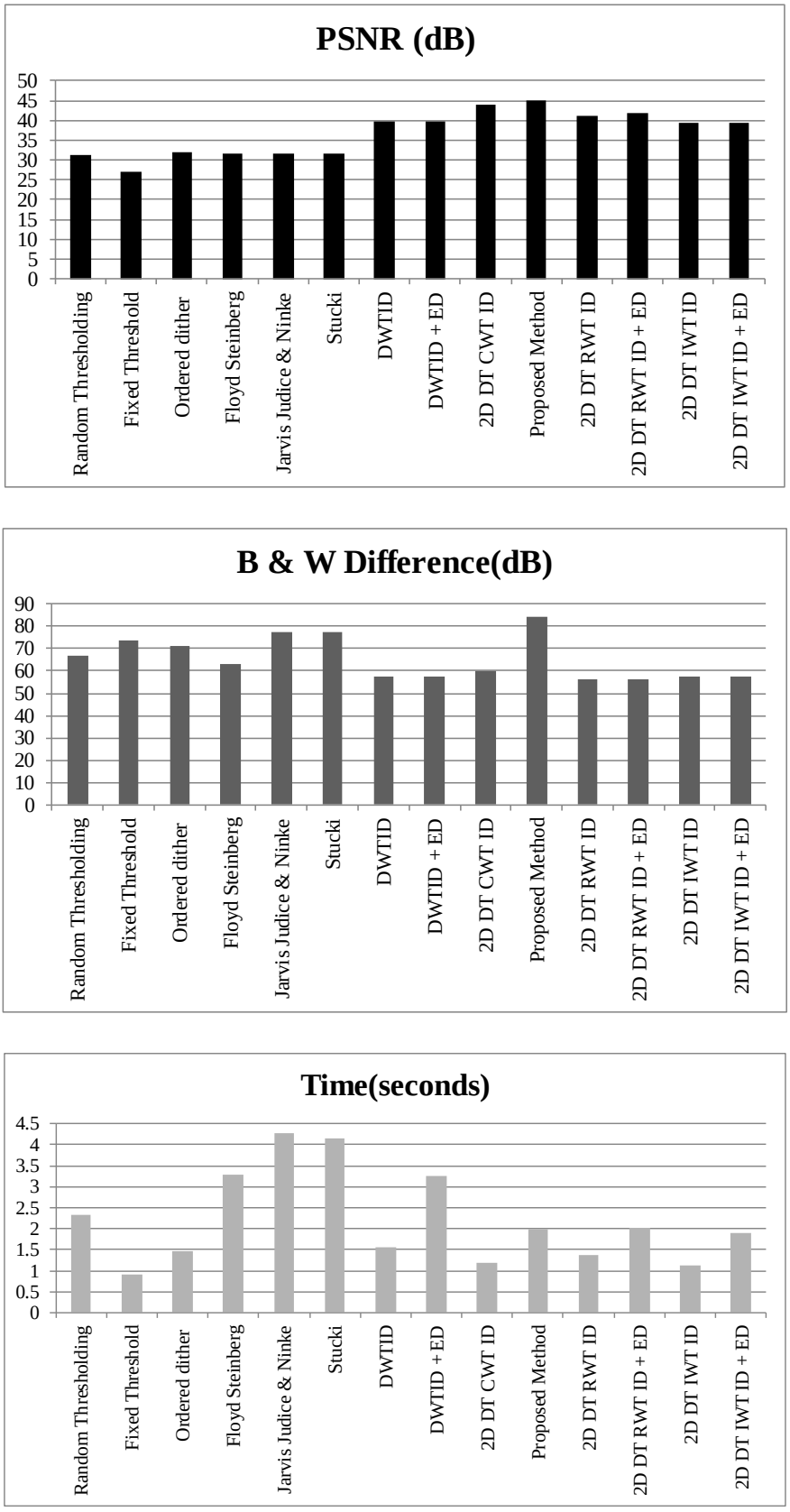

Figure 4.15 Comparison of the classical methods and the proposed method of dithering on image Lena. When it comes to PSNR and B&W difference, the **proposed method** is superior to the existing methods. In terms of processing time the proposed method is better than moderate.

4.3. Summary

This chapter has focused on the proposed work of image dithering, which is another objective of the thesis. The proposed method uses complex wavelet transforms to achieve dithering. To start with, the proposed method used the same set of amplification factors or weights that were introduced in the past to achieve wavelet-based dithering. Later on however, a new set of amplification weights that improved dither quality were also introduced in this thesis. The method proved to produce a superior dithered image that suppressed the softening effects caused by existing error diffusion methods. As a result, the output dithered image of the proposed method preserved details present in the image and also exhibited better contrast characteristics than other methods. Performance parameters such as PSNR, Black and White (B&W) difference subsequently produced favourable results for the proposed method. The processing time is also better when compared with majority of the existing methods. When it comes to PSNR and B&W difference values given by the proposed method are better by an average value of 5.135dB and 8.342dB compared to the first of the two existing methods respectively. Similarly comparing these parameters to the second of the two existing methods, the proposed method outperforms it by higher PSNR and B&W difference values of 2.449dB and 5.131dB on average.

Chapter 5- Conclusion and Future Scope

You are not a drop in the OCEAN,
You are the entire OCEAN in a drop.
-Rumi

5.1. Conclusion

This thesis ultimately aims to achieve image enhancement. Illustrations of image enhancements have been made firstly by using image fusion and secondly by image dithering. Firstly, a transform domain method to achieve image fusion has been proposed. The proposed method also incorporates power law which ultimately results in achieving contrast enhancement in the fused image along with making the details look crisper and clearer. Secondly, a new method for dithering based on complex wavelet transforms has been proposed. The proposed method produces a superior dithered image with better emphasis on detail and contrast enhancement compared to existing methods.

Starting first with image fusion, out of all the available techniques this work has mostly focused on wavelet-based image fusion. Subsequently, various experiments have been conducted in order to validate the fusion results through quantitative and qualitative methods. Later in the research, a novel method based on complex wavelet transforms has been proposed. The objective and subjective discussion has been conducted and promising results have been achieved. The evolution, development and mathematical theory of wavelet transformation has also been discussed along with the realisations of discrete wavelet transform in the first few chapters.

Many MATLAB simulations have been performed for fusing two images and achieving image dithering both in the spatial and the transform domain. Performance analysis for each of the algorithms using parameters such as RMSE, PSNR, entropy and the B&W difference has been conducted. In the case of the proposed pixel-based image fusion, both visual and mathematical assessments have been conducted and the results show an improvement in the contrast present in the final fused image. Results also have shown an improvement in entropy value by 0.9355 when compared to first existing method and 0.5717 when compared to the second existing method. Second is the proposed region-based method for image fusion. The proposed region-based method has shown an improvement of 1.4678 and 1.104 in entropy compared to existing methods respectively. Consecutively the proposed region-based based has also improved the processing time by a factor of 1.53 seconds when compared to the first existing method and 3.01 seconds compared to the second existing method. When it comes to image dithering PSNR and B&W difference values given by the proposed method are better by an average value of 5.135dB and 8.342dB compared to the

first of the two existing methods respectively. Similarly comparing these parameters to the second of the two existing methods, the proposed dithering method outperforms it by producing higher PSNR and B&W difference values of 2.449dB and 5.131dB on average.

The proposed algorithms gave promising results which point towards possible advancements. In the field of image fusion and image dithering wavelet-based algorithms can be employed for performing the fusion of source data and complex wavelets in image dithering respectively.

5.2. Future scope

The thesis points towards the immense opportunities possible for further research in image fusion and image dithering using wavelet transformation.

A first suggestion for the further research on image fusion includes a study of the various forms of noise that can be found in images such as uniform or salt and pepper noise, Gaussian noise and so on. This would pave the way for developing intelligent image fusion techniques capable of choosing the best rule based on the type of degradation models used in the source images. This thesis focuses mainly on standard discrete wavelet transformation-based fusion methods. In the future, there is a scope to implement other popular methods such as Wavelet Packet Transforms and DTCWT in order to produce better quality images.

Regarding image dithering, the proposed method could in future be extended to colour images and the computing of qualitative measures. Open source software such as Open CV could be used to implement these algorithms for other applications. The 2D DTCWT coefficients have been subjected to the sub-band weights to study the output. These coefficients can be further modified using entropy, thresholding and other techniques available and the output can be analysed further. There are other quality parameters for measuring the dither quality of an image. Some of these parameters have been mentioned below. These parameters can be used to check the quality of the dithered images.

1. Structural similarity index (SSIM).
2. Multi-scale SSIM index (MSSIM).
3. Wavelet-based Visual Signal to Noise ratio (VSNR).
4. Visual Information Fidelity (VIF).
5. Pixel-based VIF (VIFP).
6. Information fidelity criterion (IFC).
7. Noise quality measure (NQM).
8. Weighted Signal to noise ratio (WSNR).

References

1. S. Li, X. Kang, L. Fang, J. Hu, and H. Yin. "Pixel-level image fusion: A survey of the state of the art," *Information Fusion*, vol. 33, pp.100-12, January 2017.
2. S. Sharma, J. J. Zou, and G. Fang. "Detail and contrast enhancement for images using dithering based on complex wavelets," in *IEEE Region 10 Conference (TENCON), Singapore, November 22-25, 2016*, vol. 1, pp. 1388-91.
3. J. M. Guo, and Y. F. Liu. "Improved block truncation coding using optimized dot diffusion," *IEEE Transactions on Image Processing*, vol. 23, no. 3, pp. 1269-75, March 2014.
4. Y. Wang, C. Abhayaratne, R. Weerakkody, and M. Mrak. "Multi-scale dithering for contouring artefacts removal in compressed UHD video sequences", in *IEEE Global Conference on Signal and Information Processing (GlobalSIP), Atlanta, Georgia, USA, December 03-05, 2014*, vol. 1, pp. 1014-8.
5. J. S. Park, and J. K. Song. "Image quality improvement in LCDs with temporal division method using pixel dithering," *Journal of Display Technology*, vol. 11, no. 5, pp. 438-42, May 2015.
6. W. Li, X. Wan, and L. Jian. "Digital halftoning and the application to remote sensing images," in *International Conference on Computer Science and Software Engineering, Wuhan, Hubei, China, December 12-14, 2008*, vol. 6, pp. 137-40.
7. C. Varytimidis, K. Rapantzikos, Y. Avrithis, and S. Kollias. "Improving local features by dithering-based image sampling," in *Asian Conference on Computer Vision, Singapore, November 01-05, 2014*. Springer International Publishing. vol. 1, pp. 601-13.
8. I. W. Selesnick. "Hilbert transform pairs of wavelet bases," *IEEE Signal Processing Letters*, vol. 8, no. 6, pp.170-3,June 2001.
9. O. Cosma. "Image dithering based on the wavelet transform," in *Proceedings of the International Conference on Theory and Applications of Mathematics and Informatics (ICTAMI 2004), Thessaloniki, Greece,* September *15-17, 2004,* vol. 1, pp. 96-104.
10. H. G. Hosseini, M. Fatemi, and A. Alizad. "Registration of vibro-acoustography images and x-ray mammography," in *27th Annual International Conference of the Engineering in Medicine and Biology Society (IEEE-EMBS), Shanghai, China, September 01-04, 2005*, vol. 1, pp. 1846-9.
11. G. Bhatnagar, Q. J. Wu, and Z. Liu. "Directive contrast based multimodal medical image fusion in NSCT domain," *IEEE Transactions on Multimedia*, vol. 15, no. 5, pp. 1014-24, August 2013.
12. G. Moser, D. Tuia, and M. Shimoni. "2015 IEEE GRSS data fusion contest: Extremely high resolution LiDAR and optical data [Technical Committees]," *IEEE Geoscience and Remote Sensing Magazine*, vol. 3, no. 1, pp. 40-1, March 2015.
13. C. Debes, A. Merentitis, R. Heremans, J. Hahn, N. Frangiadakis, T. van Kasteren, W. Liao, R. Bellens, A. Pižurica, S. Gautama, and W. Philips. "Hyperspectral and LiDAR data fusion: Outcome of the 2013 GRSS data fusion contest," *IEEE Journal of Selected Topics in Applied Earth Observations and Remote Sensing*, vol. 7, no. 6, pp. 2405-18, June 2014.
14. N. Paramanandham, and K. Rajendiran. "A simple and efficient image fusion algorithm based on standard deviation in wavelet domain," in *International Conference on Wireless Communications, Signal Processing and Networking (WiSPNET), Chennai, India, March 23-25, 2016*, vol. 1, pp. 2207-11.

15. H. Li, Y. Chai, and Z. Li. “Multi-focus image fusion based on nonsubsampled contourlet transform and focused regions detection,” *Optik – International Journal for Light and Electron Optics*, vol. 124, no. 1, pp. 40-51, January 2013.
16. S. Savić, and Z. Babić. “Multifocus image fusion based on the first level of empirical mode decomposition,” in *19th International Conference on Systems, Signals and Image Processing (IWSSIP), Vienna, Austria,, April 11-13, 2012*, vol. 1, pp. 604-7.
17. M. Brell, C. Rogass, K. Segl, B. Bookhagen, and L. Guanter. “Improving sensor fusion: A parametric method for the geometric coalignment of airborne hyperspectral and LiDAR data,” *IEEE Transactions on Geoscience and Remote Sensing*, vol. 54, no. 6, pp. 3460-74, June 2016.
18. Q. Wei, J. Bioucas-Dias, N. Dobigeon, and J. Y. Tourneret. “Hyperspectral and multispectral image fusion based on a sparse representation,” *IEEE Transactions on Geoscience and Remote Sensing*, vol. 53, no. 7, pp. 3658-68, July 2015.
19. H. G. Hosseini, M. Fatemi, and A. Alizad. “Registration of vibro-acoustography images and x-ray mammography,” in *27th Annual International Conference of the Engineering in Medicine and Biology Society (IEEE-EMBS), Shanghai, China, September 01-04, 2005*, vol. 1, pp. 1846-9.
20. G. Bhatnagar, Q. J. Wu, and Z. Liu. “Directive contrast based multimodal medical image fusion in NSCT domain,” *IEEE Transactions on Multimedia*, vol. 15, no. 5, pp. 1014-24, August 2013.
21. P. S. Pradhan, R. L. King, N. H. Younan, and D. W. Holcomb. “Estimation of the number of decomposition levels for a wavelet-based multiresolution multisensor image fusion,” *IEEE Transactions on Geoscience and Remote Sensing*, vol. 44, no. 12, pp. 3674-86, December 2006.
22. D. Marr. *Vision: A Computational Investigation into the Human Representation and Processing of Visual Information.* New York, NY: Henry Holt, 1982.
23. E. H. Adelson, C. H. Anderson, J. R. Bergen, P. J. Burt, and J. M. Ogden. “Pyramid methods in image processing,” *RCA Engineer*, vol. 29, no. 6, pp. 33-41, November 1984.
24. P. J. Burt, and E. H. Adelson. “The laplacian pyramid as a compact image code,” *IEEE Transactions on Communications*, vol. 31, pp. 532-40, April 1983.
25. P. J. Burt, and R. J. Kolczynski. “Enhanced image capture through fusion,” in *Proceedings of the Fourth International Conference on Computer Vision, Berlin, Germany May 11-14, 1993*, pp. 173-82.
26. A. Toet, L. J. Van Ruyven, and J. M. Valeton. “Merging thermal and visual images by a contrast pyramid,” *Optical Engineering*, vol. 28, no. 7, pp. 789-92, July 1989.
27. A. Toet. “Image fusion by a ratio of low-pass pyramid,” *Pattern Recognition Letters*, vol. 9, no. 4, pp. 245-53, May 1989.
28. A. Toet. “A morphological pyramidal image decomposition,” *Pattern Recognition Letters*, vol. 9, no. 4, pp. 255-61, May 1989.
29. H. Li, B. S. Manjunath, and S. K. Mitra. “Multisensor image fusion using the wavelet transform,” *Graphical Models and Image Processing*, vol. 57, no. 3, pp. 235-45, May 1995.
30. Z. Zhang, and R. S. Blum. “A categorization of multiscale-decomposition-based image fusion schemes with a performance study for a digital camera application,” *Proceedings of the IEEE*, vol. 87, no. 8, pp.1315-26, August 1999.
31. S. D. Chen, and A. R. Ramli. “Contrast enhancement using recursive mean-separate histogram equalization for scalable brightness preservation,” *IEEE Transactions on Consumer Electronics*, vol. 49, no. 4, pp. 1301-9, November 2003.

32. S. C. Nercessian, K. A. Panetta, and S. S. Agaian. "Non-linear direct multi-scale image enhancement based on the luminance and contrast masking characteristics of the human visual system," *IEEE Transactions on Image Processing*, vol. 22, no. 9, pp. 3549-61, September 2013.
33. C. Zuo, Q. Chen, and X. Sui. "Range limited bi-histogram equalization for image contrast enhancement," *Optik – International Journal for Light and Electron Optics*, vol. 124, no. 5, pp. 425-31, March 2013.
34. S. Hashemi, S. Kiani, N. Noroozi, and M. E. Moghaddam. "An image contrast enhancement method based on genetic algorithm," *Pattern Recognition Letters*, vol. 31, no. 13, pp. 1816-24, October 2010.
35. N. Senthilkumaran, and R. Rajesh. "Edge detection techniques for image segmentation – a survey of soft computing approaches," *International Journal of Recent Trends in Engineering*, vol. 1, no. 2, pp. 250-4, May 2009.
36. F. Saitoh. "Image contrast enhancement using genetic algorithm," in *Proceedings of the 1999 IEEE International Conference on Systems, Man, and Cybernetics, Tokyo, Japan, October 12-15, 1999*, vol. 4, pp. 899-904.
37. I. Daubechies. *Ten Lectures on Wavelets* [CBMS-NSF Regional Conference Series in Applied Mathematics, vol. 61]. Philadelphia, PA: Society for Industrial and Applied Mathematics, 1991.
38. I. W. Selesnick, R. G. Baraniuk, and N. C. Kingsbury. "The dual-tree complex wavelet transform," *IEEE Signal Processing Magazine*, vol. 22, no. 6, pp. 123-51, November 2005.
39. M. Jiang, Y. Zhou, R. Wang, R. Southern, and J. J. Zhang. "Blue noise sampling using an SPH-based method," *ACM Transactions on Graphics*, vol. 34, no. 6, p. 211, November 2015.
40. J. F. Jarvis, C. N. Judice, and W. H. Ninke. "A survey of techniques for the display of continuous tone pictures on bilevel displays," *Computer Graphics and Image Processing*, vol. 5, no. 1, pp. 13-40, March 1976.
41. P. Stucki. *MECCA: A Multiple Error Correction Computation Algorithm for Bi Level Image Hardcopy Reproduction*. IBM Research, 1981.
42. S. Sharma, J. J. Zou, and G. Fang. 2016 December. "Contrast enhancement using pixel based image fusion in wavelet domain," in *2nd International Conference on Contemporary Computing and Informatics (IC3I), Noida, India, December 14-17, 2016*, vol. 1, pp. 285-90.
43. G. K. Matsopoulos, and S. Marshall. "Application of morphological pyramids: Fusion of MR and CT phantoms," *Journal of Visual Communication and Image Representation*, vol. 6, no. 2, pp. 196-207, June 1995.
44. S. Li, J. T. Kwok, and Y. Wang. "Multifocus image fusion using artificial neural networks," *Pattern Recognition Letters*, vol. 23, no. 8, pp. 985-97, June, 2002.
45. G. Pajares, and J. M. De La Cruz. "A wavelet-based image fusion tutorial," *Pattern Recognition*, vol. 37, no. 9, pp. 1855-72, September 2004.
46. K. Amolins, Y. Zhang, and P. Dare. "Wavelet based image fusion techniques – An introduction, review and comparison. *ISPRS Journal of Photogrammetry and Remote Sensing*, vol. 62, no. 4, pp. 249-63, September 2007.
47. Y. Zhang. 2004. "Understanding image fusion," *Photogrammetric Engineering and Remote Sensing*, vol. 70, no. 6, pp. 657-61.
48. S. G. Mallat. "A theory for multiresolution signal decomposition: The wavelet representation," *IEEE Transactions on Pattern Analysis and Machine Intelligence*, vol. 11, no. 7, pp. 674-93, July 1989.
49. P. D. Shukla. "Complex wavelet transforms and their applications," M.Phil. report, Department of Electronic and Electrical Engineering, University of Strathclyde, Glasgow, 2003.

50. R. R. Coifman, and D. L. Donoho. “Translation-invariant de-noising,” in *Wavelets and Statistics*, A. Antoniadis, and G. Oppenheim, Eds. New York, NY: Springer, 1995, pp. 125-50.
51. P. P. Vidyanathan. *Multirate Systems and Filter Banks*. New Jersey, Prentice Hall,1993.
52. G. Strang, and T. Nguyen. *Wavelets and Filter Banks*. Philadelphia, PA: Society for Industrial and Applied Mathematics, 1996.
53. M. Vetterli. “Filter banks allowing perfect reconstruction,” *Signal Processing*, vol. 10, no. 3, pp. 219-44, April 1986.
54. J. Kovacevic, and M. Vetterli. “Nonseparable multidimensional perfect reconstruction filter banks and wavelet bases for R/sup n,” *IEEE Transactions on Information Theory*, vol. 38, no. 2, pp. 533-55, January 1992.
55. Y. P. Lin, and P. P. Vaidyanathan. “Theory and design of two-dimensional filter banks: A review,” *Multidimensional Systems and Signal Processing*, vol. 7, no. 3-4, pp. 263-330, March 1996.
56. D. Stanhill, and Y. Y. Zeevi. “Two-dimensional orthogonal filter banks and wavelets with linear phase,” *IEEE Transactions on Signal Processing*, vol. 46, no. 1, pp. 183-90, January 1998.
57. H. Guo. “Theory and applications of the shift-invariant, time-varying and undecimated wavelet transforms,” Master’s thesis, Department of Electrical and Computer Engineering, Rice University, Houston, Texas, USA, 1995.
58. I. Cohen, S. Raz, and D. Malah. “Shift invariant wavelet packet bases,” in *1995 International Conference on Acoustics, Speech, and Signal Processing (ICASSP-95), Detroit, Michigan, USA, May 08-12, 1995*, vol. 2, pp. 1081-4.
59. L. Akarun, D. Ozdemit, and O. Yalcin. “Joint quantization and dithering of colour images,” in *Proceedings of the International Conference on Image Processing, Lausanne, Switzerland,, September 19-19, 1996*, vol. 1, pp. 557-60.
60. L. Akarun, D. Ozdemit, and O. Yalcin. “Modified quantisation algorithm for dithering of colour images,” *Electronics Letters*, vol. 32, no. 13, pp. 1185-6, June 1996.
61. A. Kaur, and C. Singh. “Contrast enhancement for cephalometric images using wavelet-based modified adaptive histogram equalization,” *Applied Soft Computing*, vol. 51, pp. 180-91, Feburary 2017.
62. G. Braudaway. “A procedure for optimum choice of a small number of colours from a large colour palette for colour imaging,” in *Proceedings of Electronic Imaging ’87, San Francisco, CA, January, 1987*, pp. 75-9.
63. M. T. Orchard, and C. A. Bouman. “Colour quantization of images,” *IEEE Transactions on Signal Processing*, vol. 39, no. 12, pp. 2677-90, December 1991.
64. Y. T. Kim. “Contrast enhancement using brightness preserving bi-histogram equalization,” *IEEE Transactions on Consumer Electronics*, vol. 43, no. 1, pp. 1-8, Feburary 1997.
65. P. Shanmugavadivu, and K. Balasubramanian. “Partical Swarm optimized multi-objective histogram equilization for image enhancement,”*Optics and Laser Technology*, vol. 57, pp. 243-53, April 2014.
66. G. Maragatham, and S. M. M. Roomi. “PSO-based stochastic resonance for automatic contrast enhancement of images,” *Signal, Image and Video Processing*, vol. 10, no. 1, pp. 207-14, January 2016.
67. Q. Wang, and R.K. Ward. “Fast image/video contrast enhancement based on weighted thresholded histogram equalization,” *IEEE Transactions on Consumer Electronics*, vol. 53, no. 2, pp. 757-764, May 2007.
68. R. W. Floyd. “An adaptive algorithm for spatial gray-scale,” in Proceedings of the Society for Information Displays, 1976, vol. 17, pp. 75-7.

69. O. Prakash, R. Srivastava, and A. Khare. “Biorthogonal wavelet transform based image fusion using absolute maximum fusion rule,” in *IEEE Conference on Information & Communication Technologies (ICT), Thuckalay, Tamil Nadu, India, April 11-12 2013,* vol. 1, pp. 577-82.
70. O. Prakash, A. Kumar, and A. Khare. “Pixel-level image fusion scheme based on steerable pyramid wavelet transform using absolute maximum selection fusion rule,” in *International Conference on Issues and Challenges in Intelligent Computing Techniques (ICICT), Ghaziabad, India February 07-08, 2014,* vol. 1, pp. 765-70.
71. Y. Yang, C. Han, X. Kang, and D. Han. “An overview on pixel-level image fusion in remote sensing,” in *IEEE International Conference on Automation and Logistics, Jinan, Japan, August 18-21, 2007*, pp. 2339-44.
72. Y. Zhang, and L. Ge. “Region-based image fusion approach using iterative algorithm,” in *Seventh IEEE/ACIS International Conference on Computer and Information Science (ICIS 08), Portland, Or, USA,,May 14-16, 2008,* pp. 202-7.
73. B. Gupta, and M. Tiwari. “Minimum mean brightness error contrast enhancement of colour images using adaptive gamma correction with colour preserving framework,” *Optik – International Journal for Light and Electron Optics*, vol. 127, no. 4, pp. 1671-6, Feburary 2016.
74. M. Sasikala, and N. Kumaravel. “A comparative analysis of feature based image fusion methods,” *Information Technology Journal*, vol. 6, no. 8, pp. 1224-30, 2007.
75. I. W. Selesnick. “Hilbert transform pairs of wavelet bases,” *IEEE Signal Processing Letters*, vol. 8, no. 6, pp.170-3, June 2001.
76. C. Barth, and R.C.P Podgurski. “Dithering digital ripple correlation control for photovoltaic maximum power point tracking,” *IEEE Transactions on Power Electronics*, vol. 30, no. 8, pp. 4548-59, August 2015.
77. R. Ulichne, *Digital halftoning*. Cambridge, MA: MIT press, 1987.
78. M. Nejati, S. Samavi, S. Shirani, "Multi-focus image fusion using dictionary-based sparse representation", *Information Fusion*, vol. 25, pp. 72-84, September 2015.
79. Figshare. (2018). *TNO image Fusion Dataset.* [online] Available at: https://figshare.com/articles/TNO_Image_Fusion_Dataset/1008029 [Accessed 28 May 2018].

Appendix A – Images used for testing

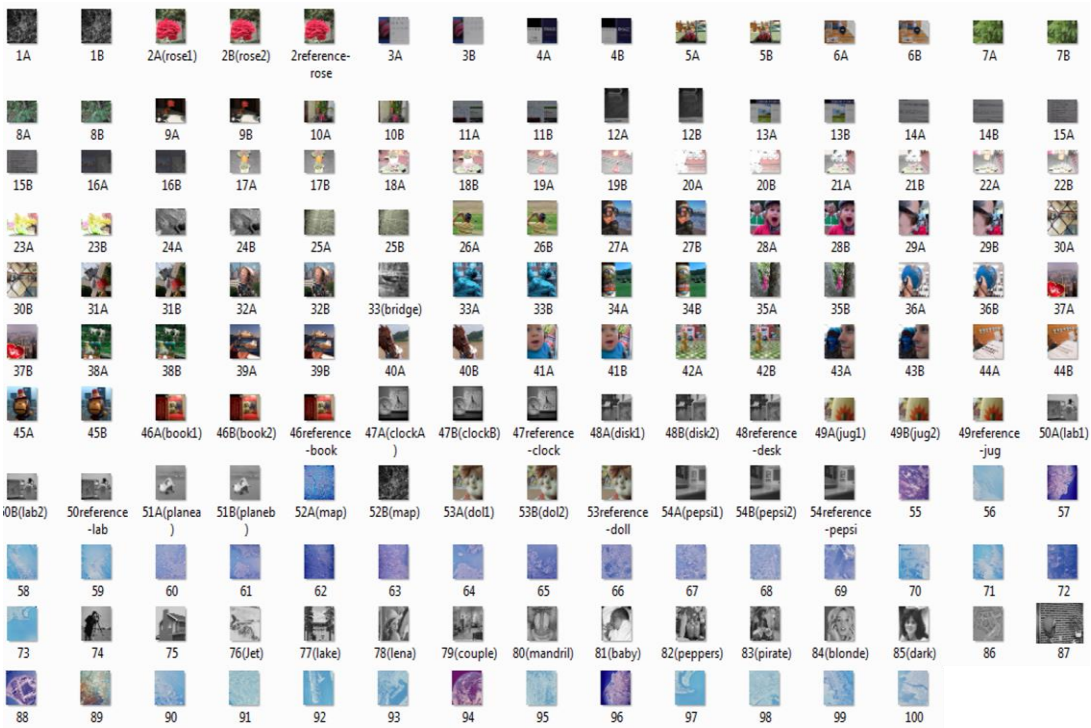

Figure A1: Dataset of test and reference images (100 in total) for dithering for image fusion. Coloured images have been converted to greyscale for processing.

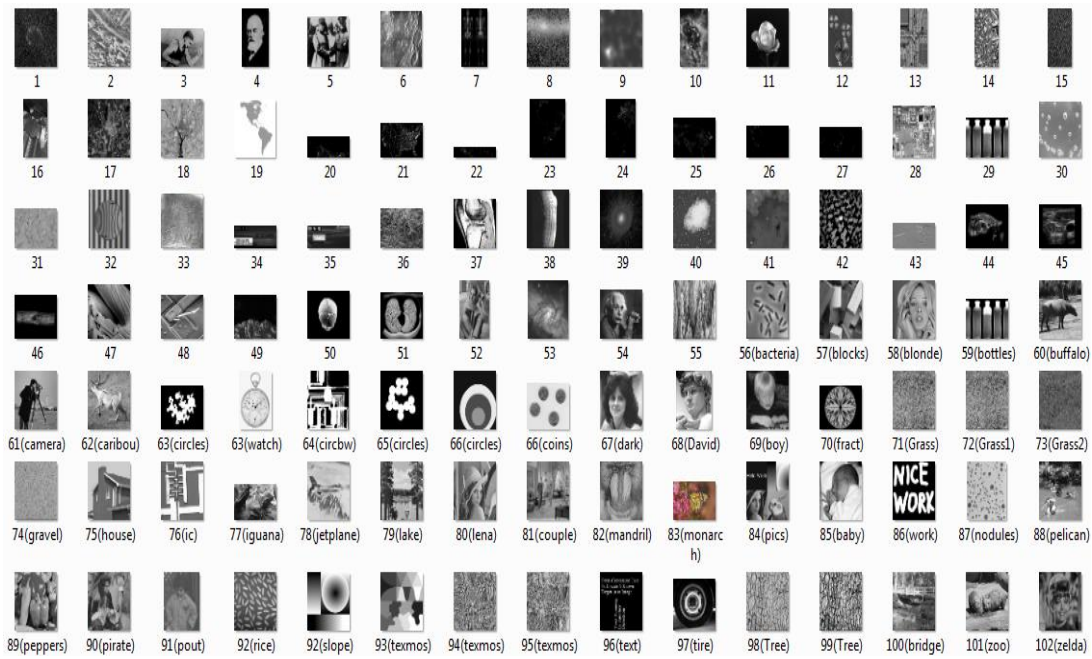

Figure A2: Dataset of test images (102 in total) for dithering. Coloured images have been converted to greyscale for processing.

Table A1 Performance parameter values of the test images for image fusion dataset (Figure A1).

Image	Fusion method	Time	Entropy		Image	Fusion method	Time	Entropy		Image	Fusion method	Time	Entropy
1	Method in [70]	5.58400361	4.26423		2	Method in [70]	7.28010361	5.39828		3	Method in [70]	6.62180361	5.625622
	Method in [14]	7.72360361	5.42562			Method in [14]	8.08580361	5.50496			Method in [14]	7.25280361	7.105684
	Proposed pixel-based method	7.679503609	5.69285			Proposed pixel-based method	8.064503609	5.86246			Proposed pixel-based method	7.206603609	6.769049
	Proposed region-based method	5.5642	5.92562			Proposed region-based method	6.55399	7.25681			Proposed region-based method	5.1533	6.769049
4	Method in [70]	7.58120361	5.10949		5	Method in [70]	6.741	6.3519		6	Method in [70]	7.62650361	6.875795
	Method in [14]	8.42000361	5.97185			Method in [14]	5.757	6.7124			Method in [14]	7.32500361	7.45698
	Proposed pixel-based method	8.324803609	6.10949			Proposed pixel-based method	6.424	7.6795			Proposed pixel-based method	7.304603609	8.168642
	Proposed region-based method	6.2136	6.89989			Proposed region-based method	5.564	7.8440			Proposed region-based method	5.4258	8.255573
7	Method in [70]	6.37610361	5.45303		8	Method in [70]	7.58400361	5.22494		9	Method in [70]	6.95580361	5.37681
	Method in [14]	7.42310361	5.61989			Method in [14]	8.68970361	7.1379			Method in [14]	6.27370361	5.638107
	Proposed pixel-based method	7.351403609	6.00273			Proposed pixel-based method	8.616803609	6.29198			Proposed pixel-based method	6.266003609	6.636099
	Proposed region-based method	5.458	6.47195			Proposed region-based method	5.4974	7.1379			Proposed region-based method	5.0745	7.076968
10	Method in [70]	8.19790361	5.39285		11	Method in [70]	8.33140361	6.10949		12	Method in [70]	6.43160361	6.008214
	Method in [14]	8.73990361	5.99932			Method in [14]	8.93410361	6.8874			Method in [14]	6.86470361	6.45684
	Proposed pixel-based method	10.71660361	6.72445			Proposed pixel-based method	8.857103609	7.06993			Proposed pixel-based method	10.81450361	6.708914
	Proposed region-based method	6.20189	7.45699			Proposed region-based method	5.9255	8.43804			Proposed region-based method	5.9657	7.450598
13	Method in [70]	6.20180361	5.56204		14	Method in [70]	7.05840361	5.3255		15	Method in [70]	7.48880361	5.52857906
	Method in [14]	7.30530361	5.80604			Method in [14]	8.14860361	5.75937			Method in [14]	7.45600361	6.316153
	Proposed pixel-based method	7.239803609	5.24356			Proposed pixel-based method	7.927303609	7.03112			Proposed pixel-based method	7.312803609	6.527612
	Proposed region-based method	5.11	6.58122			Proposed region-based method	5.0302	7.25389			Proposed region-based method	6.3547	7.1294638
16	Method in [70]	7.96330361	5.10156		17	Method in [70]	6.30250361	5.84001		18	Method in [70]	11.8319036	5.0719
	Method in [14]	8.86830361	4.88211			Method in [14]	6.64870361	6.14668			Method in [14]	10.1366036	5.86929
	Proposed pixel-based method	8.564703609	5.43269			Proposed pixel-based method	6.578103609	6.7326			Proposed pixel-based method	9.936003609	6.09049
	Proposed region-based method	6.0841	6.29485			Proposed region-based method	5.9998	7.37811			Proposed region-based method	8.12438	6.458699

19	Method in [70]	9.41100361	5.19747		20	Method in [70]	8.56290361	5.53212		21	Method in [70]	9.58230361	5.083109
	Method in [14]	6.98420361	5.99864			Method in [14]	6.86070361	5.50781			Method in [14]	7.01160361	5.602901
	Proposed pixel-based method	6.929903609	6.62987			Proposed pixel-based method	6.809203609	5.92366			Proposed pixel-based method	6.946603609	6.928072
	Proposed region-based method	6.1659	7.29829			Proposed region-based method	8.5971	6.4258			Proposed region-based method	6.399	8.168642
22	Method in [70]	9.50890361	7.01783		24	Method in [70]	9.43010361	5.59116151		25	Method in [70]	9.52500361	5.2191
	Method in [14]	6.94350361	5.75937			Method in [14]	7.12670361	6.29116151			Method in [14]	7.51200361	5.306527
	Proposed pixel-based method	6.919603609	6.66053			Proposed pixel-based method	7.118503609	7.412582			Proposed pixel-based method	7.461103609	6.716197
	Proposed region-based method	6.2555	5.68262			Proposed region-based method	6.2841	7.956328			Proposed region-based method	6.3332	7.031121
26	Method in [70]	8.40120361	6.33799		27	Method in [70]	8.34360361	4.942469		28	Method in [70]	8.50660361	5.392846
	Method in [14]	6.65520361	7.21839			Method in [14]	6.63950361	5.317635			Method in [14]	6.62820361	4.876488
	Proposed pixel-based method	7.126103609	7.91258			Proposed pixel-based method	7.130803609	5.94564			Proposed pixel-based method	10.90720361	5.678087
	Proposed region-based method	3.5487	8.02418			Proposed region-based method	5.06695	6.89469666			Proposed region-based method	4.7034	6.38308
29	Method in [70]	9.85420361	6.64523		30	Method in [70]	9.05630361	5.63692088		31	Method in [70]	13.1418836	5.636761
	Method in [14]	7.12610361	6.9856			Method in [14]	7.13080361	5.548571			Method in [14]	10.9072036	6.125869
	Proposed pixel-based method	9.419803609	7.4624			Proposed pixel-based method	14.46280361	6.381688			Proposed pixel-based method	8.746903609	6.950165
	Proposed region-based method	6.2222	8.17695			Proposed region-based method	4.8831	6.923648			Proposed region-based method	4.8054	6.125869
32	Method in [70]	11.7603036	4.0745095		33	Method in [70]	17.7160036	6.379166		34	Method in [70]	13.4661036	7.644418
	Method in [14]	9.41980361	5.181394			Method in [14]	14.4628036	6.204099			Method in [14]	8.74690361	6.82226
	Proposed pixel-based method	7.811903609	6.000348			Proposed pixel-based method	8.179603609	6.716197			Proposed pixel-based method	7.303803609	6.770702
	Proposed region-based method	4.8343	6.903456			Proposed region-based method	4.8546	7.058338			Proposed region-based method	7.4117	7.253887
35	Method in [70]	6.71240361	4.90781		36	Method in [70]	6.66810361	5.883505		37	Method in [70]	8.35240361	6.674801
	Method in [14]	7.81190361	5.97383			Method in [14]	8.17960361	5.412365			Method in [14]	7.30380361	7.729549
	Proposed pixel-based method	8.553603609	6.111809			Proposed pixel-based method	6.689603609	6.609586			Proposed pixel-based method	7.349603609	8.19382
	Proposed region-based method	9.3485	6.97781			Proposed region-based method	7.0479	6.950165			Proposed region-based method	7.0616	8.730295
38	Method in [70]	9.25060361	6.47195303		39	Method in [70]	6.54290361	5.638107		40	Method in [70]	7.14710361	7.035598
	Method in [14]	8.55360361	6.798448			Method in [14]	6.68960361	5.464093			Method in [14]	7.34960361	6.114137

	Proposed pixel-based method	7.511403609	7.615766			Proposed pixel-based method	8.806803609	5.770281			Proposed pixel-based method	6.288603609	6.631859
	Proposed region-based method	7.3033	8.4766			Proposed region-based method	6.0831	5.911966			Proposed region-based method	7.1362	5.898214
41	Method in [70]	6.98850361	5.395559		42	Method in [70]	8.20410361	**7.058338**		43	Method in [70]	6.48980361	6.008902
	Method in [14]	7.51140361	6.203238			Method in [14]	8.80680361	5.36913			Method in [14]	6.28860361	6.6235
	Proposed pixel-based method	10.78580361	6.254659			Proposed pixel-based method	9.082803609	5.464828			Proposed pixel-based method	10.92750361	6.9745
	Proposed region-based method	7.1986	6.254659			Proposed region-based method	5.4464	5.464828			Proposed region-based method	5.1513	7.436241
44	Method in [70]	14.4811036	5.614188		45	Method in [70]	11.4142036	5.795213		46	Method in [70]	7.79	6.4877
	Method in [14]	10.7858036	5.340373			Method in [14]	9.08280361	5.759368			Method in [14]	6.616	6.6681
	Proposed pixel-based method	7.410503609	6.624837			Proposed pixel-based method	8.507903609	6.082315			Proposed pixel-based method	8.553	**8.0645**
	Proposed region-based method	5.2	7.448429			Proposed region-based method	8.2437	6.34598			Proposed region-based method	5.3976	7.4407
47	Method in [70]	7.74	6.3889		48	Method in [70]	6.966	6.3676		49	Method in [70]	7.19730361	4.85569
	Method in [14]	5.641	7.2506			Method in [14]	5.641	6.3524			Method in [14]	7.79050361	5.563279
	Proposed pixel-based method	5.569	7.3248			Proposed pixel-based method	5.153	7.2066			Proposed pixel-based method	10.32630361	6.002729
	Proposed region-based method	5.167	7.7351			Proposed region-based method	4.569	7.7649			Proposed region-based method	5.3128	6.47195303
50	Method in [70]	7.08090361	5.464093		51	Method in [70]	6.84	7.4152		52	Method in [70]	9.44690361	5.933784
	Method in [14]	9.38080361	5.777106			Method in [14]	6.43	7.5623			Method in [14]	10.3263036	6.303501
	Proposed pixel-based method	7.105203609	6.2589			Proposed pixel-based method	7.72	7.7028			Proposed pixel-based method	7.127103609	6.676677
	Proposed region-based method	7.8475	7.056037			Proposed region-based method	5.39	7.7235			Proposed region-based method	7.2586	7.46856
53	Method in [70]	6.48700361	5.760402		54	Method in [70]	6.603	6.487		55	Method in [70]	6.72920361	5.563691
	Method in [14]	7.10520361	6.74352			Method in [14]	5.002	7.1471			Method in [14]	7.12710361	6.308369
	Proposed pixel-based method	7.022403609	7.011254			Proposed pixel-based method	5.458	7.3046			Proposed pixel-based method	7.637303609	6.825434
	Proposed region-based method	10.3088	7.259678			Proposed region-based method	5.132	8.0460			Proposed region-based method	7.3846	7.255573
56	Method in [70]	6.58750361	6.16645		57	Method in [70]	6.89680361	4.917233		58	Method in [70]	7.36230361	5.676677
	Method in [14]	7.02240361	6.42368			Method in [14]	7.14870361	5.564104			Method in [14]	7.63730361	5.923326
	Proposed pixel-based method	6.677703609	6.615101			Proposed pixel-based method	6.759303609	6.012398			Proposed pixel-based method	6.744803609	7.253887
	Proposed region-based method	7.4345	7.912582			Proposed region-based method	7.5004	6.89363333			Proposed region-based method	6.1141	7.900348

59	Method in [70]	6.35190361	6.372864		60	Method in [70]	**6.48770361**	5.29356388		61	Method in [70]	**6.36760361**	**6.830628**
	Method in [14]	6.67770361	6.53247			Method in [14]	6.75930361	5.548571			Method in [14]	**6.74480361**	**6.928072**
	Proposed pixel-based method	7.194803609	6.93245			Proposed pixel-based method	7.195603609	6.454225			Proposed pixel-based method	11.00100361	6.126657
	Proposed region-based method	6.2126	7.421569			Proposed region-based method	6.6666	7.3569			Proposed region-based method	9.3716	6.126657
62	Method in [70]	6.38890361	3.654247		63	Method in [70]	6.72550361	5.481543		64	Method in [70]	11.3122036	6.173619
	Method in [14]	7.19480361	5.448429			Method in [14]	7.19560361	6.345059			Method in [14]	11.0010036	6.782584
	Proposed pixel-based method	9.664303609	6.231262			Proposed pixel-based method	14.55990361	6.416197			Proposed pixel-based method	8.800203609	7.122884
	Proposed region-based method	6.9209	7.134291			Proposed region-based method	6.6867	6.716197			Proposed region-based method	6.7455	7.622044
65	Method in [70]	9.50390361	5.91909		66	Method in [70]	14.6613036	5.165871		67	Method in [70]	7.07060361	4.9282
	Method in [14]	9.66430361	6.109488			Method in [14]	14.5599036	5.411327			Method in [14]	8.80020361	5.8946
	Proposed pixel-based method	14.85080361	7.109488			Proposed pixel-based method	12.24190361	6.622044			Proposed pixel-based method	13.63780361	5.392846
	Proposed region-based method	6.8195	8.038301			Proposed region-based method	6.763	7.024448			Proposed region-based method	10.3027	6.331982
68	Method in [70]	7.67950361	5.621632		69	Method in [70]	**8.06450361**	5.636313		70	Method in [70]	7.20660361	5.93487
	Method in [14]	14.8508036	5.74574			Method in [14]	12.2419036	6.097448			Method in [14]	13.6378036	6.109488
	Proposed pixel-based method	12.20550361	6.870497			Proposed pixel-based method	15.56440361	6.465933			Proposed pixel-based method	13.76830361	6.974924
	Proposed region-based method	6.4972	7.89704			Proposed region-based method	9.8028	7.024448			Proposed region-based method	6.6519	7.053742
71	Method in [70]	8.32480361	5.33132242		72	Method in [70]	6.54540361	5.466301		73	Method in [70]	7.30460361	5.889483
	Method in [14]	12.2055036	5.97119			Method in [14]	15.5644036	5.975815			Method in [14]	13.7683036	6.002729
	Proposed pixel-based method	12.69480361	6.114137			Proposed pixel-based method	11.84730361	6.716197			Proposed pixel-based method	19.05560361	6.6258
	Proposed region-based method	6.379	6.941137			Proposed region-based method	6.4213	7.130361			Proposed region-based method	6.5056	7.31476
74	Method in [70]	7.35140361	6.0289		75	Method in [70]	**8.61680361**	6.770281		76	Method in [70]	6.26600361	5.44479897
	Method in [14]	7.35140361	6.414644			Method in [14]	11.8473036	7.12564			Method in [14]	19.0556036	5.975815
	Proposed pixel-based method	12.45580361	6.708902			Proposed pixel-based method	7.735103609	7.870497			Proposed pixel-based method	9.989903609	6.638107
	Proposed region-based method	6.9664	8.75398			Proposed region-based method	10.9173	8.762469			Proposed region-based method	6.7217	7.43810738
77	Method in [70]	10.7166036	5.403064		78	Method in [70]	8.57	7.3906		79	Method in [70]	10.8145036	5.05303
	Method in [14]	12.4558036	5.367484			Method in [14]	6.24	7.4456			Method in [14]	9.98990361	5.635865

	Proposed pixel-based method	17.03100361	5.747572			Proposed pixel-based method	7.54	7.6423			Proposed pixel-based method	15.82680361	6.008214
	Proposed region-based method	9.5019	6.615101			Proposed region-based method	5.32	7.4456			Proposed region-based method	6.8036	6.323687
80	Method in [70]	7.23980361	5.411327		81	Method in [70]	7.92730361	6.002729		82	Method in [70]	7.31280361	6.649864
	Method in [14]	17.0310036	5.306527			Method in [14]	11.7689036	6.52154			Method in [14]	15.8268036	7.010279
	Proposed pixel-based method	15.23350361	6.31224			Proposed pixel-based method	18.81920361	6.905649			Proposed pixel-based method	9.420903609	7.644418
	Proposed region-based method	6.8244	7.342023			Proposed region-based method	6.8725	7.432688			Proposed region-based method	5.8298	8.78647
83	Method in [70]	8.56470361	5.169268		84	Method in [70]	6.57810361	3.83984		85	Method in [70]	9.93600361	5.564104
	Method in [14]	15.2335036	5.769268			Method in [14]	18.8192036	5.44879			Method in [14]	9.42090361	5.308983
	Proposed pixel-based method	14.73050361	6.289128			Proposed pixel-based method	15.25470361	5.646683			Proposed pixel-based method	15.13130361	5.914432
	Proposed region-based method	10.8966	7.613314			Proposed region-based method	5.7577	6.196843			Proposed region-based method	5.6165	6.389644
86	Method in [70]	6.92990361	5.999319		87	Method in [70]	6.809	6.8968		88	Method in [70]	6.94660361	5.127612
	Method in [14]	7.7305036	6.950165			Method in [14]	5.265	7.1066			Method in [14]	15.1313036	5.126366
	Proposed pixel-based method	7.37560361	6.65897			Proposed pixel-based method	5.11	7.3248			Proposed pixel-based method	12.56710361	5.333303
	Proposed region-based method	5.6418	8.484375			Proposed region-based method	4.368	7.6446			Proposed region-based method	6.4327	5.674801
89	Method in [70]	6.91960361	4.893281		90	Method in [70]	7.11850361	5.58514		91	Method in [70]	7.46110361	5.333303
	Method in [14]	14.3756036	5.83286			Method in [14]	13.3669036	5.947356			Method in [14]	12.5671036	5.664198
	Proposed pixel-based method	16.95270361	6.659072			Proposed pixel-based method	9.34640361	7.144173			Proposed pixel-based method	9.58480361	6.420175
	Proposed region-based method	9.2247	7.037846			Proposed region-based method	6.3767	7.67344			Proposed region-based method	6.2238	6.920176
92	Method in [70]	6.65280361	5.921563		93	Method in [70]	6.58990361	6.12351		94	Method in [70]	6.58400361	5.704456
	Method in [14]	16.9527036	6.342023			Method in [14]	9.34640361	5.099381			Method in [14]	9.58480361	6.365874
	Proposed pixel-based method	9.93850361	7.442345			Proposed pixel-based method	9.59940361	6.710004			Proposed pixel-based method	8.229403609	8.850769
	Proposed region-based method	6.2635	7.931262			Proposed region-based method	6.3088	7.122884			Proposed region-based method	5.2254	7.900348
95	Method in [70]	7.09840361	6.09038		96	Method in [70]	7.09820361	5.67527		97	Method in [70]	7.82320361	5.15689
	Method in [14]	9.93850361	6.109488			Method in [14]	12.5994036	5.406498			Method in [14]	8.22940361	5.7865
	Proposed pixel-based method	9.059903609	6.65794			Proposed pixel-based method	7.241803609	6.760831			Proposed pixel-based method	9.034703609	6.966592
	Proposed region-based method	5.431	7.155266			Proposed region-based method	12.6629	7.137903			Proposed region-based method	5.1522	7.060645

98	Method in [70]	9.22160361	5.98674		99	Method in [70]	14.4014036	6.168642		100	Method in [70]	8.71580361	5.7821
	Method in [14]	9.05990361	5.98647			Method in [14]	7.24180361	6.323556			Method in [14]	9.03470361	6.5468
	Proposed pixel-based method	6.652803609	6.5262			Proposed pixel-based method	6.589903609	7.121941			Proposed pixel-based method	6.584003609	7.03649
	Proposed region-based method	7.7599	7.13591			Proposed region-based method	5.3637	7.723587			Proposed region-based method	5.0602	7.415766

Average time			Average entropy	
Method in [70]	8.164918559		Method in [70]	5.729269281
Method in [14]	9.644824821		Method in [14]	6.093085085
Proposed pixel-based method	9.645575327		**Proposed pixel-based method**	**6.66467953**
Proposed region-based method	**6.632288**		**Proposed region-based method**	**7.197090375**

Table A2 Performance parameter values of the test images for image dithering dataset (FigureA2).

Image	Dither type	PSNR	B & W difference		Image	Dither type	PSNR	B & W difference		Image	Dither type	PSNR	B & W difference
1	Floyd Steinberg	31.2227	59.8514		**2**	Floyd Steinberg	29.48743	50.83109		**3**	Floyd Steinberg	33.8892	59.33784
	WT based dithering	33.2151	62.03238			WT based dithering	33.4415	62.04961			WT based dithering	34.3902	62.04099
	Proposed method	35.0229	64.25869			**Proposed method**	35.7181	61.26657			**Proposed method**	37.2818	66.19592
4	Floyd Steinberg	31.2715	54.03064		**5**	Floyd Steinberg	33.9623	53.92846		**6**	Floyd Steinberg	**34.0991**	53.95559
	WT based dithering	32.6177	63.45059			WT based dithering	34.7402	50.99381			WT based dithering	26.4576	53.06527
	Proposed method	34.3308	74.84375			**Proposed method**	39.4438	57.98288			**Proposed method**	32.0085	54.64093
7	Floyd Steinberg	32.2055	43.79166		**8**	Floyd Steinberg	29.166	54.81543		**9**	Floyd Steinberg	32.0984	47.2351
	WT based dithering	35.1294	53.08369			WT based dithering	31.1668	53.08983			WT based dithering	**34.6825**	53.06527
	Proposed method	37.252	54.66301			**Proposed method**	34.3568	58.64828			**Proposed method**	34.4962	54.66301
10	Floyd Steinberg	26.4442	52.191		**11**	Floyd Steinberg	34.4078	55.63691		**12**	Floyd Steinberg	30.7325	55.64104
	WT based dithering	28.716	58.06044			WT based dithering	37.1697	53.40373			WT based dithering	31.9775	54.05466
	Proposed method	30.8605	59.8514			**Proposed method**	39.1263	58.83109			**Proposed method**	34.0615	59.33784
13	Floyd Steinberg	30.9858	54.11327		**14**	Floyd Steinberg	33.4086	56.14188		**15**	Floyd Steinberg	26.4383	51.77685
	WT based dithering	31.8108	**54.12365**			WT based dithering	34.8083	54.11327			WT based dithering	33.4868	54.06498
	Proposed method	33.7674	54.03064			**Proposed method**	36.7236	58.92846			**Proposed method**	33.6243	58.95559
16	Floyd Steinberg	30.2362	58.83505		**17**	Floyd Steinberg	28.2267	51.65871		**18**	Floyd Steinberg	30.9137	56.7527
	WT based dithering	27.8667	48.76488			WT based dithering	30.5352	49.23326			WT based dithering	30.7643	51.26366
	Proposed method	30.7058	56.79166			**Proposed method**	30.6291	54.81543			**Proposed method**	32.4041	61.2351

19	Floyd Steinberg	27.1367	48.78087		**20**	Floyd Steinberg	30.6528	43.76677		**21**	Floyd Steinberg	28.6945	48.74801
	WT based dithering	31.3275	51.69268			WT based dithering	31.6266	48.82113			WT based dithering	**31.5506**	48.81548
	Proposed method	31.4557	55.63691			**Proposed method**	33.528	55.64104			**Proposed method**	27.8718	54.11327
22	Floyd Steinberg	31.8763	76.13314		**23**	Floyd Steinberg	28.3038	51.01558		**24**	Floyd Steinberg	31.6718	61.72788
	WT based dithering	**32.0357**	71.37903			WT based dithering	31.9784	53.74418			WT based dithering	31.8651	70.24448
	Proposed method	31.2707	78.14188			**Proposed method**	33.3685	57.77685			**Proposed method**	36.5812	72.83505
25	Floyd Steinberg	28.5746	52.24941		**26**	Floyd Steinberg	31.3224	56.38107		**27**	Floyd Steinberg	31.476	56.36313
	WT based dithering	31.4495	53.23556			WT based dithering	31.3886	**59.50165**			WT based dithering	32.8177	**69.28072**
	Proposed method	34.385	56.7527			**Proposed method**	32.9259	56.78087			**Proposed method**	33.1416	56.76677
28	Floyd Steinberg	**33.1024**	56.35865		**29**	Floyd Steinberg	29.0322	56.36761		**30**	Floyd Steinberg	31.9629	56.30628
	WT based dithering	28.8318	69.20176			WT based dithering	32.0388	69.50165			WT based dithering	32.2497	59.98639
	Proposed method	32.1944	71.25622			**Proposed method**	32.1319	76.44418			**Proposed method**	33.4332	61.73619
31	Floyd Steinberg	26.0802	64.20175		**32**	Floyd Steinberg	33.8909	59.99319		**33**	Floyd Steinberg	30.3337	51.97469
	WT based dithering	31.5416	57.77106			WT based dithering	**34.0474**	64.38039			WT based dithering	33.9336	53.6913
	Proposed method	33.7684	70.37846			**Proposed method**	33.6929	70.17826			**Proposed method**	27.0115	67.11254
34	Floyd Steinberg	33.3214	70.56037		**35**	Floyd Steinberg	29.1611	70.69934		**36**	Floyd Steinberg	32.9248	70.58338
	WT based dithering	33.1594	71.30361			WT based dithering	33.1109	71.05684			WT based dithering	33.0478	71.20406
	Proposed method	34.9936	77.95213			**Proposed method**	35.1047	78.70281			**Proposed method**	34.1469	75.75795
37	Floyd Steinberg	34.4909	70.76968		**38**	Floyd Steinberg	34.417	56.25622		**39**	Floyd Steinberg	24.1569	**64.44418**

	WT based dithering	37.4533	71.22884			WT based dithering	36.7204	54.4879			WT based dithering	37.4493	58.93281
	Proposed method	37.7034	76.74801			**Proposed method**	37.6177	63.31982			**Proposed method**	38.5827	63.44046
40	Floyd Steinberg	34.2532	61.73619		**41**	Floyd Steinberg	37.8812	52.28017		**42**	Floyd Steinberg	34.2578	60.37846
	WT based dithering	34.3023	57.59368			WT based dithering	34.2798	57.60402			WT based dithering	34.2916	57.59368
	Proposed method	35.7898	63.42023			**Proposed method**	25.6065	66.15101			**Proposed method**	36.352	63.40006
43	Floyd Steinberg	31.5703	70.17826		**44**	Floyd Steinberg	35.8443	57.11254		**45**	Floyd Steinberg	28.0686	70.31121
	WT based dithering	36.0205	67.59368			WT based dithering	34.9443	67.62469			WT based dithering	33.4364	72.55573
	Proposed method	37.5065	75.18314			**Proposed method**	35.5795	70.76968			**Proposed method**	39.3181	74.35598
46	Floyd Steinberg	34.1806	57.95213		**47**	Floyd Steinberg	34.3798	57.70281		**48**	Floyd Steinberg	34.3273	68.75795
	WT based dithering	34.2923	67.30295			WT based dithering	37.1515	53.92846			WT based dithering	27.3039	79.00348
	Proposed method	37.1949	70.53742			**Proposed method**	37.7535	60.9038			**Proposed method**	37.572	81.76954
49	Floyd Steinberg	31.446	66.74801		**50**	Floyd Steinberg	31.8054	63.31982		**51**	Floyd Steinberg	27.5019	63.44046
	WT based dithering	**36.8647**	**79.31262**			WT based dithering	33.5318	72.12582			WT based dithering	31.7964	74.12582
	Proposed method	32.9505	73.72864			**Proposed method**	35.1736	74.57866			**Proposed method**	32.376	79.32688
52	Floyd Steinberg	30.4551	63.42023		**53**	Floyd Steinberg	32.5927	63.37993		**54**	Floyd Steinberg	29.5875	46.15101
	WT based dithering	32.7713	56.46683			WT based dithering	36.66	51.27612			WT based dithering	34.5358	59.67244
	Proposed method	34.333	74.50598			**Proposed method**	38.8217	58.89483			**Proposed method**	36.1235	65.81215
55	Floyd Steinberg	26.468	63.40006		**56**	Floyd Steinberg	29.2874	65.18314		**57**	Floyd Steinberg	29.5582	54.18273
	WT based dithering	34.4088	56.38107			WT based dithering	34.2685	61.14137			WT based dithering	34.3477	61.09488
	Proposed method	39.6242	67.25616			**Proposed method**	38.2766	74.48429			**Proposed method**	39.0745	64.5096

58	Floyd Steinberg	29.4882	62.76968		**59**	Floyd Steinberg	29.4191	60.35598		**60**	Floyd Steinberg	34.3913	49.53742
	WT based dithering	30.9606	61.11809			WT based dithering	34.1708	61.09488			WT based dithering	26.556	49.42469
	Proposed method	34.98892	64.4879			**Proposed method**	36.3705	63.16153			**Proposed method**	30.4148	54.92108
61	Floyd Steinberg	33.9102	59.6921		**62**	Floyd Steinberg	24.9528	50.9038		**63**	Floyd Steinberg	29.8651	61.76954
	WT based dithering	43.8980	57.4452			WT based dithering	31.0151	55.07814			WT based dithering	29.4392	65.9049
	Proposed method	53.1722	52.5388			**Proposed method**	37.20994	59.7119			**Proposed method**	41.1423	69.71849
64	Floyd Steinberg	35.0394	63.72864		**65**	Floyd Steinberg	35.085	55.32117		**66**	Floyd Steinberg	35.0735	57.57866
	WT based dithering	29.7894	60.02729			WT based dithering	37.2213	67.08214			WT based dithering	36.7506	60.08902
	Proposed method	39.9267	80.38301			**Proposed method**	41.641	69.17635			**Proposed method**	38.6497	65.64104
67	Floyd Steinberg	35.056	54.32688		**68**	Floyd Steinberg	33.1558	74.50598		**69**	Floyd Steinberg	27.4189	74.36241
	WT based dithering	36.29	60.02729			WT based dithering	34.2603	84.15766			WT based dithering	38.5207	**78.70497**
	Proposed method	36.7166	65.64929			**Proposed method**	41.4455	85.64929			**Proposed method**	41.9115	76.35865
70	Floyd Steinberg	33.6457	58.89483		**71**	Floyd Steinberg	29.1896	50.81215		**72**	Floyd Steinberg	34.0974	59.25616
	WT based dithering	36.1124	70.81688			WT based dithering	35.3031	54.54225			WT based dithering	36.2541	61.44173
	Proposed method	41.1646	87.14644			**Proposed method**	40.9335	56.19886			**Proposed method**	41.0499	64.4574
73	Floyd Steinberg	35.81	51.81394		**74**	Floyd Steinberg	35.5115	54.48429		**75**	Floyd Steinberg	35.0338	54.5096
	WT based dithering	37.8479	61.68642			WT based dithering	36.5836	64.68642			WT based dithering	36.8507	61.68642
	Proposed method	41.2889	65.48571			**Proposed method**	38.6839	65.48571			**Proposed method**	41.6438	66.02901
76	Floyd Steinberg	31.7573	54.4879		**77**	Floyd Steinberg	29.7306	54.4879		**78**	Floyd Steinberg	30.7661	63.16153

	WT based dithering	38.509	57.47572			WT based dithering	36.5496	57.24448			WT based dithering	39.3891	**62.54659**
	Proposed method	41.5275	63.03501			**Proposed method**	41.4016	60.10279			**Proposed method**	41.5433	62.10152
79	Floyd Steinberg	27.3022	54.92108		**80**	Floyd Steinberg	31.50421	62.86755		**81**	Floyd Steinberg	30.8822	59.7119
	WT based dithering	37.5043	55.62455			WT based dithering	39.8365	57.4452			WT based dithering	37.5468	67.16197
	Proposed method	41.234	62.03238			**Proposed method**	45.0971	83.9405			**Proposed method**	41.7789	73.45059
82	Floyd Steinberg	30.7817	59.71849		**83**	Floyd Steinberg	35.7660	59.4731		**84**	Floyd Steinberg	34.2998	47.38301
	WT based dithering	41.175	67.10004			WT based dithering	46.6803	57.6429			WT based dithering	34.7994	**53.25434**
	Proposed method	41.6431	70.99381			**Proposed method**	50.3881	55.7323			**Proposed method**	41.7419	53.08369
85	Floyd Steinberg	25.9731	53.17635		**86**	Floyd Steinberg	34.3384	55.64104		**87**	Floyd Steinberg	30.766	55.64929
	WT based dithering	32.6992	59.14432			WT based dithering	**36.929**	63.1224			WT based dithering	36.0724	52.43561
	Proposed method	41.4053	63.08983			**Proposed method**	36.8186	68.06044			**Proposed method**	38.6269	63.40373
88	Floyd Steinberg	33.9102	55.64929		**89**	Floyd Steinberg	34.1098	55.63279		**90**	Floyd Steinberg	34.0608	56.35865
	WT based dithering	35.642	56.24837			WT based dithering	34.1675	66.00019			WT based dithering	39.8283	59.09586
	Proposed method	38.4695	64.05466			**Proposed method**	41.0602	71.12365			**Proposed method**	40.4513	64.11327
91	Floyd Steinberg	33.9927	67.14644		**92**	Floyd Steinberg	35.7673	56.19886		**93**	Floyd Steinberg	35.0808	57.98448
	WT based dithering	36.2989	76.22044			WT based dithering	38.7198	67.60831			WT based dithering	39.5679	**53.8308**
	Proposed method	40.0663	80.76488			**Proposed method**	40.9242	74.23326			**Proposed method**	39.806	51.26366
94	Floyd Steinberg	36.0921	55.4574		**95**	Floyd Steinberg	32.6897	55.48571		**96**	Floyd Steinberg	35.766	55.48571
	WT based dithering	38.5485	62.53887			WT based dithering	38.6219	63.33303			WT based dithering	38.7007	62.89128
	Proposed method	41.5854	68.69268			**Proposed method**	40.8262	68.82113			**Proposed method**	40.7794	71.37903

97	Floyd Steinberg	36.0361	55.47356		**98**	Floyd Steinberg	35.9915	56.02901		**99**	Floyd Steinberg	35.9023	63.03501
	WT based dithering	38.6058	62.94849			WT based dithering	39.7296	62.93893			WT based dithering	**39.7872**	62.91984
	Proposed method	39.514	63.74418			**Proposed method**	41.8648	70.24448			**Proposed method**	37.4142	69.50165
100	Floyd Steinberg	36.0511	55.10279		**101**	Floyd Steinberg	31.1874	53.67484		**102**	Floyd Steinberg	34.3568	59.7053
	WT based dithering	37.4184	59.11966			WT based dithering	34.4627	54.65933			WT based dithering	49.0810	56.1244
	Proposed method	39.2737	69.28072			**Proposed method**	37.3163	69.20176			**Proposed method**	61.5787	52.5533

Average PSNR(dB)	
Floyd Steinberg	31.81133
WT based dithering	34.49794
Proposed method	**36.946**

Average B & W difference(dB)	
Floyd Steinberg	57.93166186
WT based dithering	61.14275608
Proposed method	**66.2730101**

Appendix B – Visual illustrations of methods discussed in Sections 2.1.1 and 2.2.2

(1) (2)

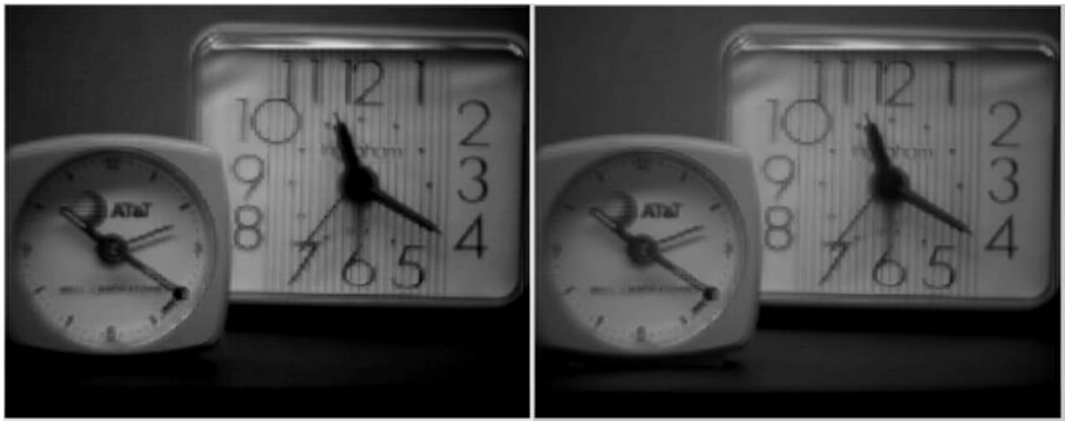

(3) (4)

(5)

Figure B1 Visual illustrations of the existing fusion methods as discussed in Section 2.1.1. (1) Noised image 1 (2) Noised image 2 (3) Fused image using PCA (4) Fused image using IHS (5) Fused image using BT.

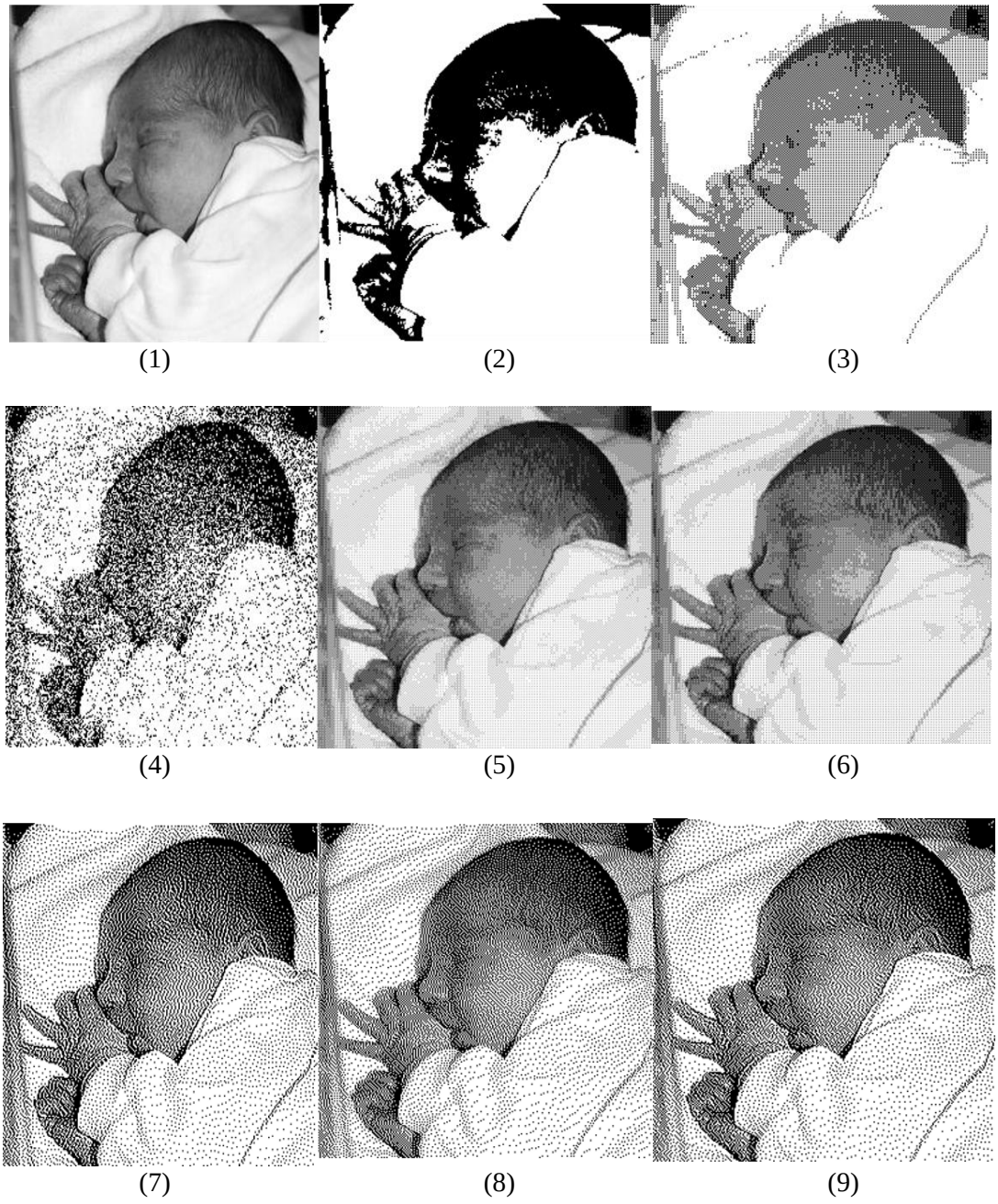

Figure B2 Visual illustrations of the existing dithering methods as discussed in Section 2.2.2. (1) Original image (2) Fixed-thresholding image (3) Ordered dither image (4) Random dither image (5) Ordered 4- level dither (6) Ordered 8-level dither (7) Floyds-Steinberg ED image (8) Jarvis ED image (9) Stucki ED image